Quantification and functional characterization of *Sinorhizobium meliloti* chemotaxis proteins

Timofey Dmitryevich Arapov

Dissertation submitted to the faculty of the Virginia Polytechnic Institute and State University in partial fulfillment of the requirements for the degree of

Doctor of Philosophy
In
Biological Sciences

Birgit E. Scharf, Chair
David L. Popham
Florian D. Schubot
Roderick V. Jensen

February 20, 2020
Blacksburg, VA

Keywords: chemotaxis, protein quantification, *Sinorhiozbium*

Quantification and functional characterization of *Sinorhizobium meliloti* chemotaxis proteins

Timofey Dmitryevich Arapov

ABSTRACT

The flagellated soil-dwelling bacterium *Sinorhizobium meliloti* is known for its symbiotic relationship with several leguminous genera. The symbiosis between the bacterium and its host plants facilitates fixation of atmospheric nitrogen and ultimately replenishment of nitrogen to the soil. However, before nitrogen fixation can occur, the bacterial cells must actively travel to the plant's roots and successfully induce formation of a plant organ called a root nodule. To initiate the nodulation process, the bacterium needs to be in direct contact with the root hairs. This requires free living bacterial cells within the soil to sense the presence of their host plant and travel to its roots. *S. meliloti* is able to do this through a process called chemotaxis. Chemotaxis is the ability to respond to chemical gradients within the environment by directed movement. It is facilitated by **M**ethyl-accepting **C**hemotaxis **P**roteins (MCPs) as part of a two-component signal transduction system. These receptor proteins are able to bind ligands and influence the state of the signal transduction system, ultimately controlling flagellar behavior. The chemotaxis system of *Escherichia coli* has been well characterized and serves as a useful point of comparison to that of *S. melilot* throughout this work.

Within this work we have determined the stoichiometry of all chemotaxis proteins of *S. meliloti* by means of quantitative immunoblotting. Chapter 2 addresses the stoichiometry of MCPs and the histidine kinase CheA. The eight MCPs were grouped by total abundance within the cell, in high abundance (McpV), low abundance (IcpA, McpU, McpX, and McpW), and very low abundance (McpY, McpZ and McpT). The approximate cellular ratio of these three receptor

groups is 300:30:1. The chemoreceptor-to-CheA ratio is 22.3:1, highly similar to the 23:1 ratio known for *Bacilius subtiltis.*

Chapter 3 continues the investigation of the protein stoichiometry, expanding to all chemotaxis proteins. We compare ratios of *S. meliloti* chemotaxis proteins to those of *E. coli* and *B. subtilis.* We address the possible reasons for the high ratio of CheR / CheB to the total amount of receptors. Proteins again can be grouped by abundance: CheD, CheY1, and CheY2 are the most abundant. CheR and CheB appear in lower amounts, CheS and CheT appear to be auxiliary proteins, and finally CheW1 and CheW2, which directly interact with the receptors and CheA.

Chapter 4 focuses on altered receptor abundance in *S. meliloti* due to the fusion of common epitope tags to the C-terminus. The fusion of these tags promotes greater cellular abundance of many receptors including McpU. The fusion of charged residues to the C-terminus promotes a greater increase in McpU abundance thanthe addition of single amino acid residues. Truncations of McpU were made to investigate the presence of a protease recognition site near the C-terminus. These truncations resulted in an increase in abundance similar to those resulting from epitope tag fusions. As epitope tags are widely used in protein studies to help determine protein stoichiometry, this study obviates a potential stumbling block for future experimenters.

The function of CheT, a small protein (13.4 kDa) encoded by the last gene in *S. meliloti*'s major chemotaxis operon, is the subject of chapter 5. A *cheT* deletion strain is chemotactically deficient compared to the *S. meliloti* wild-type strain. Through two separate experiments (a glutaraldehyde cross-linking assay and co-purification) we demonstrated that CheT interacts with the methyltransferase CheR. We also investigate its possible role in CheR's methylation activity through a series of methylation assays.

This work contributes to our understanding of *Sinorhizobium meliloti's* chemotaxis signal transduction system. We have discovered evidence for new a protein-protein interaction within our system and have revealed the abundance of all chemotaxis proteins within the cell. We also showed that fusions of epitope tags to various chemotaxis proteins can dramatically influence their abundance. We shed light on the possible function of a previously uncharacterized protein, although more work is required to determine its exact role.

Quantification and functional characterization of *Sinorhizobium meliloti* chemotaxis proteins

Timofey Dmitrievich Arapov

GENERAL AUDIENCE ABSTRACT

Sinorhizboium meliloti is a bacterium that lives in the soil and forms a symbiotic relationship with many plants including alfalfa, a commonly grown cover crop. This symbiotic relationship is important because it allows for nitrogen to be replenished into the soil without the use of artificial fertilizer. However, to form this relationship the bacterial cells in the soil must be able to colonize the plant roots. The soil is a complex environment with many different kinds of chemical molecules and sources of nutrients. Like many other types of bacteria, *S. meliloti* uses flagella (long helical structures that rotate much like a propeller) to move through the soil. Control of the flagella falls to what is known as a chemotaxis signal transduction system, which can be thought of as a navigation system for each bacterial cell. The system has proteins that act as receptors to sense different chemical molecules. The bacterial cells can sense signals for the plant and move towards their host. This work shows the abundance of each type of receptor and other components within the cell. It also examines the function of a previously unknown protein, CheT, within the chemotaxis system.

DEDICATION

To my family who always listened to my many complaints

ACKNOWLEDGEMENTS

My graduate career has so far been the single longest and most difficult endeavor of my life.

However, I could not have begun it without two specific people from my academic career; Dr. Bruce Turner – who was my professor for evolutionary biology during my undergraduate years at Virginia Tech, and my first research advisor, and Dr. Stephen Melville, my second research advisor for whom I first worked studying for my first bacterium. Thank you both for your confidence in me.

Although the path has been tumultuous I would like to thank these other people in no particular order. My advisor Dr. Birgit Scharf, thank you. For being supportive of my research ideas and letting me explore all the avenues that it has led us down. For understanding when I made mistakes (which were numerous). For providing all the tangible resources (which were also numerous) to complete this work.

My committee for attending all the committee meetings (including those which ran long) and giving your professional opinion about each and every data point.

Dr. Benjamin Webb, for providing a good example.

Rafael Castaneda and Dr. Hardik Zatakia for struggling with blots with me and leaving lots of work to do.

Anna, Rachel, Maya, Jiwoo for letting me mentor you during your time here.

My wife, Floricel Gonzalez for everything, listing of which would consume the entire length of this work.

Table of Contents

Chapter 1 Introduction 1
REFERENCES 11
Chapter 2 Cellular stoichiometry of methyl-accepting chemotaxis proteins in *Sinorhizobium meliloti* 19
ABSTRACT 20
INTRODUCTION 22
MATERIALS AND METHODS 26
RESULTS 33
DISCUSSION 38
ACKNOWLEDGMENTS 41
REFERENCES 47
Chapter 3 Cellular stoichiometry of chemotaxis proteins in *Sinorhizobium meliloti* 58
ABSTRACT 59
INTRODUCTION 60
RESULTS 64
DISCUSSION 68
MATERIALS AND METHODS 74
ACKNOWLEDGMENTS 81
REFERENCES 86
Chapter 4 Features in the C-terminal region control McpU degradation in *Sinorhizobium meliloti* 97
ABSTRACT 98
INTRODUCTION 99
RESULTS 103
DISCUSSION 108
MATERIALS AND METHODS 112
ACKNOWLEDGMENTS 115
REFERENCES 118
Chapter 5 CheT, a novel chemotaxis protein in the legume symbiont *Sinorhizobium meliloti*, is part of the adaptation system 130
ABSTRACT 131
INTRODUCTION 132
RESULTS 136
DISCUSSION 141

MATERIALS AND METHODS 145
ACKNOWLEDGMENTS 150
REFERENCES 153
Chapter 6 – Final Discussion 164
REFERENCES 170

List of Figures

Chapter 1

Figure 1.1 Basic illustration of chemotaxis 14
Figure 1.2 *E. coli* chemotaxis signal transduction system and flagellar motor. 15
Figure 1.3 *B. subtilis* chemotaxis signal transduction system. 16
Figure 1.4 *S. meliloti* chemotaxis signal transduction system. 16
Figure 1.5 Multiple chemotaxis signal transduction systems of *R. sphaeroides*. 17
Figure 1.6 Classification of various alphaproteobacterial chemotaxis operons. 18

Chapter 2

Figure 2.1 Representative immunoblot used to quantify transmembrane chemoreceptors. 54
Figure 2.2 Representative immunoblot used to quantify cytosolic receptors and CheA. 56
Figure 2.3 Localization of McpU, McpV, IcpA, and CheA fused to e-GFP in *S. meliloti* cells by fluorescence microscopy 57
Figure 2.4 Sequence comparison of the 15 C-terminal amino acid residues in the NWETF-motif containing *E. coli* (E.c.) receptors Tar and Tsr and all eight *S. meliloti* (S.m.) chemoreceptors.. 57

Chapter 3

Figure 3.1 Representative immunoblots used to quantify chemotaxis proteins. 91
Figure 3.2 Representative immunoblot used to quantify 3xFLAG-CheS 92
Figure 3.3 Relationship analysis and sequence alignment of CheW proteins from various bacterial species 93
Figure 3.4 Chemotactic responses of various *S. meliloti cheW* mutant strains in a quantitative swim plate assay compared to the wild-type strain 94
Figure 3.5 Cartoon of *in vivo* stoichiometries in *S. meliloti, B. subtilis*, and *E. coli* signaling complexes 95

Chapter 4

Figure 4.1 Mutational analysis of the C-terminal region of McpU and its results on stability. . 122
Figure 4.2 Representative immunoblots for direct comparison of McpU abundance in cell lysates of wild type compared to mutant strains. 123
Figure 4.3 Representative immunoblots used to quantify the relative abundance of McpU in cell lysates of wild type compared to mutant strains. 124
Figure 4.4 Relative abundance of McpU in mutant strains compared to wild type 125
Figure 4.5 Representative immunoblots used to quantify chemotaxis proteins with C-terminal 3xFLAG fusions 126
Figure 4.6 Relative swim ring diameter of *S. meliloti* mutant strains in Bromfield and Rhizobium Basal medium containing 10^{-4} M lysine. 128
Figure 4.7 Comparison of the region comprising 47 amino acid residues proximal to the carboxy-terminus of *C. crescentus* McpA and McpB, five *S. meliloti* MCPs and *S. meliloti* CheW1. 129

Chapter 5

Figure 5.1 Alignment of the amino acid sequence of *S. meliloti* CheT with five paralogues from related alphaproteobacteria 157
Figure 5.2 Chemotactic responses of various *S. meliloti che* mutant strains in a quantitative swim plate assay compared to the wild-type strain (RU11/001) 158
Figure 5.3 Free swimming speed of *S. meliloti* wild-type and chemotaxis gene deletion strains 159
Figure 5.4 Immunoblot analysis to assess the binding of S. meliloti CheT and selected chemotaxis proteins 160
Figure 5.5 Copurification of His_6-CheR and CheT 161
Figure 5.6 Time course of McpX methylation by CheR using [^{3}H]-S-adenosylmethionine (SAM[^{3}H]) as substrate 162
Figure 5.7 McpX methylation by CheR using [^{3}H]-S-adenosylmethionine (SAM[^{3}H]) as substrate with various supplements 163

List of Tables

Chapter 2

Table 2.1 Bacterial strains and plasmids..... 42
Table 2.2 *In vivo mcp* promoter activities in wild type (WT), Δ*visN/R*, Δ*rem*, and Δ*flbT* mutant strains..... 44
Table 2.3 Cellular content of chemoreceptors and CheA chemotaxis protein contents in *S. meliloti* strain RU11/001..... 45
Table 2.4 Proportion of *S. meliloti* cells with fluorescent polar foci expressing eGFP fusions from native chromosomal gene loci..... 46

Chapter 3

Table 3.1 Cellular content of chemotaxis proteins in *S. meliloti* strain RU11/001..... 82
Table 3.2 Cellular stoichiometry of chemotaxis proteins normalized to a CheA dimer in *E. coli, B. subtilis,* and *S. meliloti*..... 83
Table 3.3 Bacterial strains and plasmids..... 84

Chapter 4

Table 4.1 Absolute protein abundance of chemotaxis proteins with C-terminal 3xFLAG epitope..... 116
Table 4.2 Bacterial strains and plasmids..... 117

Chapter 5

Table 5.1.Bacterial strains and plasmids..... 151

Chapter 1 Introduction

Chemotaxis and motility are important factors in both, bacterial pathogenesis and symbiosis, by allowing bacteria to find nutrient rich zones and to avoid toxic environments (2, 3). An incredibly vast array of bacteria swim by rotating one or more flagella, and swimming motility is a highly energy consuming process. Not only does rotation of the flagellum require energy but assembly of the flagellum itself is a genetically complex process involving the use of over 50 different genes and a high degree of regulation. Although the chemotaxis system has been thoroughly described for *Escherichia coli,* other organisms are not as well understood. Certain bacteria including *Sinorhizobium meliloti* have developed a significantly divergent chemotaxis system relative to that observed in *E. coli.*

S. meliloti is a gram-negative bacterium that belongs to the *Rhizobiaceae* family within the alpha class of proteobacteria. Like many other Rhizobia, it is primarily found within the soil and is often associated with roots of legumes. It lives in symbiosis with these legumes, fixing nitrogen in exchange for carbon sources. Most importantly, it is motile, chemotactically active, and moves through its environment using rotating peritrichous flagella. *S. meliloti* possesses a genome of one large 3.65 Mb chromosome and two megaplasmids, pSymA (1.35 Mb) and pSymB (1.68 Mb). Previous studies have revealed that pSymA is important to its symbiotic lifestyle (4). This contrasts with pSymB, which contains several essential genes for growth including *S. meliloti's* only $_{\text{Arg}}\text{tRNA}^{\text{CCG}}$ (5).

With a large degree of homology to other alpha proteobacteria, the chemotaxis system of *S. meliloti* presents a relatively simple system that can be studied to better understand signal transduction pathways that deviate from the *E. coli* paradigm.

Motility and Chemotaxis

Many bacteria use flagella as their primary mode of locomotion. They are able to navigate through their environment through a series of "runs" and "tumbles" that result in a "random walk" (6). By altering the time in the run behavior or frequency of the tumbles they are able to bias this random walk towards the source of the attractant (7). Chemotaxis constitutes the ability to sense chemical gradients and respond with directed movement. It is important to note that not all motile bacteria are capable of chemotaxis; these traits are controlled by two separate systems.

Previous studies have shown that a number of chemoreceptors known as methyl-accepting chemotaxis proteins (MCPs) are responsible for sensing the presence of repellents and attractants. MCPs localize to a single cluster at a cell pole (8). These chemoreceptors respond to a variety of different molecules, which can serve as repellents or attractants. Depending on the state of these MCPs, bacteria are able to change flagellar movement. Each MCP binds a specific set of ligands, and the numbers, amounts, and identities of MCPs vary from species to species. *E. coli* is known to have five while *S. meliloti* has eight chemoreceptors (9). MCPs are vital to controlling movement up or down a concentration gradient.

Chemosensory signal transduction and adaptation in *E. coli*

To navigate chemical gradients, bacteria need to compare the state of their environment (chemical stimuli) relative to the past. In other words: "are things getting better or worse?" *E. coli* is widely used as a model system for chemotaxis. Like many other bacteria it uses a set of peritrichous flagella. When rotating counter clockwise (CCW), these flagella form a bundle used to propel a cell forward. Similar to other signal transduction systems, *E. coli* uses a histidine-aspartate phosphorelay system (HAP). The first component is an auto-histidine kinase, CheA,

which interacts with MCPs. The second is a response regulator CheY, which interacts with motor proteins when phosphorylated. Phosphorylated CheY (CheY-P) is then responsible for binding to the flagellar motor and switching the direction of rotation from CCW to CW (10, 11).

When a chemoattractant is bound to an MCP, a conformational change occurs in the cytoplasmic domain inhibiting CheA autokinase activity. This change stops signaling to the flagellar motor. In the absence of attractant or when a repellent is bound, autokinase activity of CheA instead goes up. CheY-P is able to interact with the motor and change the direction of motor rotation from counter clockwise to clockwise. A change in rotation causes the flagellar bundle to fall apart, the result is a random reorientation in space called a tumble. Although CheY-P has some autophosphatase activity, a phosphatase CheZ is responsible for a tenfold increase in the dephosphorylatin rate of CheY-P (12).

Simply turning CheA activity on and off is not enough to allow for effective chemotaxis in the presence of constant stimuli and continued sensitivity over a broad range of stimuli concentrations. A truly adaptive system is needed. All adaptation systems solve the fundamental problem of returning the system state back to the prestimulus level in the presence of an increased or decreased concentration of attractant or repellent (13). Without an adaptation system, chemoreceptors remain saturated with signal and continuously inhibit the activity of the kinase. *E. coli* has one sensory adaptation system. The system is composed of CheR, a methyltransferase, and CheB, a methylesterase and deamidase. CheR is constitutively active and adds methyl groups to conserved glutamic acid residues found in the MCPs, whereas CheB is activated through phosphorylation by CheA (14). Methylation of the receptor reduces its affinity for the ligand and increases its ability to stimulate CheA (15). The *E. coli* receptor Tsr, responsible for sensing serine, has five methylation sites. Four of these sites have a nine amino

acid motif that contains a conserved glutamate or glutamine. The glutamines can be irreversibly deamidated by CheB to become glutamate residues. CheR is then able to methylate these glutamates to form glutamyl-methyl esters (16). However, the fifth site does not follow the nine amino acid motif and has a slightly different role than the other four sites, suggesting that not all methylation sites serve the same purpose. When an MCP inhibits CheA activity, the activity of CheB is also reduced. CheB-P counters CheR activity by returning MCPs to their original state, via demethylation, thereby returning CheA autokinase activity to higher levels.

However, all of these processes do not occur at the same time scale. When the concentration of an attractant is increasing, the level of receptor methylation will rise, resulting in longer runs and fewer tumbles. If the cell moves to a lower concentration of attractant, the level of methylation will drop and a tumble becomes more likely. Because there is a difference between the slower time scale of methylation and demethylation of the MCPs and the more rapid motor control by CheY-P, a memory mechanism is created. The steeper the gradient of attractant concentration, the longer it will take for CheA activity to be restored to base levels. This memory feature allows bacteria to navigate spatial chemical gradients (13).

Since effective chemotaxis requires an adaptation system and the adaptation system requires methylation and demethylation of MCPs, one would expect that CheB and CheR are essential for all chemotaxis systems. However, exceptions exist such as in *Helicobacter pylori*, which lacks CheB and CheR homologues, and in *Azospirillum brasilense*, where CheB and CheR appear to be not essential for chemotaxis (17, 18). Although other adaptation mechanisms exist, the chemotaxis architecture that employs CheR and CheB for adaptation is wide spread as evidenced by the presence of both CheR and CheB in the approximately 85% of sequenced bacterial genomes (19).

Chemotaxis and Adaptation in *Bacillus subtilis*Another well studied model is the chemotaxis system of gram-positive *Bacillus subtilis. B. subtilis* retains the two integral HAP components CheA and CheY, as well as the methylation and demethylation apparatus. Unlike in *E. coli*, binding of an attractant increases histidine kinase activity. High levels of CheY-P in *B. subtilis* promotes "run" behavior as opposed to *E. coli*, where low levels of CheY-P promote "run" behavior. The function of CheR and CheB remain the same, but the system of methylation and demethylation of MCPs is significantly different.

Evidence suggests that both, methylation and demethylation, occurs on sites of MCPs in response to the addition or removal of attractant. Methylation of individual sites on the same MCP has dissimilar effects on kinase activity. Depending on which sites are modified, kinase activity can be increased or decreased (20). However, the net level of methylation remains constant regardless of attractant concentration (21). This phenomenon contrasts with the *E. coli* system, which only removes methyl groups when attractant is removed and the net level of methylation changes (22, 23).

Furthermore, *B. subtilis* lacks a CheZ homologue to remove phosphate from CheY-P, but replaces it with two additional systems. One system relies on CheD and CheC, the other system relies on CheV. These systems are not unique to *B. subtilis,* with the CheC/CheD system present in >40% of chemotactic bacteria and CheV in ~30% (19).

CheD is a deamidase that converts glutamine residues in MCPs to glutamic acid residues, which are then able to be methylated by CheR leading to modulated CheA activity. CheC has a number of functions, it is a phosphatase of CheY-P and an indirect regulator of adaptation. CheC is able to bind to CheY-P and act as a phosphatase. The CheC/CheY-P complex has a high

affinity for CheD. The CheD/CheC/CheY-P complex exhibits increased phosphatase activity on CheY-P by a factor of five compared to CheC. When CheY-P concentration is low, CheD is mostly bound to the chemoreceptors promoting CheA autokinase activity, however, the mechanism by which it influences CheA activity is unknown This contributes to increased levels of CheY-P and increased formation of the CheC/CheY-P complex, which captures CheD from chemoreceptors, thereby decreasing the level of CheA-P, while also decreasing CheY-P levels through the phosphatase function of the complex (24).

CheV duplicates the function of CheW as an adaptor protein but it also has a receiver domain that is phosphorylated by CheA-P. CheV-P is then able to inhibit CheA autokinase activity, although it is currently unknown how. The result is a feedback inhibition loop (25). There is evidence that CheV and the CheC/CheD complex interact with the methylation system but not with each other (26). While no individual system is vital for chemotaxis in *B. subtilis*, they work in concert to provide a more robust chemotactic response.

Chemotaxis and Adaptation in *Sinorhizobium meliloti*

S. meliloti also differs significantly from *E. coli*. It lacks a CheZ homologue and instead employs a phosphate sink mechanism (27, 28). The flagellar motor of *S. meliloti* can only rotate in the CW direction and rotation is slowed down by the activated response regulator. At full, synchronized speed, the CW rotation of the flagella causes bundle formation. However, when one or more individual flagella slow down at a different rate the bundle flies apart. Coordinated increase in rotary speed reforms the bundle and allows for continued movement (29).

The phosphate sink mechanism is possible through two CheY homologues, CheY1 and CheY2. CheY2 is the response regulator that is able to interact with the motor when phosphorylated, while CheY1 serves to hold excess phosphate and to facilitate its rapid removal

from the system. CheY2 competes for phosphorylation with both CheB and the phosphate sink CheY1 (28).

Furthermore, phosphate groups can be shuttled from CheY2 back to CheA. With the help of an auxiliary protein CheS, which binds to CheA, phosphate groups can be rapidly removed from CheY1. CheS functions by effectively increasing the affinity of CheY1 to CheA approximately 100-fold. CheS does not have direct phosphatase activity but effectively replaces the phosphatase function of CheZ. Although it is not yet clear what is the exact mechanism that allows for this increase in affinity between CheY1 and the CheS, but likely does not require a direct interaction between CheY1 and CheS (28).

Chemotaxis and Adaptation in *Rhodobacter sphaeroides*

R. sphaeroides has possibly the most complex chemotaxis signal transduction system currently discovered. *R. sphaeroides* has a unidirectional motor that is capable of completely stopping and causing a tumble; there is also data indicating it can bias this new orientation (30).

R. sphaeroides possesses three different chemotaxis operons for controlling two different types of flagella. It also has six CheY homologues, four CheW homologues, four CheA homologues, three CheR homologues, three CheB homologues, and one CheD homologue. Fla1-mediated chemotaxis has been studied far more intensively than Fla2, and is controlled by genes from both chemotaxis operon two ($cheOp_2$) and chemotaxis operon three ($cheOp_3$) (Figure 1.5) . However, there are additional genes in all three operons with unknown function.

Another major difference to *E. coli* is the presence of a cytoplasmic chemosensory cluster. The sensory proteins in the cluster have no transmembrane domain and use completely separate homologues of CheA and CheW, suggesting a high degree of specificity to the internal

sensory cluster (31, 32). Signals from this cytoplasmic cluster and its respective chemotaxis adaption proteins are then funneled to $CheY_6$ (33).

A number of other novel interactions emerge within this vastly more complex system. For example, the P1 domain of $CheA_3$ can be phosphorylated by $CheA_4$ (34). Furthermore, we see specificity of CheAs and their ability to phosphorylate various CheYs. $CheA_1$-P can phosphorylate $CheY_1$, $CheY_2$, and $CheY_5$, while $CheA_2$-P can phosphorylate only $CheY_1$, $CheY_6$, and $CheB_2$ (34-36).

The roles of the CheY homologues are complex as well. For example, a deletion of *cheY*$_6$ results in a chemotaxis negative phenotype. A double deletion of *cheY*$_3$ and *cheY*$_4$ also results in a chemotaxis negative phenotype, however, chemotaxis is unaffectedwhen *cheY*$_3$ and *cheY*$_4$ are deleted individually. This indicates a level of redundancy within the system, where some CheYs can compensate for the roles of others (37).

R. sphaeroides also lacks a CheZ homologue and does not use the CheD/CheC; instead, a phosphate sink mechanism is used in conjunction with the phosphatase activity of abifunctional histidine kinase, $CheA_3$ to inactive the phosphorylated motor response regulator (33). $CheY_6$ acts similarly to CheY1 in *S. meliloti*; however,unlike CheY1 in *S. meliloti* it also directly interacts with the motor and is capable of independently stopping the motor in the absence of other CheYs (37).

Chemotaxis Genomics and Operon structure

Genes encoding chemoreceptors, *cheA* and *cheW* are found in >95% of genomes that contain at least one chemotaxis gene. Along with *cheY*, their gene products form the core of the chemotaxis signal transduction system (19).

cheR and *cheB* are present in up to 90% of all genomes with chemotaxis components. Hence, with a few exceptions, their gene products can be included in the core chemotaxis system. All other chemotaxis proteins such as CheC, CheZ, CheV, and the *S. meliloti* CheS can be considered auxiliary in their purpose.

Genomic analysis also shows that >20% of genomes with chemotaxis components do not have an identifiable phosphatase suggesting a great degree of evolutionary variability. Many relatives of *S. meliloti* seem to not have a known phosphatase and likely use a very similar phosphate sink mechanism.

A comparison of the gene order from known chemotaxis operons in alphaproteobacteria showed three distinct groups (Figure 1.6). A phylogeny of alpha proteobacteria based on the sequence of CheA confirms these findings. One surprising bit of information is that the major chemotaxis operon of *S. meliloti* corresponds to $cheOp_3$ which has a relatively minor role in *R. sphaeroides* chemotaxis .(11, 38).

The operon structure is quite variable among bacteria. In *E. coli,* flagellar, chemotaxis, and motility genes are in four different clusters. But in *S. meliloti*, the flagellar, chemotaxis, and motility genes are all found in one 56-kb region of the genome (39, 40). In *B. subtilis*, the majority of flagella, chemotaxis, and motility genes are in a large operon 26-kb in size. However, some chemotaxis genes such as *cheV* are elsewhere in the genome.

Motivations

Previous work has revealed important differences between *S. meliloti, E. coli* and *B. subtilis* particularly in the terms of phosphotransfer (27, 28, 41, 42). It is clear that a great amount of diversity exists in chemotaxis systems. Addressing this diversity is critical to understanding bacterial chemotaxis beyond the well-established enteric paradigm. Data are available regarding

the protein stoichiometry for the constituent members of the *E. coli* and *B. subtilis* chemotaxis systems (43, 44). Stoichiometric data for the *E. coli* chemotaxis system were foundational for determining ratios of the core signaling complex, which are the basic units of the array, and the receptor composition of the *E. coli* chemotaxis array. Stoichiometric data also revealed the difference between *E. coli* and *B. subtilis* chemotaxis architecture (43). Given the known differences in phosphotransfer, knowledge of *S. meliloti* chemotaxis protein stoichiometries will reveal how its chemotaxis system has been remodeled by natural selection regarding receptor composition and abundance of histidine kinase and response regulators. Of particular interest is the highly understudied adaptation system. Furthermore, the final open reading frame in the major chemotaxis operon of *S. meliloti* remains uninvestigated. Determining the concentration of all the chemotaxis proteins and establishing a role for *orf10* (*cheT)* will serve as a foundation for further research of chemotaxis in *S. melilot* and other alphaproteobacteria. This information will contribute to predictive models of *S. meliloti* chemotactic behavior. Models could later translate into engineering *S. meliloti* strains, which can outcompete native strains in the environment, and ultimately increase crop yields.

REFERENCES

1. Porter SL, Wadhams GH, Armitage JP. 2011. Signal processing in complex chemotaxis pathways. Nature Reviews Microbiology 9:153-165.
2. Williams SM, Chen Y-T, Andermann TM, Carter JE, McGee DJ, Ottemann KM. 2007. *Helicobacter pylori* chemotaxis modulates inflammation and bacterium-gastric epithelium interactions in infected mice. Infection and Immunity 75:3747-3757.
3. Miller LD, Yost CK, Hynes MF, Alexandre G. 2007. The major chemotaxis gene cluster of *Rhizobium leguminosarum* bv. viciae is essential for competitive nodulation. Mol Microbiol 63:348-362.
4. Barnett MJ, Fisher RF, Jones T, Komp C, Abola AP, Barloy-Hubler F, Bowser L, Capela D, Galibert F, Gouzy J, Gurjal M, Hong A, Huizar L, Hyman RW, Kahn D, Kahn ML, Kalman S, Keating DH, Palm C, Peck MC, Surzycki R, Wells DH, Yeh K-C, Davis RW, Federspiel NA, Long SR. 2001. Nucleotide sequence and predicted functions of the entire *Sinorhizobium meliloti* pSymA megaplasmid. Proc Natl Acad Sci U S A 98:9883-9888.
5. Finan TM, Weidner S, Wong K, Buhrmester J, Chain P, Vorhölter FJ, Hernandez-Lucas I, Becker A, Cowie A, Gouzy J, Golding B, Pühler A. 2001. The complete sequence of the 1,683-kb pSymB megaplasmid from the N2-fixing endosymbiont *Sinorhizobium meliloti*. Proc Natl Acad Sci U S A 98:9889-9894.
6. Berg HC, Brown DA. 1972. Chemotaxis in *Escherichia coli* analysed by three-dimensional tracking. Nature 239:500-4.
7. Berg HC. 1993. Random walks in biology. Princeton University Press.
8. Meier VM, Scharf BE. 2009. Cellular localization of predicted transmembrane and soluble chemoreceptors in *Sinorhizobium meliloti*. J Bacteriol 191:5724-5733.
9. Meier VM, Muschler P, Scharf BE. 2007. Functional analysis of nine putative chemoreceptor proteins in *Sinorhizobium meliloti*. J Bacteriol 189:1816-26.
10. Wadhams GH, Armitage JP. 2004. Making sense of it all: bacterial chemotaxis. Nat Rev Mol Cell Biol 5:1024-1037.
11. Porter SL, Wadhams GH, Armitage JP. 2011. Signal processing in complex chemotaxis pathways. Nat Rev Microbiol 9:153-165.
12. Wang H, Matsumura P. 1996. Characterization of the CheAS/CheZ complex: a specific interaction resulting in enhanced dephosphorylating activity on CheY-phosphate. Mol Microbiol 19:695-703.
13. Vladimirov N, Sourjik V. 2009. Chemotaxis: how bacteria use memory. Biol Chem 390:1097-1104.
14. Nowlin DM, Bollinger J, Hazelbauer GL. 1987. Sites of covalent modification in Trg, a sensory transducer of *Escherichia coli*. J Biol Chem 262:6039-6045.
15. Hulko M, Berndt F, Gruber M, Linder JU, Truffault V, Schultz A, Martin J, Schultz JE, Lupas AN, Coles M. 2006. The HAMP domain structure implies helix rotation in transmembrane signaling. Cell 126:929-940.
16. Han X-S, Parkinson JS. 2014. An unorthodox sensory adaptation site in the *Escherichia coli* serine chemoreceptor. J Bacteriol 196:641-649.
17. Stephens BB, Loar SN, Alexandre G. 2006. Role of CheB and CheR in the complex chemotactic and aerotactic pathway of *Azospirillum brasilense*. J Bacteriol 188:4759-4768.

18. Spohn G, Scarlato V. 2001. Motility, Chemotaxis, and Flagella. *In* Mobley HL, Mendz GL, Hazell SL (ed), *Helicobacter pylori*: Physiology and Genetics. ASM Press, Washington (DC).
19. Wuichet K, Zhulin IB. 2010. Origins and diversification of a complex signal transduction system in prokaryotes. Sci Signal 3:ra50-ra50.
20. Glekas GD, Cates JR, Cohen TM, Rao CV, Ordal GW. 2011. Site-specific methylation in *Bacillus subtilis* chemotaxis: effect of covalent modifications to the chemotaxis receptor McpB. Microbiology 157:56-65.
21. Thoelke MS, Kirby JR, Ordal GW. 1989. Novel methyl transfer during chemotaxis in *Bacillus subtilis*. Biochemistry 28:5585-9.
22. Kirsch ML, Peters PD, Hanlon DW, Kirby JR, Ordal GW. 1993. Chemotactic methylesterase promotes adaptation to high concentrations of attractant in *Bacillus subtilis*. J Biol Chem 268:18610-6.
23. Kirsch ML, Zuberi AR, Henner D, Peters PD, Yazdi MA, Ordal GW. 1993. Chemotactic methyltransferase promotes adaptation to repellents in *Bacillus subtilis*. J Biol Chem 268:25350-6.
24. Glekas GD, Plutz MJ, Walukiewicz HE, Allen GM, Rao CV, Ordal GW. 2012. Elucidation of the multiple roles of CheD in *Bacillus subtilis* chemotaxis. Mol Microbiol 86:743-56.
25. Rao CV, Glekas GD, Ordal GW. 2008. The three adaptation systems of *Bacillus subtilis* chemotaxis. Trends Microbiol 16:480-487.
26. Walukiewicz HE, Tohidifar P, Ordal GW, Rao CV. 2014. Interactions among the three adaptation systems of *Bacillus subtilis* chemotaxis as revealed by an in vitro receptor-kinase assay. Mol Microbiol 93:1104-18.
27. Sourjik V, Schmitt R. 1998. Phosphotransfer between CheA, CheY1, and CheY2 in the chemotaxis signal transduction chain of *Rhizobium meliloti*. Biochemistry 37:2327-2335.
28. Dogra G, Purschke FG, Wagner V, Haslbeck M, Kriehuber T, Hughes JG, Van Tassell ML, Gilbert C, Niemeyer M, Ray WK, Helm RF, Scharf BE. 2012. *Sinorhizobium meliloti* CheA complexed with CheS exhibits enhanced binding to CheY1, resulting in accelerated CheY1 dephosphorylation. J Bacteriol 194:1075-1087.
29. Scharf B. 2002. Real-time imaging of fluorescent flagellar filaments of *Rhizobium lupini* H13-3: flagellar rotation and pH-induced polymorphic transitions. J Bacteriol 184:5979-86.
30. Rosser G, Baker RE, Armitage JP, Fletcher AG. 2014. Modelling and analysis of bacterial tracks suggest an active reorientation mechanism in *Rhodobacter sphaeroides*. J R Soc Interface 11:20140320.
31. Wadhams GH, Martin AC, Armitage JP. 2000. Identification and localization of a methyl-accepting chemotaxis protein in *Rhodobacter sphaeroides*. Mol Microbiol 36:1222-1233.
32. Wadhams GH, Martin AC, Warren AV, Armitage JP. 2005. Requirements for chemotaxis protein localization in *Rhodobacter sphaeroides*. Mol Microbiol 58:895-902.
33. Porter SL, Roberts MA, Manning CS, Armitage JP. 2008. A bifunctional kinase-phosphatase in bacterial chemotaxis. Proc Natl Acad Sci U S A 105:18531-18536.
34. Porter SL, Armitage JP. 2004. Chemotaxis in *Rhodobacter sphaeroides* requires an atypical histidine protein kinase. J Biol Chem 279:54573-54580.

35. Porter SL, Armitage JP. 2002. Phosphotransfer in *Rhodobacter sphaeroides* chemotaxis. J Mol Biol 324:35-45.
36. Ind AC, Porter SL, Brown MT, Byles ED, de Beyer JA, Godfrey SA, Armitage JP. 2009. Inducible-expression plasmid for *Rhodobacter sphaeroides* and *Paracoccus denitrificans*. Appl Environ Microbiol 75:6613-6615.
37. Porter SL, Wadhams GH, Martin AC, Byles ED, Lancaster DE, Armitage JP. 2006. The CheYs of *Rhodobacter sphaeroides*. J Biol Chem 281:32694-32704.
38. Hauwaerts D, Alexandre G, Das SK, Vanderleyden J, Zhulin IB. 2002. A major chemotaxis gene cluster in *Azospirillum brasilense* and relationships between chemotaxis operons in α-proteobacteria. FEMS Microbiol Lett 208:61-67.
39. Sourjik V, Sterr W, Platzer J, Bos I, Haslbeck M, Schmitt R. 1998. Mapping of 41 chemotaxis, flagellar and motility genes to a single region of the *Sinorhizobium meliloti* chromosome. Gene 223:283-290.
40. Rotter C, Mühlbacher S, Salamon D, Schmitt R, Scharf B. 2006. Rem, a new transcriptional activator of motility and chemotaxis in *Sinorhizobium meliloti*. J Bacteriol 188:6932-6942.
41. Sourjik V, Schmitt R. 1996. Different roles of CheY1 and CheY2 in the chemotaxis of *Rhizobium meliloti*. Mol Microbiol 22:427-436.
42. Riepl H, Maurer T, Kalbitzer HR, Meier VM, Haslbeck M, Schmitt R, Scharf B. 2008. Interaction of CheY2 and CheY2-P with the cognate CheA kinase in the chemosensory-signalling chain of *Sinorhizobium meliloti*. Mol Microbiol 69:1373-1384.
43. Cannistraro VJ, Glekas GD, Rao CV, Ordal GW. 2011. Cellular stoichiometry of the chemotaxis proteins in *Bacillus subtilis*. J Bacteriol 193:3220-3227.
44. Li M, Hazelbauer GL. 2004. Cellular stoichiometry of the components of the chemotaxis signaling complex. J Bacteriol 186:3687-3694.
45. Boldog T, Grimme S, Li M, Sligar SG, Hazelbauer GL. 2006. Nanodiscs separate chemoreceptor oligomeric states and reveal their signaling properties. Proceedings of the National Academy of Sciences 103:11509-11514.
46. Hauwaerts D, Alexandre G, Das SK, Vanderleyden J, Zhulin IB. 2002. A major chemotaxis gene cluster in *Azospirillum brasilense* and relationships between chemotaxis operons in α-proteobacteria. FEMS Microbiology Letters 208:61-67.

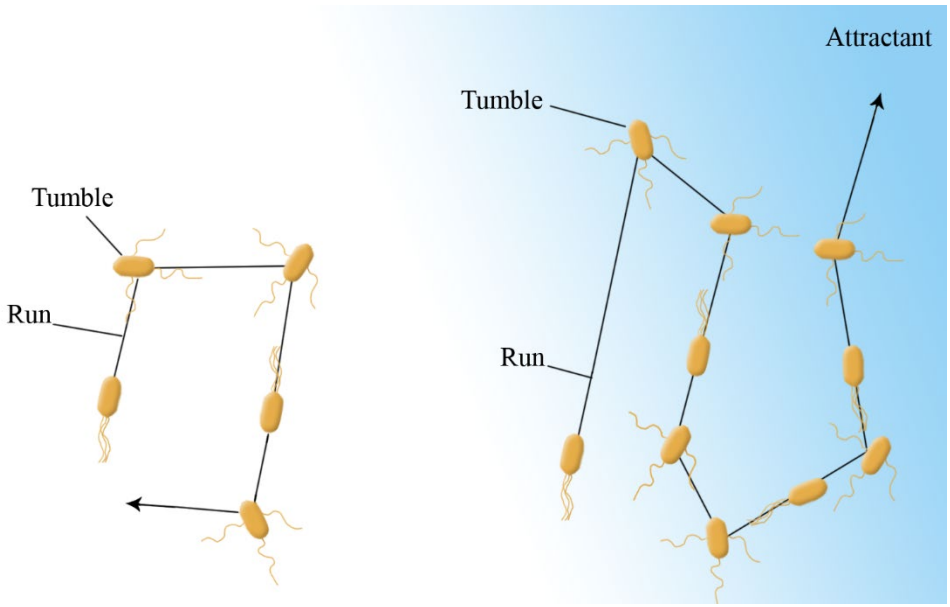

Figure 1.1 Basic illustration of chemotaxis On the left: a depiction of a random walk in the absence of chemical gradient. On the right the “biased random walk” in the presence of a chemical gradient in green and white (with green being the highest concentration of chemoattractant)., (45)

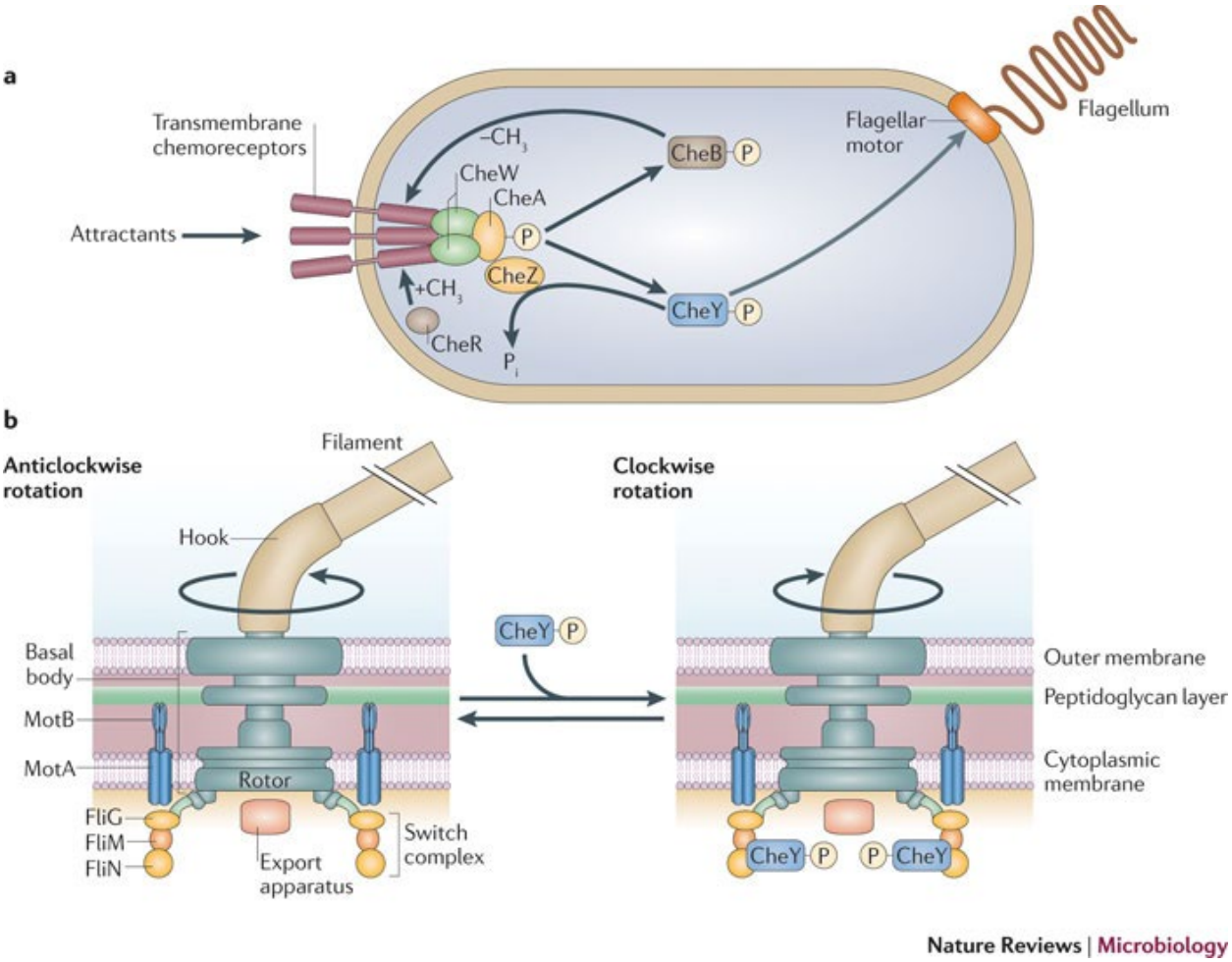

Figure 1.2 *E. coli* chemotaxis signal transduction system and flagellar motor. a. The image demonstrates the histidine-aspartate phosphorelay system and the flow of phosphates in the system. b. A model of the *E. coli* flagellar motor and directional switching in the presence of CheY-P. Image used with permission from Porter *et al* (11).

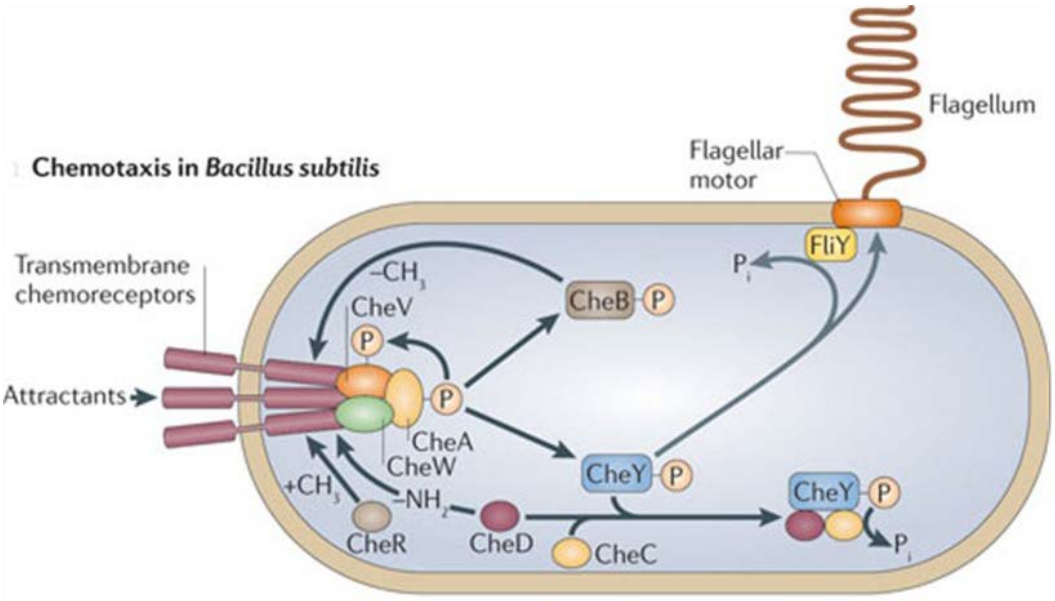

Figure 1.3 *B. subtilis* chemotaxis signal transduction system. The image demonstrates the histidine-aspartate phosphorelay system and the flow of phosphates in *B. subtilis*. Note the presence of CheV in the chemosensory cluster and the replacement of CheZ with the CheD/CheC/CheY complex. Image used with permission from Porter *et al.* (1).

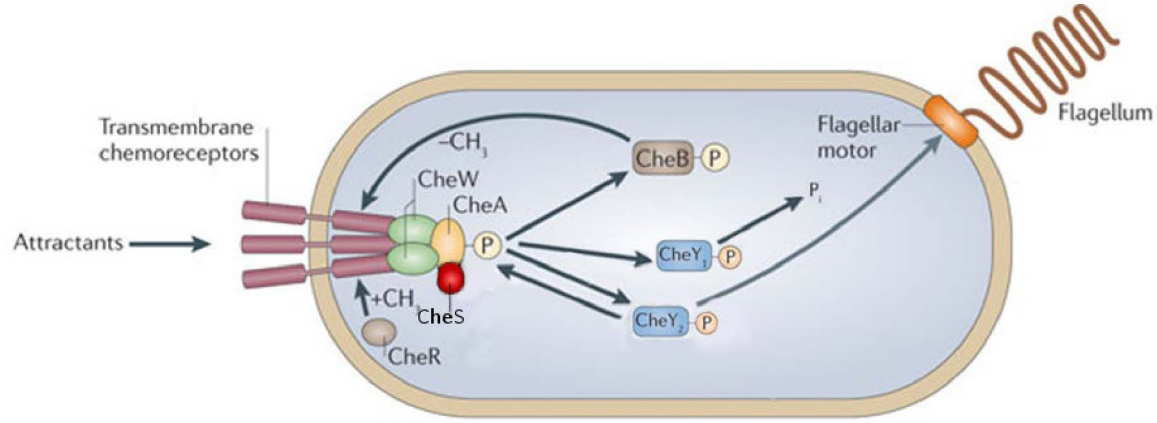

Figure 1.4 *S. meliloti* chemotaxis signal transduction system. The image demonstrates the histidine-aspartate phosphorelay system and the flow of phosphates in *B. subtilis*. Note the complex of CheS with CheA and the reverse movement of phosphate groups. Image used with permission from Porter *et al (11).*

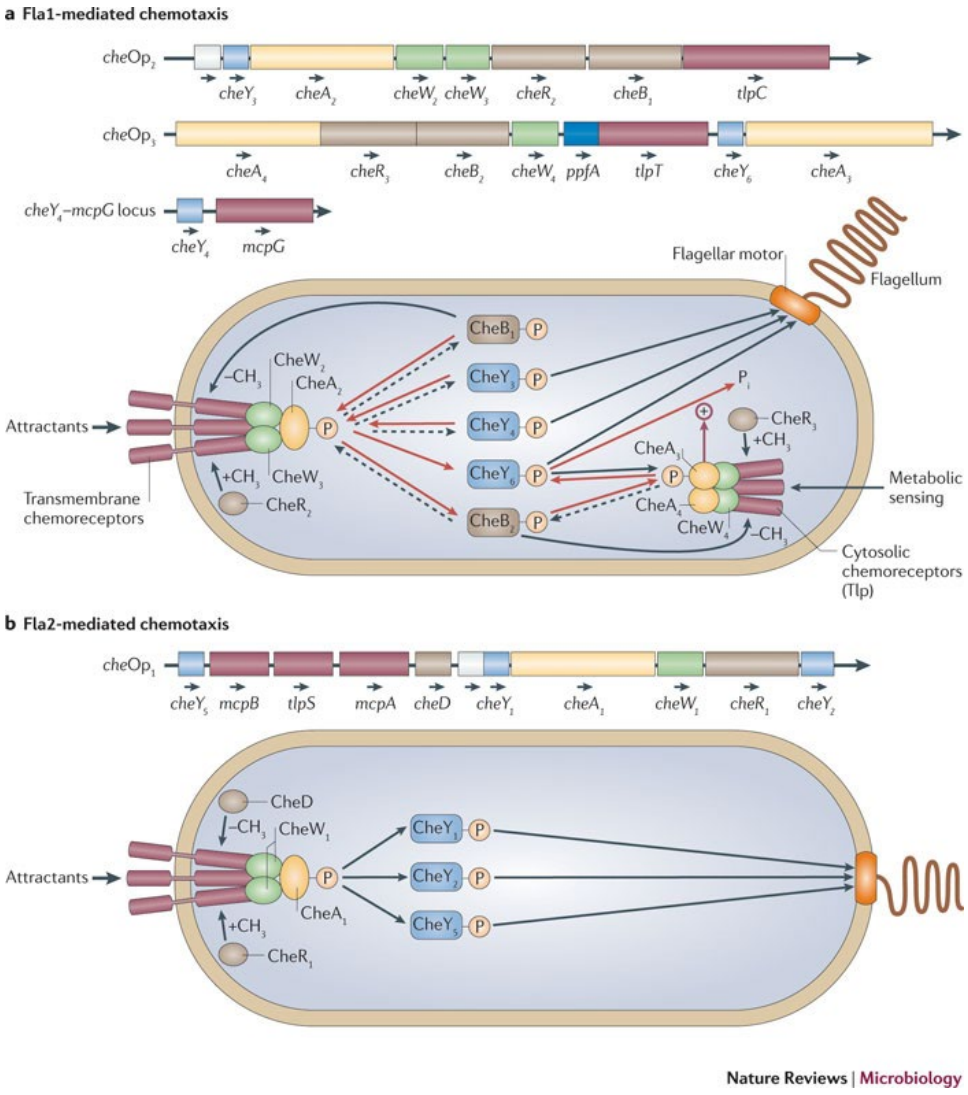

Figure 1.5 Multiple chemotaxis signal transduction systems of *R. sphaeroides.* Fla1-mediated chemotaxis genes, with *cheOp*$_2$ and *cheOp*$_3$ shown respectively. Note multiple paths for phosphorylation of CheA and each CheY (not all discussed) b. The *cheOp*$_1$ and a plausible mechanism for control of Fla2 flagella. Image used with permission from Porter *et al (11).*

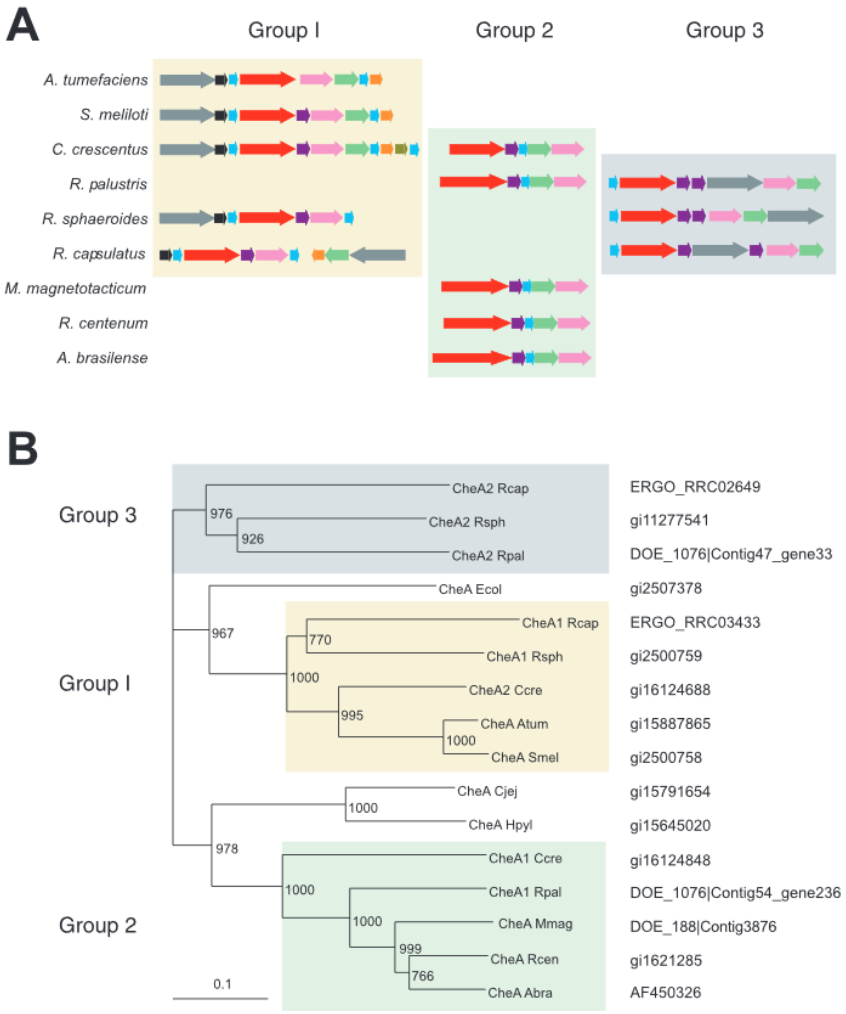

Figure 1.6 Classification of various alphaproteobacterial chemotaxis operons. **A.** Chemotaxis operon classification, color code of operon structure classification ; CheA, red, CheW, dark purple, CheY, light blue, CheB, green, CheR magenta, Chemotactic transducer genes, grey CheS black, CheD, orange CheU, brown . **B.** Phylogenetic tree built on the sequence of histidine-kinase homologues CheA (46). Image used with permission from Hauwaert *et al.* (38)

Chapter 2 Cellular stoichiometry of methyl-accepting chemotaxis proteins in *Sinorhizobium meliloti*

HARDIK M. ZATAKIA[1 #], TIMOFEY D. ARAPOV[1 #], VERONIKA M. MEIER[2+], BIRGIT E. SCHARF[1,2*]

[1]Department of Biological Sciences, Life Sciences I, Virginia Polytechnic Institute and State University, Blacksburg, VA 24061, USA

[2] Lehrstuhl für Genetik, Universität Regensburg, D-93040 Regensburg, Germany

[#] H.M.Z. and T.D.A. equally contributed to the work.

Running title: Stoichiometry of *Sinorhizobium meliloti* chemoreceptors

Key words: alfalfa, chemoreceptors, flagellar motor, plant symbiosis, transcriptional control

* For correspondence:
E-mail bscharf@vt.edu
Tel (+1) 540 231 0757
Fax (+1) 540 231 4043
Biological Sciences, Life Sciences I
Virginia Tech
Blacksburg, VA 24061, USA

[+] Present Address: BKD (bloembollenkeuringsdienst), Zwartelaan 2, NL-2161 AL Lisse, Veronika.Wallner@bkd.eu

First published in ASM Journal of Bacteriology, February 23, 2018 - https://doi.org/10.1128/JB.00614-17

Attribution: TDA has generated portions of Figure 2.2 relating to quantification of CheA and IcpA, Figure 2.3, and Table 2.4. HMZ generated portions of Figure 2.1 and Figures 2.2 relating to McpY. VMM contributed to the results section "The *mcp* genes are part of the flagellar regulon and transcribed as class III genes". HMZ, TDA and BES drafted the final manuscript

ABSTRACT

The chemosensory system in *Sinorhizobium meliloti* has several important deviations from the widely studied enterobacterial paradigm. To better understand the differences between the two systems and how they are optimally tuned, we determined the cellular stoichiometry of the methyl-accepting chemotaxis proteins (MCPs) and the histidine kinase CheA in *S. meliloti*. Quantitative immunoblotting was used to determine the total amount of MCPs and CheA per cell in *S. meliloti*. The MCPs are present in the cell in high abundance (McpV), low abundance (IcpA, McpU, McpX, and McpW), and very low abundance (McpY and McpZ), whereas McpT was below detection limit. The approximate cellular ratio of these three receptor groups is 300:30:1. The chemoreceptor to CheA ratio is 23.5:1, highly similar to that seen in *Bacillus subtilis* (23:1) and about 10 times higher than that in *Escherichia coli* (3.4:1). Different from *E. coli*, the high abundance receptors in *S. meliloti* are lacking the carboxy-terminal NWETF pentapeptide that binds the CheR methyltransferase and CheB methylesterase. Using transcriptional *lacZ* fusions, we showed that chemoreceptors are positively controlled by the master regulators of motility, VisNR and Rem. In addition, FlbT, a class IIA transcriptional regulator of flagellins, also positively regulates the expression of most chemoreceptors except for McpT and McpY, placing chemoreceptors as class III genes. Taken together, these results demonstrate that the chemosensory complex and the adaptation system in *S. meliloti* deviates significantly from the established enterobacterial paradigm, but shares some similarities with *B. subtilis*.

‘

The symbiotic soil bacterium *Sinorhizobium meliloti* is of great agricultural importance because of its nitrogen-fixing properties, which enhances growth of its plant symbiont alfalfa. Chemotaxis provides a competitive advantage for bacteria to sense their environment and interact with their eukaryotic hosts. For a better understanding of the role of chemotaxis in these processes, detailed knowledge on the regulation and composition of the chemosensory machinery is essential. Here, we show that chemoreceptor gene expression in *S. meliloti* is controlled through the main transcriptional regulators of motility. Chemoreceptor abundance is much lower in *S. meliloti* compared to *Escherichia coli* and *Bacillus subtilis*. Moreover, chemoreceptor to kinase CheA ratio is different from *E. coli* but similar to *B. subtilis*.

INTRODUCTION

Chemotaxis is a mechanism by which bacteria rapidly respond to their immediate environment, ultimately moving toward favorable niches and away from repellents (34-36). It has been implicated in various bacterial processes like pathogenicity, nodulation, and biofilm production (37, 38). Chemotaxis has been most widely studied in the enterobacterium *Escherichia coli*, which swims in series of runs and tumbles through the rotation of peritrichous flagella. During runs, flagella rotate counter-clockwise (CCW) leading to the formation of a flagellar bundle with synchronized rotation. In *E. coli*, tumbles are achieved by reverting the rotation of one or more flagella in the clockwise (CW) direction, which causes the flagellar bundle to splay apart, and randomly reorients the cell in three dimensional space (39). However, the flagellar motors of certain bacterial species exhibit only unidirectional rotation. In the case of *Rhodobacter sphaeroides*, pausing rotation of the single polar flagellum causes the cell to tumble, while resuming flagellar rotation results in a straight run (40). In *Sinorhizobium meliloti*, the asynchrony caused by the slowing down of one or more of the strictly CW rotating flagella results in a tumble (33, 41-43).

Bacterial chemotaxis is accomplished through the sensing of environmental signals by chemoreceptors called methyl-accepting chemotaxis proteins (MCPs). *E. coli* has four transmembrane MCPs: Tap, Tar, Trg, and Tsr. While Tap senses dipeptides, Tar mediates taxis towards aspartate and maltose, Trg recognizes ribose and galactose, and Tsr responds to serine and 3,4-dihydroxymandelic acid, a catabolite of norepinephrine (44-46). A fifth receptor, Aer, which is anchored to the inside of the cytoplasmic membrane, acts as an oxygen sensor (45, 46). The number of different chemoreceptors varies within species. While *Mesorhizobium loti* has only one putative chemoreceptor gene, *Vibrio cholerae* has 45 (47). Chemoreceptors form stable

homodimers that are in turn arranged in trimers. These 'trimers of dimers' along with other cytoplasmic chemotaxis proteins are packaged in large hexagonal arrays called 'chemoreceptor clusters'. MCPs typically consist of a periplasmic ligand-binding domain, two membrane-spanning helices, and a cytoplasmic signaling domain. Binding of ligand to the periplasmic domain causes a piston-like movement through the transmembrane domains to the cytoplasmic domain, where it acts as a signal to the cytosolic chemotaxis proteins (46, 48). While the periplasmic domains of MCPs are vastly diverse to accommodate various ligands, the cytoplasmic signaling domains are highly conserved, even amongst different species (36). A two-component system using the histidine-aspartate phosphorelay mediates the chemotactic signal transduction from the chemoreceptor cluster to the flagellar motors. The first component, CheA, is the histidine kinase that binds to the cytoplasmic domain of the MCPs via a coupling protein, CheW. The second component, CheY, is the response regulator that interacts with the flagellar motor complex, thereby controlling its rotation. Binding of an attractant to the periplasmic domain of an MCP induces a conformational change in the cytoplasmic domain that inhibits the autophosphorylation of CheA. In *E. coli*, when CheA is inactive and no signal is being passed to the flagellar motors, continued CCW rotation results in a run. In absence of a bound attractant or presence of a repellent, ATP-dependent CheA autophosphorylation is stimulated. Phosphorylated CheA (CheA-P) transfers the phosphate group to a conserved aspartate residue in CheY (35, 36). CheY-P interacts with FliM of the flagellar motor complex and signals the motor to switch to the CW direction, subsequently resulting in a tumble (49, 50). In *E. coli*, CheZ is a phosphatase which increases the dephosphorylation rate of CheY-P and thereby allows for signal termination (51-53). An adaptation system involving CheR and CheB is employed for increased sensitivity and real-time modulation of chemotactic activity based on the local environment. CheR is a methyltransferase

that constitutively adds methyl groups to conserved sites on the cytoplasmic signaling domain of MCPs. CheB acts as a methylesterase and is activated through its phosphorylation by CheA-P (36, 47). In *E. coli*, only the high abundant MCPs, Tar and Tsr, have a conserved pentapeptide NWETF at their carboxy terminus, which serves as the site for CheR and CheB docking (54). The concerted addition and removal of methyl groups by CheR and CheB, respectively, brings about the conformational changes in MCPs required for the resetting and adaptation of the chemotaxis system (55, 56).

The importance of bacterial chemotaxis in establishing symbiosis with plant hosts has been well documented for members of the *Rhizobiaceae* family including *S. meliloti* (57-60). Recent studies of *S. meliloti* motility and chemotaxis have uncovered marked deviations from the enterobacterial paradigm (42, 61). Unlike *E. coli*, *S. meliloti* not only has six transmembrane chemoreceptors (McpT-McpX, and McpZ) but also has two soluble cytosolic receptors (McpY and IcpA). The size of the ligand-binding domains of *S. meliloti* chemoreceptors vary greatly between 160 to 390 amino acids residues (62). Our group has shown that McpU and McpX play a role in host interaction by sensing plant-derived amino acids and quaternary ammonium compounds, respectively (63-66). However, the function of the remaining six chemoreceptors is not known. Furthermore, *S. meliloti* does not utilize a CheZ phosphatase but employs an indirect phosphate sink mechanism for signal termination. Here, phosphate groups from the response regulator CheY2 are shuttled back via CheA to an additional response regulator protein, CheY1 (67). *S. meliloti* involves three additional proteins in chemotaxis as compared to *E. coli* , namely CheD, CheS, and CheT (68). A CheD analog in *Bacillus subtilis* serves as an MCP deamidase and thus plays a role in adaptation (69). However, it is unclear whether *S. meliloti* CheD exerts a similar function. CheS and CheT have no homologs in enteric bacteria but display homology to some unassigned proteins

in other α-proteobacteria like *Caulobacter crescentus* and *Rhizobium leguminosarum*. CheS enhances the phosphate flow from CheA-P to CheY1 by increasing the affinity between CheA-P and CheY1 by 100-fold (70). The one kinase-two response regulator system and presence of an auxiliary protein allows the implementation of a tunable switch-like signal processing (71). The function of CheT in chemotaxis is currently unknown.

Up to now, two studies have investigated the cellular quantities of bacterial chemotaxis proteins, one in *E. coli* and one in *B. subtilis* (72, 73). While total protein amounts may change depending on growth conditions and nutrient availability, cellular ratios of chemotaxis proteins were fairly robust. Both studies also revealed that ratios between certain proteins, such as CheA and CheW, remained constant, while the ratio of others, such as CheA and the MCPs, differed greatly between species (72, 73). To gain a better understanding of deviations evolved in the *S. meliloti* chemotaxis system and to understand how the system is tuned for optimum performance and sensitivity, we determined the cellular amounts and ratios of CheA and all eight chemoreceptors in *S. meliloti* using quantitative immunoblots. Furthermore, we explored the regulation of chemoreceptor gene expression within the flagellar gene hierarchy. Ultimately, computational models can be used to simulate the interactions of all chemotaxis proteins and to evaluate the chemotaxis system holistically under various physiologically relevant conditions (74).

MATERIALS AND METHODS

Bacterial strains and plasmids

Derivatives of *E. coli* K12 and *S. meliloti* MV II-1 and the plasmids used are listed in Table 2.1. RU11/001 is a spontaneous streptomycin-resistant derivative of MVII-1 (75).

Media and growth conditions

E. coli strains were grown in lysogeny broth (LB) (76) at indicated temperatures. *S. meliloti* strains were grown in TYC (0.5 % tryptone, 0.3 % yeast extract, 0.13 % $CaCl_2.6H_2O$ [pH 7.0]) (77) or SMM (Sinorhizobium motility medium; RB [6.1 mM K_2HPO_4, 3.9 mM KH_2PO_4, 1 mM $MgSO_4$, 1 mM $(NH_4)_2SO_4$, 0.1 mM $CaCl_2$, 0.1 mM NaCl, 0.01 mM Na_2MoO_4, 0.001 mM $FeSO_4$, 2 µg/l biotin] (78), 0.2 % Mannitol. 2 % TY) (79). Motile cells for immunoblots and fluorescence microscopy were grown in SMM for two days, diluted to an OD_{600} of 0.02 and incubated at 30 °C to an OD_{600} of 0.25. The following antibiotics were used in their final concentrations: for *E. coli*, ampicillin at 100 µg/ml, kanamycin at 50 µg/ml and tetracycline at 10 µg/ml; for *S. meliloti*, neomycin at 120 µg/ml, streptomycin at 600 µg/ml, and tetracycline at 10 µg/ml.

Genetic and DNA manipulations

S. meliloti DNA was isolated and purified as described previously (80). Plasmid DNA, DNA fragments or PCR products were purified according to manufacturers' instructions, and PCR amplification of chromosomal DNA was carried out according to published protocols (80). The *flbT* strain was generated *in vitro* by overlap extension PCR as described (81). Constructs containing the mutations were cloned into the mobilizable suicide vector pK18*mobsac*B, used to transform *E. coli* S17-1, and conjugally transferred to *S. meliloti* by filter mating (82, 83). Allelic

replacement was achieved by sequential selections on neomycin and 10 or 15 % sucrose as described previously (80). Confirmation of allelic replacement and elimination of the vector was obtained by gene-specific primer PCR and DNA-sequencing. Derivatives of the broad-host-range plasmids pPHU235 and pPHU236 were used to transform *E. coli* S17-1 and conjugally transferred to *S. meliloti* by streptomycin-tetracycline double selection as described above (84).

β-galactosidase assays

Cultures of *S. meliloti* containing *lacZ* fusions grown on over-layered Bromfield agar plates were sampled, diluted 1:1 in Z buffer (85), permeabilized with 1 drop of toluene, and assayed for β-galactosidase activity by the method of Miller (85) as previously described (62).

Purification of recombinant proteins

McpT-LBD (ligand-binding domain) (aa 30 – 178) was expressed from pBS1030, McpU-LBD (aa 40 – 287) was expressed from pBS353, McpV-LBD (aa 31 – 189) from pBS0409, McpW-LBD (aa 39 – 180) from pBS1031, McpX-LBD (aa 34 – 320) from pBS352, McpZ-LBD (aa 39 – 445) from pBS426, and CheA from (pBS57) in *E. coli* ER2566 (Table 2.1) as described by Riepl *et al. (86)*. Briefly, cells were grown to an OD_{600} of 0.6 - 0.8 at 37 °C in LB, and expression was induced by 0.3 mM isopropyl-β-$_D$-thiogalactopyranoside (IPTG) at 16 °C for 16 h. Cells were harvested, suspended in IMPACT buffer (500 mM NaCl, and 1 mM EDTA, 1 mM phenylmethylsulfonyl fluoride [PMSF], 20 mM Tris/HCl, pH 8.0), and lysed by three passages through a French pressure cell at 20,000 lb/in^2 (SLM Aminco, Silver Spring, MD). A modified IMPACT buffer (2 M NaCl, 1 mM EDTA, 1 mM PMSF, 20 mM Tris/HCl, pH 8.0) along with Halt™ Protease Inhibitor cocktail (Life Technologies) was used for CheA purification. The soluble fraction was loaded on

a Chitin agarose (NEBiolabs, Beverly, MA) column (6 cm x 5 cm) and Intein-mediated cleavage was induced by equilibration of the column with IMPACT buffer containing 50 mM dithiothreitol (DTT) and incubation at 4 °C for 2-3 days. Proteins were eluted with IMPACT buffer and pooled fractions of each protein were further purified by fast-performance liquid chromatography (FPLC, Äktaprime Plus, GE Healthcare) gel filtration on HiPrep 26/60 Sephacryl S-200 HR (GE Healthcare). The column was equilibrated and developed using 100 mM NaCl, 5 % (v/v) glycerol, 80 mM Na_2HPO_4, 20 mM NaH_2PO_4, pH 7.5 at 0.5 ml/min, and protein-containing fractions were combined.

McpY protein was overproduced in inclusion bodies from plasmid pRU2790 in *E. coli* BL21(DE3) (Table 2.1). Cells were grown at 37 °C in LB at 300 rpm to an OD_{600} of 0.6 - 0.8, and expression was induced by 1 mM IPTG. Cells were harvested after 4 h of incubation at 37 °C, suspended in 20 ml 0.5 mM EDTA, 20 mM Tris/HCl, pH 7.5, and cell lysates were prepared as described before. The lysate was centrifuged at 55,000 g and 4 °C for 20 min, the soluble fraction was discarded, and the pellet was washed twice with 1 % (v/v) Triton X-100, 1 mM EDTA, 20 mM Tris/HCl, pH 7.5. Inclusion bodies were suspended in 10 ml denaturation buffer (8 M urea, 5 mM DTT, 50 mM Tris/HCl, pH 8.0), centrifuged and the supernatant was filtered through a 0.2 µm cellulose acetate syringe filter. Ten-ml samples were subjected to FPLC (Äktaprime Plus, GE Healthcare) gel filtration on HiPrep 26/60 Sephacryl S-200 HR (GE Healthcare). The column was equilibrated and developed in denaturation buffer at 0.5 ml/min, and protein-containing fractions were combined. The protein was then refolded by dialysis against a 30-fold volume of 100 mM NaCl, 1 mM EDTA, 1 mM DTT, 20 % (v/v) glycerol, 50 mM Tris/HCl, pH 8.0 for 24 h at 4 °C. Subsequently, dialysis was performed with 100 mM NaCl, 1 mM EDTA, 1 mM DTT, 10 % (v/v) glycerol, 50 mM Tris/HCl, pH 8.0 for 24 h at 4 °C. Lastly, the protein was dialyzed in phosphate-buffered saline

(PBS; 100 mM NaCl, 80 mM Na_2HPO_4, 20 mM NaH_2PO_4, pH 7.5) for 24 h at 4 °C and stored in 5 % glycerol at -80 °C.

IcpA was overproduced as a fusion protein with 6x-histidine tagged maltose-binding protein (MBP) from pBS487 in *E. coli* BL21(DE3) (Table 2.1). Cells were grown to an OD_{600} of 0.6 - 0.8 at 37 °C in LB, and expression was induced by 0.3 mM IPTG. Cells were harvested after 4 h of incubation at 25 °C, then suspended in Ni-NTA column buffer (500 mM NaCl, 25 mM imidazole, 1 mM PMSF, 20 mM $NaPO_4$, pH 7.4). Cells were lysed by three passages through a French pressure cell at 20,000 psi (SLM Aminco, Silver Spring, MD). The soluble fraction was loaded onto a 5 ml NTA column (GE Healthcare Life Sciences) charged with Ni^{2+}. Protein was eluted from the column using a linear gradient in Ni-NTA column buffer and elution buffer (500 mM NaCl, 350 mM imidazole, 1mM PMSF, 20 mM $NaPO_4$, pH 7.0). Fusion protein containing fractions were pooled, and Tobacco Etch Virus nuclear-inclusion-a endopeptidase (TEV protease) was added to a final concentration of 0.2 mg/ml. After incubation at room temperature for 24 h, the solution was centrifuged at 55,000 g and 4 °C for 30 min. Precipitated IcpA in the pellet fraction was solubilized at room temperature for 25 min in Ni-NTA column buffer contain 50 mM sodium cholate and filtered through a 0.22 μm filtered cellulose acetate syringe filter. To remove any remaining MBP, the filtrate was loaded onto a 5 ml Ni-NTA column, and the IcpA-containing flow-through fractions were pooled, concentrated, dialyzed against 300 mM NaCl, 50 mM sodium cholate, 5 % glycerol, 40 mM Tris/HCl, pH 7.4, and stored at -80 °C.

Immunoblotting

Polyclonal antibodies raised against purified ligand-binding domains of McpT-McpX, and McpZ were purified as described here (77). Briefly, one mg of purified protein was separated on a 12.5

% acrylamide gel and transferred to a nitrocellulose membrane (Amersham Protran 0.45 NC, GE Healthcare). Proteins were stained on the membrane using 1 % Ponceau S and the protein containing membrane was cut into pieces (1 cm x 0.5 cm). Membrane pieces were then incubated 16 h at 4 °C with two ml of crude serum. The blots were washed three times with PBS/0.1 % bovine serum albumin (BSA), twice with PBS/0.1 % BSA/0.1 % Nonidet P40, and three times with PBS/0.1 % BSA for 5 min per wash step. The specific antibodies were eluted from the membrane by incubating with 750 µl of 0.2 M glycine/HCl, pH 2.5 for 1 min followed by neutralization with 375 µl of prechilled 1 M potassium phosphate, pH 9.0. The elution was repeated once and the combined eluates were dialyzed three times against PBS and stored at -80 °C.

Samples for immunoblots were prepared as follows. For whole cell extracts, one ml cell culture of RU11/001 at OD_{600} 0.250 ± 0.002 was pelleted and suspended in 15 µl of supernatant and 15 µl of Laemmli buffer (4.5 % SDS, 18.75 mM Tris/HCl pH 6.5, 43.5 % Glycerin, 0.0125 % Bromophenol Blue, and 5 % β-mercaptoethanol). Samples were then boiled at 100 °C for 10 min and stored at -30 °C. Control samples comprised cell extracts from appropriate deletion strains treated identically. Standard curves were made by adding defined quantities of protein to appropriate deletion strain lysates. Immunoblots were carried out as described here (87). Briefly, proteins from cell extracts were separated on 12.5 % acrylamide gels and then transferred to a 0.45 µm nitrocellulose membrane. The membrane was blocked overnight with 5 % non-fat dry milk solution made in PBS/0.1 % Tween 20. The blots were probed with 1:200 dilution of purified antibodies or 1:5,000 dilution of crude serum. Mouse monoclonal anti-GFP was used at 1:5,000 dilution to detect McpW-eGFP fusion protein. Blots were washed three times with PBS/0.1 % Tween 20 and then probed with 1:5,000 dilution of donkey anti-rabbit horseradish peroxidase-

linked whole antibody. The blots were washed three times with PBS/0.1 % Tween 20. Detection was performed by chemiluminescence (Amersham ECL Western Blotting Detection Kit or SuperSignal™ West Femto Maximum Sensitivity Substrate for McpY) using Hyperfilm ECL (GE Healthcare). Images were captured by using an Epson Perfection 1640SU scanner and intensities were quantified using ImageJ. Variations caused by improper blotting of proteins and manual error were minimized by only using those blots for quantification that had a standard curve with an R^2 value of > 0.95.

Protein concentrations were initially determined by the standard Bradford Assay using Quick Start™ Bradford 1x Dye Reagent (BIO-RAD) and a bovine serum albumin standard curve as per manufacturer's protocol. Amounts of proteins stated in the figure legends were calculated using this method. Accurate protein concentrations were obtained by quantitative amino acid analyses after total acid hydrolysis performed at the Protein Chemistry Lab, Texas A&M University.

Fluorescence microscopy

Motile cells were pelleted and suspended in 15 µl of PBS. Five microliters were placed on slide coated with poly-L-lysine, a cover slip was placed on top of the cell suspension droplet, and the edges were sealed with acrylic polymer to prevent drying. Images were taken with an Olympus IX71 microscope, using a 100× NA 1.4UPIanSApo objective lens equipped with a charge coupled-device camera (Photometrics CoolSNAP HQ2CCD) and processed using SoftWorx software (Applied Precision). Fluorescence images of eGFP (enhanced green fluorescent protein; excitation, 470 nm) were detected using a FITC (525 nm) filter. Images were analyzed with MicrobeTracker, a MATLAB (Mathworks) based software package (88).

Determination of dry weight

Dry weight was determined as previously described (50). Five 25-ml samples were harvested by centrifugation, resuspended in 77 mM ammonium acetate, pH 7.0, transferred to tared Sarstedt tubes, centrifuged, washed in the same buffer, and lyophilized for 3 days. Medium and buffer were prefiltered (0.2 μm). A value of 0.053 ± 0.008 mg/ml of culture (mean ± SD for five determinations) was obtained. The cytoplasmic volume/ mg dry weight as 1.4 μl was taken from Stock et al., 1977) (89).

RESULTS

The *mcp* genes are part of the flagellar regulon and transcribed as class III genes

Previously, we have shown that all genes in the flagellar gene cluster are organized in a four-class hierarchy (79, 87). The LuxR-type VisNR and the OmpR-like Rem act as class IA and IB transcriptional regulators, respectively. They control the expression of class II (comprising flagellar assembly and motility genes) and class III (comprising flagellin and chemotaxis genes), which requires class IIA for expression (79). FlbT is a class IIA positive flagellar regulator (90). While *icpA* is the first gene of the *che* operon and therefore classified as a class III gene, the regulation of the remaining seven chemoreceptor genes is unknown. With the exception of *mcpW*, which is co-transcribed with a putative *cheW*, all other *mcp* genes are monocistronic and scattered throughout the genome (62, 91). To answer whether expression of *mcp* genes follow the same control mechanisms, we transferred vectors with translational fusions of six of the *mcp* promotors and of the promoter of the *che* operon as control (62) to RU11/001 (WT), RU11/814 (Δ*visNR*), RU11/555 (Δ*rem*), and RU13/110 (Δ*flbT*), and assayed for ß-galactosidase activity as listed in Table 2.2. We found that all three genes were required for the transcription of chemoreceptor genes. Only two of the genes with weaker promoters, namely *mcpT* and *mcpY*, exhibited some residual transcriptional activity in Δ*visNR* and Δ*rem* and about 80% activity in Δ*flbT* compared to those measured in wild type. In conclusion, *mcp* genes are part of the flagellar regulon and positively regulated by its master transcriptional regulators with a certain degree of decoupling for *mcpT* and *mcpY*.

Quantification of transmembrane chemoreceptors

To quantify the six transmembrane chemoreceptors (McpT-X, and McpZ), we purified and raised polyclonal antibodies against the periplasmic ligand-binding region of each MCP. This way, we avoided generating antibodies targeting the highly conserved cytosolic domains and obviate cross reactivity with other chemoreceptors in the cell extracts. An important factor for attaining consistent results during quantitative immunoblot analysis is the choice of the appropriate growth phase for cell harvest. In *S. meliloti*, expression of flagellar and chemotaxis genes (including the *che* operon) are under a tight transcriptional control through the activity of a class IB regulator, Rem (79). Furthermore, it has been previously shown that chemoreceptors in *S. meliloti* follow the expression pattern of Rem and are maximally expressed at mid-exponential phase (92). Thus, an OD_{600} of 0.25 was selected for harvesting cells for immunoblots (62). Standard curves were established by adding varying amounts of the purified periplasmic regions of each MCP to cell extracts of corresponding deletion strains. Signals from immunoblots were detected using X-ray films with different exposures, and band intensities were determined with ImageJ.

A representative blot for McpV (65.34 kDa) showed a distinct band below the 75 kDa marker in lanes 2-4 containing wild-type cell extracts, which is markedly absent in lane 1 containing the *mcpV* deletion cell extract (Figure. 2.1A). McpV-LBD (20.23 kDa) which was used to create a standard curve can be seen below the 25 kDa marker in the lanes containing *mcpV* deletion cell extracts and purified McpV-LBD in decreasing amounts. A similar blot is seen for McpZ (90.15 kDa), with varying amounts of McpZ-LBD (45.97 kDa) added to extracts from the *mcp*Z deletion strain (Figure. 2.1B).

Purified McpU-LBD (27.66 kDa) and McpX-LBD (32.55 kDa) were used to quantify the corresponding proteins (McpU, 74.38 kDa and McpX, 83.73 kDa) in *S. meliloti* wild-type cell

extracts. Although the proteins were separated under denaturing conditions and a reducing agent was added to the loading buffer, both proteins existed in monomeric and dimeric forms (Figure. 2.1C & D). The McpU-LBD standard curve showed that the ratio of monomer to dimer was approximately 80:20. In contrast, McpX-LBD mainly existed as a dimer with the ratio of monomer to dimer being approximately 20:80. Thus, the intensities of both bands, monomer and dimer, were added for the quantification of McpU and McpX.

For immunoblots probed with anti-McpW antibodies, McpW-LBD (15.96 kDa) was used as a standard. We observed that the McpW (72.50 kDa) band in wild-type cell extracts overlapped with a cross-reacting band of similar size, as indicated in Figure. 2.1E. This produced a more intense band as marked by an asterisk compared to lane 4 containing the *mcpW* deletion strain extract. To confirm that the additional band intensity was caused by McpW, we loaded extracts of strain RU13/143 expressing McpW-eGFP from its native chromosomal locus in lane 1 and 3. McpW-eGFP (104.84 kDa) appeared above the 100 kDa marker band, and the band intensity of the 75-kDa band was decreased to that of the *mcpW* deletion strain (Figure. 2.1E, lane 4). Next, we subtracted the 75-kDa band appearing in the *mcpW* deletion strain extract from the 75-kDa band of the wild-type extract to quantify McpW. Additionally, we quantified the band intensity of McpW-eGFP. Both quantification methods yielded the same amount of McpW.

To quantify the number of MCP molecules per cell, we determined the number of *S. meliloti* cells in one ml of cell culture grown in minimal medium at OD_{600} 0.25. Using serial dilutions and spread plating, we determined that one ml cell culture of *S. meliloti* at OD_{600} 0.25 contained $2.56 \pm 0.31 \times 10^8$ cells. For the six transmembrane chemoreceptors, the numbers ranged from a few molecules to several hundred per cell (Table 2.3). However, we were unable to quantify McpT. Neither crude serum nor affinity-purified antibodies raised against McpT-LBD allowed detection of a band

corresponding to purified McpT-LBD or McpT in wild-type cell extracts. As an alternative strategy for quantifying McpT, extracts of a strain expressing McpT-eGFP from its native chromosomal locus (RU13/142) were probed using anti-eGFP antibodies. We were able to detect purified eGFP at amounts as low as 5 pg. No corresponding bands were detected in extracts of the McpT-eGFP strain. In conclusion, of the five transmembrane receptors quantified, McpV was the most abundant chemoreceptor, being present in more than six fold higher numbers compared to the next highest abundant receptor, McpU (Table 2.3). The other receptors followed the order: McpU > McpX > McpW > McpZ.

Quantification of cytosolic chemoreceptors

For the two cytosolic chemoreceptors, IcpA (57.54 kDa) and McpY (64.30 kDa), full length proteins were used to serve as controls for a standard curve, because antibodies raised against these proteins have been generated previously (62). While the IcpA antibodies had few cross-reactivities with other proteins in the cell lysates, the McpY antibody reacted non-specifically with a number of proteins in the lysates (Figure. 2.2 A & B). IcpA was present at levels comparable to McpW. The amounts of McpY were the lowest of any chemoreceptor that could be quantified (Table 2.3).

Quantification of CheA

To determine the stoichiometry of chemoreceptors to the kinase CheA and to compare our data with the *E. coli* and *B. subtilis* studies (72, 73), we quantified the cellular amounts of CheA. Purified full length CheA (81.12 kDa) and existing polyclonal antibodies were used for quantification (67). A typical blot (Figure. 2.2 C) exhibited a band above the 75 kDa marker in WT cell lysates, which was absent in the lane containing Δ*cheA* cell lysates. As before, a standard

curve was established by adding increasing amounts of the purified full-length CheA protein. CheA was found to be present in low abundance and at levels similar to McpW and IcpA (Table 3).

Fluorescence microscopy of eGFP expressing strains

The low amounts of chemoreceptor proteins detected in immunoblots raised the question whether only a sub-population of cells displayed expression. We chose four representative proteins to assess their expression in individual cells via C-terminal EGFP fusions (92), namely two transmembrane receptors (McpU and McpV), a cytosolic receptor (IcpA), and the autokinase CheA. We showed previously that all four fusion proteins localize to one or both cell poles (92). Cultures were grown as described for quantitative immunoblots, and cells from three biological replicates per strain were analyzed by fluorescence microscopy in conjunction with computerized image analysis to determine their fluorescent patterns (Table 2.4). For the four strains, between 24 and 45% of the cells displayed fluorescent foci predominantly at one cell pole. Representative images for each strain are depicted in Figure. 2.3. Thus, between one half to one quarter of cells in a population do not express the chemosensory cluster.

DISCUSSION

Chemotaxis is a complex process, which ultimately aids in the survival of bacteria in a rapidly changing environment. Since it consumes considerable amounts of the cell's energy, tight regulation of the expression of all components of the chemotaxis machinery is required (93). Our group has shown previously that motility and chemotaxis genes in the *S. meliloti* flagellar regulon are expressed in a transcriptional hierarchy (79). Our current studies expand the previously established scheme by including the *mcp* genes as class III genes and FlbT (class IIA) as a positive regulator for class III genes (with *mcpT* and *mcpY* as exceptions). Similar to the coordinated regulation in enterobacteria (94), class III gene expression is dependent on the completion of basal body structure and flagellar export. This suggests that a control mechanism comparable to the one operating in enterobacteria exists in *S. meliloti*. Expression of chemotaxis and motility genes is not only dependent on growth phase and temperature, but can also vary based on the richness of the medium. While enterobacteria are typically motile in rich media (95), *S. meliloti* exerts higher motility under nutrient-poor conditions (96). Furthermore, it remains to be seen whether expression of chemoreceptors is induced by their respective chemoeffector, as shown for certain C- and N-sources in *Pseudomonas putida (97).*

A number of different chemotaxis proteins have to interact to bring about the desired changes in motility. The cellular amounts of these proteins must be at the exact levels tuned for optimal performance. We set out to quantify the amounts of chemoreceptors and the histidine kinase CheA in an *S. meliloti* cell. The total molecule amount of all eight chemoreceptors in an *S. meliloti* cell is 423 ± 56 (Table 2.3). This is extremely low as compared to 59,960 ± 5,960 in *B. subtilis* and 26,000 ± 1,800 in *E. coli* (72, 73). From our viable cell counts and dry weight analyses, it is evident that an *S. meliloti* cell is about half the size of an *E. coli* cell (50). The smaller size may enable the

S. meliloti cell to function efficiently with a lower total amount of chemoreceptors. Additionally, not all cells expressed detectable quantities of eGFP fusion proteins under these culture conditions (Table 2.4). Therefore, it is possible that amounts for those cells expressing chemotaxis proteins is actually two to three times higher. However, this observation does not have an effect on the determined protein ratios.

In *E. coli*, the chemoreceptors are present in high (Tsr and Tar) and low (Trg, Tap, and Aer) abundance (54, 72). In *S. meliloti*, one chemoreceptor, McpV, is present at high levels, four in low amounts (McpU, McpW, McpX, and IcpA), and two in extremely low abundance (McpY and McpZ), and one was not detectable (McpT). The approximate ratios of receptors are 1 (McpY, McpZ) : 15 (McpU, McpW, McpX, IcpA) : 150 (McpV). The high abundance of McpV correlates with its CheA- and CheW-independent localization in *S. meliloti* (92). It can be hypothesized that the abundance of McpV enables its localization at the pole independently of other chemotaxis proteins and, in fact, that it may act as scaffold receptor to recruit other receptors to localize at the poles. Interestingly, when observing the localization of McpV-eGFP through cell division, new clusters are formed in midcell near the septum of the new daughter cells (98). A similar behavior has been described for *E. coli* chemoreceptors, which localize to future division sites (99). The function of McpV in sensing environmental cues is not known and subject of current investigations. However, we identified the low-abundance receptors McpU and McpX as general amino acid and quaternary ammonium compound sensors, respectively (63-65). In *B. subtilis*, the major receptors for taxis towards all amino acids and sugars, McpB and McpC, are also present in relatively low cellular abundance (73). This feature might be a commonplace in soil bacteria as it is not seen in *E. coli*, where the high abundance receptor Tsr mediates taxis toward serine, and Tar mediates taxis towards aspartate and maltose (54).

Finally, two of the three receptors that are present in very low numbers (McpT and McpY) appear to be regulated differently from the other receptors. Although their expression is partially dependent on VisNR and Rem, their transcription is not controlled by the class IIA regulator FlbT. Furthermore, we have preliminary data showing that both genes exhibit 30-40 % residual expression in alfalfa root nodules while all other chemoreceptors are not expressed (data not shown). Due to these differences, we speculate that McpT and McpY might play a role *in planta*, which could explain their extremely low expression levels under our assay conditions.

In *E. coli*, the presence of the carboxy-terminal pentapeptide, representing the CheR and CheB binding site, correlates with receptor abundance (100, 101). Despite the absence of this binding motif in low-abundance receptors of *E. coli*, receptor methylation and demethylation occur efficiently due to assistance by high-abundance receptors within chemoreceptor clusters (102). In *S. meliloti*, the highest abundant receptor, McpV, is lacking the motif. Instead, only McpT, McpW, McpX, and McpY, which are low or extremely-low abundance chemoreceptors possess the conserved carboxy-terminal pentapeptide (Figure. 2.4) (62). The adaptation process in *S. meliloti* has not been investigated, and the composition of chemoreceptor arrays is unknown. Therefore, the reason for the opposite correlation of receptor abundance and presence of the CheR/CheB binding motif remains to be elucidated.

The ratio of chemoreceptors to CheA in *S. meliloti* is approximately 23.5:1. This ratio is lower in *E. coli* (3.4:1) but is at the same level in *B. subtilis* (23:1) (72, 73). Presumably, this difference in chemoreceptor to CheA ratio reflects the more variable biotopes of soil bacteria (bulk soil versus rhizosphere) compared to gut bacteria. It remains to be investigated whether the structure of the CheA-CheW-receptor complex is different in *S. meliloti* from the one described for *E. coli* (103). Apparently, ratios of chemotaxis proteins across genera are adapted and optimized according to

their lifestyles. Our ongoing efforts to determine the amounts of cytosolic chemotaxis proteins would provide us with a snapshot of chemotaxis protein stoichiometry in *S. meliloti*. This in turn would shed more light on the various deviations of the *S. meliloti* chemosensory system from the enterobacterial paradigm, and their corresponding benefits to the different (free-living versus symbiotic) life styles of *S. meliloti*.

ACKNOWLEDGMENTS

This study was supported by grant Scha914/2-1/2 from the Deutsche Forschungsgemeinschaft and NSF grant MCB-1253234. We are indebted to Amanda Sebastian for performing the dry weight measurements, Jorge Escalante-Semerena for providing plasmid pKLD66, Jordan Mancl and Manisha Shrestha for providing TEV protease, Jinny Johnson for her help with the amino acid analyses, and members of the Scharf lab for critical reading of the manuscript.

Table 2.1 Bacterial strains and plasmids

Strains/Plasmids	Relevant Characteristics/Sequence	Reference or Source
Strain		
E. coli		
BL21(DE3)	F^- *ompT hsdS*$_B$(r_b^- m_b^-) *gal dcm* λ (DE3)	Novagen
ER2566	*lon ompT lacZ*::*T7*	NEBiolabs
S17-1	*recA endA thi hsdR* RP4-2 Tc::Mu::Tn7 Tp^r Sm^r	(82)
S. meliloti		
RU11/001	Sm^r, spontaneously streptomycin-resistant wild-type strain	(96)
RU11/310	Sm^r, Δ*cheA*	(80)
RU11/555	Sm^r, Δ*rem*	(79)
RU11/803	Sm^r, Δ*mcpW*	(62)
RU11/804	Sm^r, Δ*mcpY*	(62)
RU11/805	Sm^r, Δ*mcpX*	(62)
RU11/814	Sm^r, Δ*visNR*	(87)
RU11/815	Sm^r, Δ*icpA*	(62)
RU11/818	Sm^r, Δ*mcpZ*	(62)
RU11/828	Sm^r, Δ*mcpU*	(62)
RU11/830	Sm^r, Δ*mcpV*	(62)
RU11/838	Sm^r, Δ*mcpT*	(62)
RU13/142	Sm^r, *mcpT-egfp*	(92)
RU13/143	Sm^r, *mcpW-egfp*	(92)
RU13/243	Sm^r, *cheA-egfp*	(92)
RU13/301	Sm^r, *mcpU-egfp*	(92)
RU13/303	Sm^r, *icpA-egfp*	(92)
RU13/310	Sm^r, Δ*flbT*	This study
Plasmids		
pHT28	Ap^r, expression vector for *E. coli fliM*	(104)
pK18*mobsacB*	Km^r, *lacZ mob sacB*	(105)
pKLD66	Ap^r, expression vecto	(106)
pTYB1	Ap^r, expression vector	NEBiolabs
pTYB11	Ap^r, expression vector	NEBiolabs
pBS352	Ap^r, 858 bp *Nde*I/*Sap*I PCR fragment containing periplasmic domain of *mcpX* cloned into pTYB1	This study
pBS353	Ap^r, 741 bp *Nde*I/*Sap*I PCR fragment containing periplasmic domain of *mcpU* cloned into pTYB1	This study
pBS409	Ap^r, 474 bp *Sap*I/*Pst*I PCR fragment containing periplamic domain of *mcpV* cloned into pTYB11	This study

pBS426	Ap^r, 1218 bp *Sap*I/*Spe*I PCR fragment containing periplamic domain of *mcpZ* cloned into pTYB11	This study
pBS487	Ap^r, 1602 bp *Kpn*I/*Hin*dIII PCR fragment containing *icpA* cloned into pKLD66	This study
pBS1030	Ap^r, 444 bp *Nde*I/*Pst*I PCR fragment containing periplamic domain of *mcpT* cloned into pTYB1	This study
pBS1031	Ap^r, 423 bp *Nde*I/*Pst*I PCR fragment containing periplamic domain of *mcpW* cloned into pTYB1	This study
pRU2250	Tc^r, *icpA* (1974 bp)-*lacZ* (*che*) fusion cloned into pPHU236	(62)
pRU2782	Tc^r, *mcpT* (320 bp)-*lacZ* fusion cloned into pPHU235	(62)
pRU2783	Tc^r, *mcpU* (456 bp)-*lacZ* fusion cloned into pPHU236	(62)
pRU2784	Tc^r, *mcpW* (303 bp)-*lacZ* fusion cloned into pPHU236	(62)
pRU2787	Tc^r, *mcpZ* (409 bp)-*lacZ* fusion cloned into pPHU236	(62)
pRU2790	Ap^r, 1779 bp *Kpn*I/*Pst*I PCR fragment containing *mcpY* replacing *E. coli fliM* in pHT28	(62)
pRU2898	Tc^r, *mcpY* (786 bp)-*lacZ* fusion cloned into pPHU236	(62)
pRU2994	Tc^r, *mcpX* (590 bp)-*lacZ* fusion cloned into pPHU236	(62)

Table 2.2 *In vivo mcp* promoter activities in wild type (WT), Δ*visN/R*, Δ*rem*, and Δ*flbT* mutant strains

Plasmid [a] (*lacZ*-fusion)	β-galactosidase activity [b] (Miller units)			
	RU11/001[c] WT	RU11/814 Δ*visNR*	RU11/555 Δ*rem*	RU13/110 Δ*flbT*
pRU2728 (*mcpT*)	42	7	7	35
pRU2283 (*mcpU*)	235	0	0	4
pRU2784 (*mcpW*)	127	2	0	6
pRU2994 (*mcpX*)	417	0	0	6
pRU2898 (*mcpY*)	29	13	12	23
pRU2787 (*mcpZ*)	154	0	0	17
pRU2250 (*icpA* = *che*)	156	0	0	25

[a] Transcription from nine chemoreceptor promoters was assessed with plasmid-borne *lacZ* fusions in wild-type (RU11/001), Δ*visN/R* (RU11/814), Δ*rem* (RU11/555), and Δ*flbT* (RU13/110) during exponential growth. Cells diluted in RB were layered on Bromfield agar plates and grown to an OD_{600} of 0.15-0.25. The *che*-operon (*che*) is composed of the genes *icpA orf2 cheY1 cheA cheW cheR cheB cheY2 cheD orf10*.

[b] β-galactosidase activities (85) of three to five independent experiments were averaged. Standard deviations were between 0.5-6%.

[c] Values for wild type were taken from Meier *et al.* (2007; (62)).

Table 2.3 Cellular content of chemoreceptors and CheA chemotaxis protein contents in *S. meliloti* strain RU11/001

Protein	No. of molecules/cell [a]
McpT	B.D.L.
McpU	47 ± 6
McpV	299 ± 55
McpW	17 ± 4
McpX	39 ± 7
McpY	1 ± 1
McpZ	3 ± 1
IcpA	17 ± 6
Receptor total	423 ± 56
CheA	18 ± 5

[a] Mean ± standard deviation. Values were obtained from six independent immunoblots.
[b] B.D.L., below detection limit.

Table 2.4 Proportion of *S. meliloti* cells with fluorescent polar foci expressing eGFP fusions from native chromosomal gene loci

Strain	Protein fusion	% of cells with fluorescent polar foci [a]
RU13/212	McpV-eGFP	24 ± 4
RU13/243	CheA-eGFP	44 ± 5
RU13/301	McpU-eGFP	28 ± 3
RU13/303	IcpA-eGFP	42 ± 1

[a] Mean ± standard deviation. Values were obtained from 5000 to 6400 cells in three independent experiments. Wild-type cells had no detectable fluorescent signal.

REFERENCES

1. Porter SL, Wadhams GH, Armitage JP. 2011. Signal processing in complex chemotaxis pathways. Nature Reviews Microbiology 9:153-165.
2. Vladimirov N, Sourjik V. 2009. Chemotaxis: how bacteria use memory. Biological Chemistry 390:1097-1104.
3. Williams SM, Chen Y-T, Andermann TM, Carter JE, McGee DJ, Ottemann KM. 2007. Helicobacter pylori Chemotaxis Modulates Inflammation and Bacterium-Gastric Epithelium Interactions in Infected Mice. Infection and Immunity 75:3747-3757.
4. Miller LD, Yost CK, Hynes MF, Alexandre G. 2007. The major chemotaxis gene cluster of *Rhizobium leguminosarum* bv. viciae is essential for competitive nodulation. Molecular Microbiology 63:348-362.
5. Barnett MJ, Fisher RF, Jones T, Komp C, Abola AP, Barloy-Hubler F, Bowser L, Capela D, Galibert F, Gouzy J, Gurjal M, Hong A, Huizar L, Hyman RW, Kahn D, Kahn ML, Kalman S, Keating DH, Palm C, Peck MC, Surzycki R, Wells DH, Yeh K-C, Davis RW, Federspiel NA, Long SR. 2001. Nucleotide sequence and predicted functions of the entire *Sinorhizobium meliloti* pSymA megaplasmid. Proceedings of the National Academy of Sciences 98:9883-9888.
6. Finan TM, Weidner S, Wong K, Buhrmester J, Chain P, Vorhölter FJ, Hernandez-Lucas I, Becker A, Cowie A, Gouzy J, Golding B, Pühler A. 2001. The complete sequence of the 1,683-kb pSymB megaplasmid from the N2-fixing endosymbiont *Sinorhizobium meliloti*. Proceedings of the National Academy of Sciences of the United States of America 98:9889-9894.
7. Berg HC, Brown DA. 1972. Chemotaxis in *Escherichia coli* analysed by three-dimensional tracking. Nature 239:500-4.
8. Meier VM, Scharf BE. 2009. Cellular Localization of Predicted Transmembrane and Soluble Chemoreceptors in *Sinorhizobium meliloti*. Journal of Bacteriology 191:5724-5733.
9. Meier VM, Muschler P, Scharf BE. 2007. Functional analysis of nine putative chemoreceptor proteins in *Sinorhizobium meliloti*. J Bacteriol 189:1816-26.
10. Wadhams GH, Armitage JP. 2004. Making sense of it all: bacterial chemotaxis. Nature Reviews Molecular Cell Biology 5:1024-1037.
11. Wang H, Matsumura P. 1996. Characterization of the CheAS/CheZ complex: a specific interaction resulting in enhanced dephosphorylating activity on CheY-phosphate. Molecular Microbiology 19:695-703.
12. Nowlin DM, Bollinger J, Hazelbauer GL. 1987. Sites of covalent modification in Trg, a sensory transducer of *Escherichia coli*. Journal of Biological Chemistry 262:6039-6045.
13. Han X-S, Parkinson JS. 2014. An Unorthodox Sensory Adaptation Site in the Escherichia coli Serine Chemoreceptor. Journal of Bacteriology 196:641-649.
14. Hulko M, Berndt F, Gruber M, Linder JU, Truffault V, Schultz A, Martin J, Schultz JE, Lupas AN, Coles M. 2006. The HAMP Domain Structure Implies Helix Rotation in Transmembrane Signaling. Cell 126:929-940.
15. Stephens BB, Loar SN, Alexandre G. 2006. Role of CheB and CheR in the Complex Chemotactic and Aerotactic Pathway of *Azospirillum brasilense*. Journal of Bacteriology 188:4759-4768.

16. Spohn G, Scarlato V. 2001. Motility, Chemotaxis, and Flagella. *In* Mobley HL, Mendz GL, Hazell SL (ed), *Helicobacter pylori*: Physiology and Genetics. ASM Press, Washington (DC).
17. Glekas GD, Cates JR, Cohen TM, Rao CV, Ordal GW. 2011. Site-specific methylation in *Bacillus subtilis* chemotaxis: effect of covalent modifications to the chemotaxis receptor McpB. Microbiology 157:56-65.
18. Thoelke MS, Kirby JR, Ordal GW. 1989. Novel methyl transfer during chemotaxis in *Bacillus subtilis*. Biochemistry 28:5585-5589.
19. Kirsch ML, Peters PD, Hanlon DW, Kirby JR, Ordal GW. 1993. Chemotactic methylesterase promotes adaptation to high concentrations of attractant in *Bacillus subtilis*. Journal of Biological Chemistry 268:18610-6.
20. Kirsch ML, Zuberi AR, Henner D, Peters PD, Yazdi MA, Ordal GW. 1993. Chemotactic methyltransferase promotes adaptation to repellents in *Bacillus subtilis*. Journal of Biological Chemistry 268:25350-6.
21. Wuichet K, Zhulin IB. 2010. Origins and Diversification of a Complex Signal Transduction System in Prokaryotes. Science Signaling 3:ra50-ra50.
22. Glekas GD, Plutz MJ, Walukiewicz HE, Allen GM, Rao CV, Ordal GW. 2012. Elucidation of the multiple roles of CheD in *Bacillus subtilis* chemotaxis. Mol Microbiol 86:743-56.
23. Rao CV, Glekas GD, Ordal GW. 2008. The three adaptation systems of *Bacillus subtilis* chemotaxis. Trends in microbiology 16:480-487.
24. Walukiewicz HE, Tohidifar P, Ordal GW, Rao CV. 2014. Interactions among the three adaptation systems of *Bacillus subtilis* chemotaxis as revealed by an in vitro receptor-kinase assay. Mol Microbiol 93:1104-18.
25. Sourjik V, Schmitt R. 1998. Phosphotransfer between CheA, CheY1, and CheY2 in the Chemotaxis Signal Transduction Chain of *Rhizobium meliloti*. Biochemistry 37:2327-2335.
26. Dogra G, Purschke FG, Wagner V, Haslbeck M, Kriehuber T, Hughes JG, Van Tassell ML, Gilbert C, Niemeyer M, Ray WK, Helm RF, Scharf BE. 2012. *Sinorhizobium meliloti* CheA Complexed with CheS Exhibits Enhanced Binding to CheY1, Resulting in Accelerated CheY1 Dephosphorylation. Journal of Bacteriology 194:1075-1087.
27. Scharf B. 2002. Real-time imaging of fluorescent flagellar filaments of R*hizobium lupini* H13-3: flagellar rotation and pH-induced polymorphic transitions. J Bacteriol 184:5979-86.
28. Rosser G, Baker RE, Armitage JP, Fletcher AG. 2014. Modelling and analysis of bacterial tracks suggest an active reorientation mechanism in *Rhodobacter sphaeroides*, vol 11.
29. Poggio S, Abreu-Goodger C, Fabela S, Osorio A, Dreyfus G, Vinuesa P, Camarena L. 2007. A complete set of flagellar genes acquired by horizontal transfer coexists with the endogenous flagellar system in *Rhodobacter sphaeroides*. J Bacteriol 189:3208-16.
30. Hauwaerts D, Alexandre G, Das SK, Vanderleyden J, Zhulin IB. 2002. A major chemotaxis gene cluster in *Azospirillum brasilense* and relationships between chemotaxis operons in α-proteobacteria. FEMS Microbiology Letters 208:61-67.
31. Sourjik V, Sterr W, Platzer J, Bos I, Haslbeck M, Schmitt R. 1998. Mapping of 41 chemotaxis, flagellar and motility genes to a single region of the *Sinorhizobium meliloti* chromosome1. Gene 223:283-290.

32. Rotter C, Muhlbacher S, Salamon D, Schmitt R, Scharf B. 2006. Rem, a new transcriptional activator of motility and chemotaxis in *Sinorhizobium meliloti*. J Bacteriol 188:6932-42.
33. Scharf B. 2002. Real-time imaging of fluorescent flagellar filaments of *Rhizobium lupini* H13-3: flagellar rotation and pH-induced polymorphic transitions. J Bacteriol 184:5979-5986.
34. Bren A, Eisenbach M. 2000. How signals are heard during bacterial chemotaxis: protein-protein interactions in sensory signal propagation. J Bacteriol 182:6865-6873.
35. Porter SL, Wadhams GH, Armitage JP. 2011. Signal processing in complex chemotaxis pathways. Nat Rev Microbiol 9:153-65.
36. Wadhams GH, Armitage JP. 2004. Making sense of it all: bacterial chemotaxis. Nat Rev Mol Cell Biol 5:1024-37.
37. Duan Q, Zhou M, Zhu L, Zhu G. 2013. Flagella and bacterial pathogenicity. J Basic Microbiol 53:1-8.
38. Pratt LA, Kolter R. 1998. Genetic analysis of *Escherichia coli* biofilm formation: roles of flagella, motility, chemotaxis and type I pili. Mol Microbiol 30:285-93.
39. Berg HC. 2000. Constraints on models for the flagellar rotary motor. Phil Trans R Soc Lond 355:491-501.
40. Armitage JP, Macnab RM. 1987. Unidirectional, intermittent rotation of the flagellum of *Rhodobacter sphaeroides*. J Bacteriol 169:514-518.
41. Platzer J, Sterr W, Hausmann M, Schmitt R. 1997. Three genes of a motility operon and their role in flagellar rotary speed variation in *Rhizobium meliloti*. J Bacteriol 179:6391-6399.
42. Scharf B, Schmitt R. 2002. Sensory transduction to the flagellar motor of *Sinorhizobium meliloti*. J Mol Microbiol Biotechnol 4:183-186.
43. Attmannspacher U, Scharf B, Schmitt R. 2005. Control of speed modulation (chemokinesis) in the unidirectional rotary motor of *Sinorhizobium meliloti*. Mol Microbiol 56:708-718.
44. Pasupuleti S, Sule N, Cohn WB, MacKenzie DS, Jayaraman A, Manson MD. 2014. Chemotaxis of *Escherichia coli* to norepinephrine (NE) requires conversion of NE to 3,4-dihydroxymandelic acid. J Bacteriol 196:3992-4000.
45. Parkinson JS. 2003. Bacterial chemotaxis: a new player in response regulator dephosphorylation. J Bacteriol 185:1492-1494.
46. Falke JJ, Hazelbauer GL. 2001. Transmembrane signaling in bacterial chemoreceptors. Trends Biochem Sci 26:257-265.
47. Szurmant H, Ordal GW. 2004. Diversity in chemotaxis mechanisms among the bacteria and archaea. Microbiol Mol Biol Rev 68:301-319.
48. Hazelbauer GL, Falke JJ, Parkinson JS. 2008. Bacterial chemoreceptors: high-performance signaling in networked arrays. Trends Biochem Sci 33:9-19.
49. Bren A, Eisenbach M. 1998. The N terminus of the flagellar switch protein, FliM, is the binding domain for the chemotactic response regulator, CheY. J Mol Biol 278:507-14.
50. Scharf BE, Fahrner KA, Turner L, Berg HC. 1998. Control of direction of flagellar rotation in bacterial chemotaxis. Proc Natl Acad Sci U S A 95:201-206.
51. Scharf BE, Fahrner KA, Berg HC. 1998. CheZ has no effect on flagellar motors activated by CheY13DK106YW. J Bacteriol 180:5123-5128.

52. Blat Y, Eisenbach M. 1994. Phosphorylation-dependent binding of the chemotaxis signal molecule CheY to its phosphatase, CheZ. Biochemistry 33:902-906.
53. McEvoy MM, Bren A, Eisenbach M, Dahlquist FW. 1999. Identification of the binding interfaces on CheY for two of its targets, the phosphatase CheZ and the flagellar switch protein FliM. J Mol Biol 289:1423-33.
54. Feng X, Baumgartner JW, Hazelbauer GL. 1997. High- and low-abundance chemoreceptors in *Escherichia coli*: differential activities associated with closely related cytoplasmic domains. J Bacteriol 179:6714-6720.
55. Djordjevic S, Goudreau PN, Xu Q, Stock AM, West AH. 1998. Structural basis for methylesterase CheB regulation by a phosphorylation-activated domain. Proc Natl Acad Sci USA 95:1381-1386.
56. Anand GS, Goudreau PN, Stock AM. 1998. Activation of methylesterase CheB: evidence of a dual role for the regulatory domain. Biochemistry 37:14038-47.
57. Caetano-Anolles G, Wall LG, De Micheli AT, Macchi EM, Bauer WD, Favelukes G. 1988. Role of motility and chemotaxis in efficiency of nodulation by *Rhizobium meliloti*. Plant Physiol 86:1228-35.
58. Miller LD, Yost CK, Hynes MF, Alexandre G. 2007. The major chemotaxis gene cluster of *Rhizobium leguminosarum* bv. *viciae* is essential for competitive nodulation. Mol Microbiol 63:348-62.
59. Gulash M, Ames P, Larosiliere RC, Bergman K. 1984. Rhizobia are attracted to localized sites on legume roots. Appl Environ Microbiol 48:149-152.
60. Scharf BE, Hynes MF, Alexandre GM. 2016. Chemotaxis signaling systems in model beneficial plant-bacteria associations. Plant Mol Biol doi:10.1007/s11103-016-0432-4.
61. Schmitt R. 2002. Sinorhizobial chemotaxis: a departure from the enterobacterial paradigm. Microbiology 148:627-631.
62. Meier VM, Muschler P, Scharf BE. 2007. Functional analysis of nine putative chemoreceptor proteins in *Sinorhizobium meliloti*. J Bacteriol 189:1816-1826.
63. Webb BA, Compton KK, Castaneda Saldana R, Arapov T, Ray WK, Helm RF, Scharf BE. 2017. *Sinorhizobium meliloti* chemotaxis to quaternary ammonium compounds is mediated by the chemoreceptor McpX. Mol Microbiol 103:333-346.
64. Webb BA, Helm RF, Scharf BE. 2016. Contribution of individual chemoreceptors to *Sinorhizobium meliloti* chemotaxist towards amino acids of host and nonhost seed exudates. Mol Plant Microbe Interact 29:231-239.
65. Webb BA, Hildreth S, Helm RF, Scharf BE. 2014. *Sinorhizobium meliloti* chemoreceptor McpU mediates chemotaxis toward host plant exudates through direct proline sensing. Appl Environ Microbiol 80:3404-15.
66. Webb BA, Compton KK, Del Campo JSM, Taylor D, Sobrado P, Scharf BE. 2017. *Sinorhizobium meliloti* chemotaxis to multiple amino acids is mediated by the chemoreceptor McpU. Mol Plant Microbe Interact 30:770-777.
67. Sourjik V, Schmitt R. 1998. Phosphotransfer between CheA, CheY1, and CheY2 in the chemotaxis signal transduction chain of *Rhizobium meliloti*. Biochemistry 37:2327-2335.
68. Sourjik V, Sterr W, Platzer J, Bos I, Haslbeck M, Schmitt R. 1998. Mapping of 41 chemotaxis, flagellar and motility genes to a single region of the *Sinorhizobium meliloti* chromosome. Gene 223:283-290.

69. Glekas GD, Mulhern BJ, Kroc A, Duelfer KA, Lei V, Rao CV, Ordal GW. 2012. The *Bacillus subtilis* chemoreceptor McpC senses multiple ligands using two discrete mechanisms. J Biol Chem 287:39412-8.
70. Dogra G, Purschke FG, Wagner V, Haslbeck M, Kriehuber T, Hughes JG, Van Tassell ML, Gilbert C, Niemeyer M, Ray WK, Helm RF, Scharf BE. 2012. *Sinorhizobium meliloti* CheA complexed with CheS exhibits enhanced binding to CheY1, resulting in accelerated CheY1 dephosphorylation. J Bacteriol 194:1075-87.
71. Amin M, Kothamachu VB, Feliu E, Scharf BE, Porter SL, Soyer OS. 2014. Phosphate sink containing two-component signaling systems as tunable threshold devices. PLoS Comput Biol 10:e1003890.
72. Li M, Hazelbauer GL. 2004. Cellular stoichiometry of the components of the chemotaxis signaling complex. J Bacteriol 186:3687-3694.
73. Cannistraro VJ, Glekas GD, Rao CV, Ordal GW. 2011. Cellular stoichiometry of the chemotaxis proteins in *Bacillus subtilis*. J Bacteriol 193:3220-7.
74. Levin MD, Morton-Firth CJ, Abouhamad WN, Bourret RB, Bray D. 1998. Origins of individual swimming behavior in bacteria. Biophys J 74:175-81.
75. Krupski G, Götz R, Ober K, Pleier E, Schmitt R. 1985. Structure of complex flagellar filaments in *Rhizobium meliloti*. J Bacteriol 162:361-366.
76. Bertani G. 1951. Studies on lysogenesis. I. The mode of phage liberation by lysogenic *Escherichia coli*. J Bacteriol 62:293-300.
77. Scharf B, Schuster-Wolff-Bühring H, Rachel R, Schmitt R. 2001. Mutational analysis of *Rhizobium lupini* H13-3 and *Sinorhizobium meliloti* flagellin genes: importance of flagellin A for flagellar filament structure and transcriptional regulation. J Bacteriol 183:5334-5342.
78. Götz R, Limmer N, Ober K, Schmitt R. 1982. Motility and chemotaxis in two strains of *Rhizobium* with complex flagella. J Gen Microbiol 128:789-798.
79. Rotter C, Mühlbacher S, Salamon D, Schmitt R, Scharf B. 2006. Rem, a new transcriptional activator of motility and chemotaxis in *Sinorhizobium meliloti*. J Bacteriol 188:6932-6942.
80. Sourjik V, Schmitt R. 1996. Different roles of CheY1 and CheY2 in the chemotaxis of *Rhizobium meliloti*. Mol Microbiol 22:427-436.
81. Higuchi R. 1989. Using PCR to engineer DNA, p 61-70. *In* Erlich HA (ed), PCR technology Principles and applications for DNA amplification. Stockton Press, New York.
82. Simon R, O'Connell M, Labes M, Pühler A. 1986. Plasmid vectors for the genetic analysis and manipulation of rhizobia and other gram-negative bacteria. Methods Enzymol 118:640-659.
83. Simon R, Priefer U, Pühler A. 1983. A broad host range mobilisation system for *in vivo* genetic engineering: Transposon mutagenesis in gram negative bacteria. Bio/Technology 1:783-791.
84. Labes M, Pühler A, Simon R. 1990. A new family of RSF1010-derived expression and lac-fusion broad-host- range vectors for gram-negative bacteria. Gene 89:37-46.
85. Miller JH. 1972. Experiments in molecular genetics. Cold Spring Harbor Laboratory Press, Cold Spring Harbor.

86. Riepl H, Maurer T, Kalbitzer HR, Meier VM, Haslbeck M, Schmitt R, Scharf B. 2008. Interaction of CheY2 and CheY2-P with the cognate CheA kinase in the chemosensory-signalling chain of *Sinorhizobium meliloti*. Mol Microbiol 69:1373-84.
87. Sourjik V, Muschler P, Scharf B, Schmitt R. 2000. VisN and VisR are global regulators of chemotaxis, flagellar, and motility genes in *Sinorhizobium (Rhizobium) meliloti*. J Bacteriol 182:782-788.
88. Sliusarenko O, Heinritz J, Emonet T, Jacobs-Wagner C. 2011. High-throughput, subpixel precision analysis of bacterial morphogenesis and intracellular spatio-temporal dynamics. Mol Microbiol 80:612-27.
89. Stock JB, Rauch B, Roseman S. 1977. Periplasmic space in *Salmonella typhimurium* and *Escherichia coli*. J Biol Chem 252:7850-61.
90. Hoang HH, Gurich N, González JE. 2008. Regulation of motility by the ExpR/Sin quorum-sensing system in *Sinorhizobium meliloti*. J Bacteriol 190:861-71.
91. Galibert F, Finan TM, Long SR, Pühler A, Abola P, Ampe F, Barloy-Hubler F, Barnett MJ, Becker A, Boistard P, Bothe G, Boutry M, Bowser L, Buhrmester J, Cadieu E, Capela D, Chain P, Cowie A, Davis RW, Dreano S, Federspiel NA, Fisher RF, Gloux S, Godrie T, Goffeau A, Golding B, Gouzy J, Gurjal M, Hernandez-Lucas I, Hong A, Huizar L, Hyman RW, Jones T, Kahn D, Kahn ML, Kalman S, Keating DH, Kiss E, Komp C, Lelaure V, Masuy D, Palm C, Peck MC, Pohl TM, Portetelle D, Purnelle B, Ramsperger U, Surzycki R, Thebault P, Vandenbol M, et al. 2001. The composite genome of the legume symbiont *Sinorhizobium meliloti*. Science 293:668-672.
92. Meier VM, Scharf BE. 2009. Cellular localization of predicted transmembrane and soluble chemoreceptors in *Sinorhizobium meliloti*. J Bacteriol 191:5724-33.
93. Soutourina O, Bertin PN. 2003. Regulation cascade of flagellar expression in Gram-negative bacteria. FEMS Microbiol Rev 27:505-523.
94. Aldridge P, Hughes KT. 2002. Regulation of flagellar assembly. Curr Opin Microbiol 5:160-165.
95. Adler J, Templeton B. 1967. The effect of environmental conditions on the motility of *Escherichia coli*. J Gen Microbiol 46:175-84.
96. Pleier E, Schmitt R. 1991. Expression of two *Rhizobium meliloti* flagellin genes and their contribution to the complex filament structure. J Bacteriol 173:2077-2085.
97. Lopez-Farfan D, Reyes-Darias JA, Krell T. 2017. The expression of many chemoreceptor genes depends on the cognate chemoeffector as well as on the growth medium and phase. Curr Genet 63:457-470.
98. Meier VM. 2007. Funktionsanalyse und zellulaere Lokalisierung der neun Chemorezeptoren von *Sinorhizobium meliloti*. PhD thesis, University of Regensburg, Germany.
99. Thiem S, Kentner D, Sourjik V. 2007. Positioning of chemosensory clusters in *E. coli* and its relation to cell division. EMBO J 26:1615-23.
100. Wu J, Li J, Li G, Long DG, Weis RM. 1996. The receptor binding site for the methyltransferase of bacterial chemotaxis is distinct from the sites of methylation. Biochemistry 35:4984-4993.
101. Barnakov AN, Barnakova LA, Hazelbauer GL. 1999. Efficient adaptational demethylation of chemoreceptors requires the same enzyme-docking site as efficient methylation. Proc Natl Acad Sci U S A 96:10667-10672.

102. Li M, Hazelbauer GL. 2005. Adaptational assistance in clusters of bacterial chemoreceptors. Mol Microbiol 56:1617-1626.
103. Gegner JA, Graham DR, Roth AF, Dahlquist FW. 1992. Assembly of an MCP receptor, CheW, and kinase CheA complex in the bacterial chemotaxis signal transduction pathway. Cell 70:975-982.
104. Kovach ME, Elzer PH, Hill DS, Robertson GT, Farris MA, Roop RM, 2nd, Peterson KM. 1995. Four new derivatives of the broad-host-range cloning vector pBBR1MCS, carrying different antibiotic-resistance cassettes. Gene 166:175-176.
105. Schäfer A, Tauch A, Jager W, Kalinowski J, Thierbach G, Pühler A. 1994. Small mobilizable multi-purpose cloning vectors derived from the *Escherichia coli* plasmids pK18 and pK19: selection of defined deletions in the chromosome of *Corynebacterium glutamicum*. Gene 145:69-73.
106. Rocco CJ, Dennison KL, Klenchin VA, Rayment I, Escalante-Semerena JC. 2008. Construction and use of new cloning vectors for the rapid isolation of recombinant proteins from *Escherichia coli*. Plasmid 59:231-7.

FIGURES

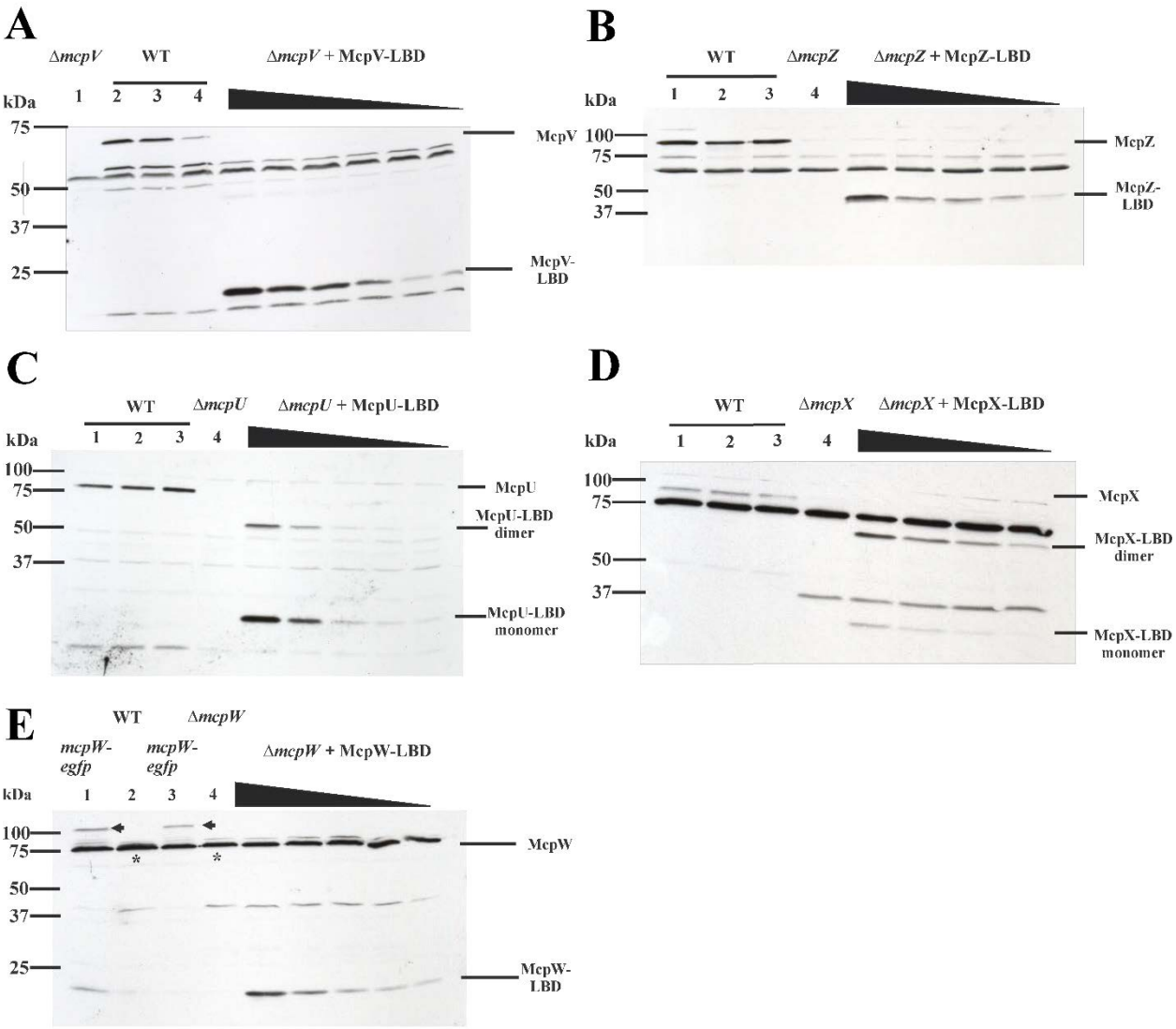

Figure 2.1 Representative immunoblot used to quantify transmembrane chemoreceptors. **A.** McpV; lane 1 (Δ*mcpV*) contains RU11/830 (*mcpV* deletion strain) cell lysate from 1 ml culture at OD_{600} 0.25. Lanes 2 - 4 contain RU11/001 (WT) cell lysates from 1 ml of culture at OD_{600} 0.25. Δ*mcpV* + McpV-LBD lanes contain purified McpV-LBD (7.5, 5.0, 4.0, 3.0, 2.0, and 1.0 ng) mixed with RU11/830 cell lysates.Representative immunoblots used to quantify transmembrane chemoreceptors. **B.** McpZ; lanes 1 - 3 contain RU11/001 (WT) cell lysates from 1 ml of culture at OD_{600} 0.25. Lane 4 (Δ*mcpZ*) contains RU11/818 (*mcpZ* deletion strain) cell lysate from 1 ml

culture at OD_{600} 0.25. Δ*mcpZ* + McpZ-LBD lanes contain purified McpZ-LBD (2.6, 1.3, 0.78, 0.52, and 0.26 ng) mixed with RU11/830 cell lysates. **C.** McpU; lanes 1 - 3 contain RU11/001 (WT) cell lysates from 1 ml of culture at OD_{600} 0.25. Lane 4 (Δ*mcpU*) contains RU11/828 (*mcpU* deletion strain) cell lysate from 1 ml culture at OD_{600} 0.25. Δ*mcpU* + McpU-LBD lanes contain purified McpU-LBD (2.0, 1.0, 0.5, 0.1, and 0.05 ng) mixed with RU11/828 cell lysates. McpU-LBD exists in a monomeric and dimeric form, as indicated. **D.** McpX; lanes 1 - 3 contain RU11/001 (WT) cell lysates from 1 ml of culture at OD_{600} 0.25. Lane 4 (Δ*mcpX*) contains RU11/805 (*mcpX* deletion strain) cell lysate from 1 ml culture at OD_{600} 0.25. Δ*mcpX* + McpX-LBD lanes contain purified McpX-LBD (1.0, 0.75, 0.5, and 0.25 ng) mixed with RU11/805 cell lysates. McpX-LBD exists in a monomeric and dimeric form, as indicated. **E.** McpW; lanes 1 and 3 contain RU13/143 (*mcpW-egfp*) cell lysates from 1 ml of culture at OD_{600} 0.25. Lane 2 contains RU11/001(WT) cell lysates from 1 ml of culture at OD_{600} 0.25. Lane 4 (Δ*mcpW*) contains RU11/803 (*mcpW* deletion strain) cell lysate from 1 ml culture at OD_{600} 0.25. Δ*mcpW* + McpW-LBD lanes contain purified McpW-LBD (0.5, 0.25, 0.1, 0.075, and 0.05 ng) mixed with RU11/803 cell lysates. The intensity of the McpW-GFP band in lanes 1 and 3 (arrows) is equal to the difference in intensities between the band in lane 2 (asterisk) and its corresponding non-specific band in lane 4.

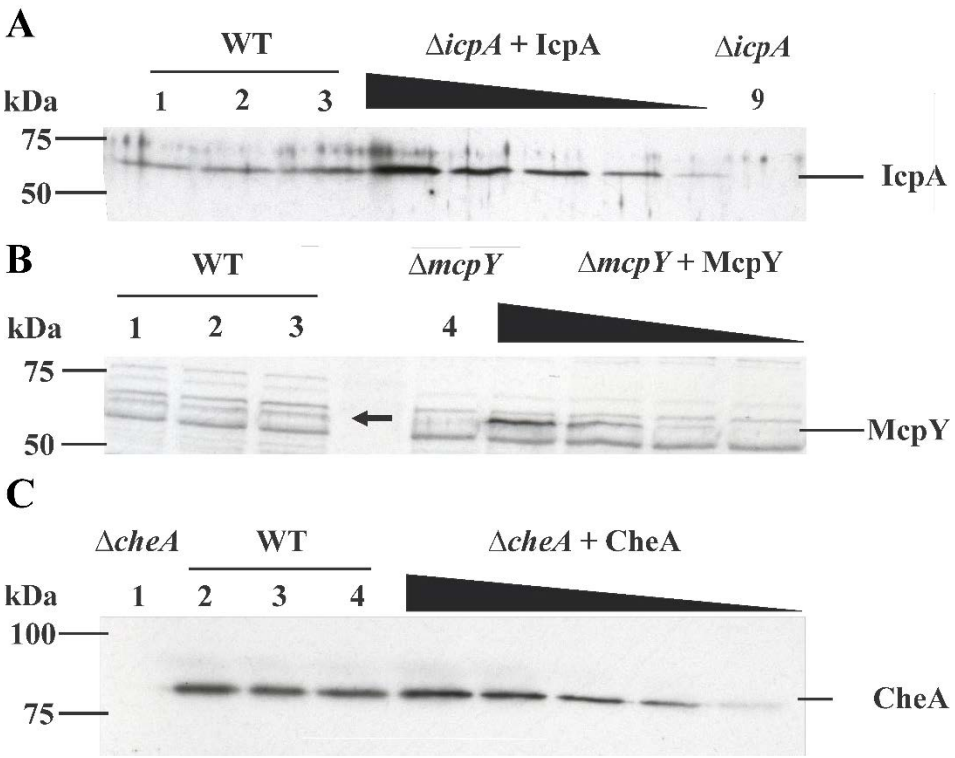

Figure 2.2 Representative immunoblot used to quantify cytosolic receptors and CheA. **A.** McpY; lanes 1 - 3 contain RU11/001 (WT) cell lysates from 1 ml of culture at OD_{600} 0.25. Lane 4 (Δ*mcpY*) contains RU11/804 (*mcpY* deletion strain) cell lysate from 1 ml culture at OD_{600} 0.25. Δ*mcpY* + McpY lanes contain purified McpY (0.1, 0.05, 0.01, and 0.005 ng) mixed with RU11/804 cell lysates. Arrow indicates the McpY protein in the WT cell lysates. **B.** IcpA; lanes 1 - 3 contain RU11/001 (WT) cell lysates from 1 ml of culture at OD_{600} 0.25. Lane 9 (Δ*icpA*) contains RU11/815 (*icpA* deletion) cell lysate from 1 ml culture at OD_{600} 0.25. Δ*icpA* + IcpA lanes contain purified IcpA (1.28, 0.96, 0.64, 0.32, 0.16 ng) mixed with RU11/815 cell lysates. **C.** CheA; lane 1 (Δ*cheA*) contains RU11/310 (*cheA* deletion strain) cell lysate from 1 ml culture at OD_{600} 0.25. Lanes 2 - 4 contain RU11/001 (WT) cell lysates from 1 ml of culture at OD_{600} 0.25. Δ*cheA* + CheA lanes contain purified CheA (1.0, 0.8, 0.6, 0.4, and 0.2 ng) mixed with RU11/310 cell lysates.

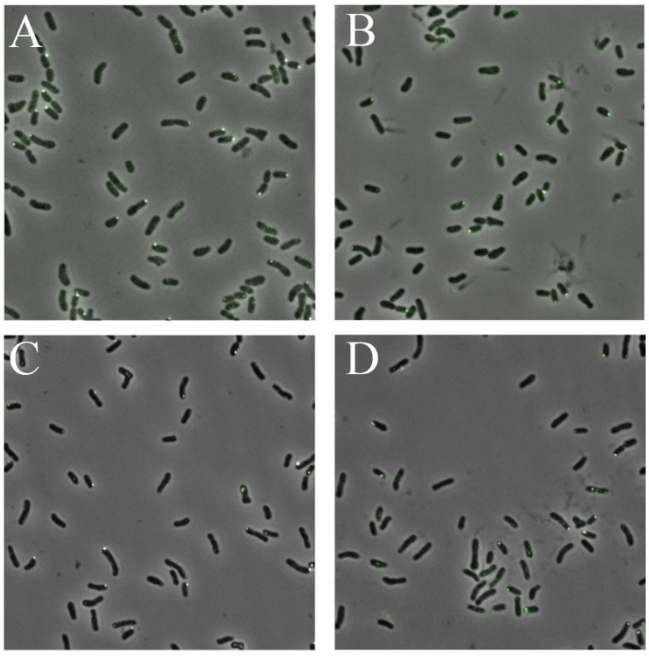

Figure 2.3 Localization of McpU, McpV, IcpA, and CheA fused to e-GFP in *S. meliloti* cells by fluorescence microscopy . **A.** McpU-eGFP; **B**. McpV-eGFP; **C**. IcpA-eGFP; **D**. CheA-eGFP.

Chemoreceptor	Carboxy-terminal sequence	Length of protein (aa)
E.c. Tar	P R L R I A E Q D P **N W E T F**	553
E.c. Tsr	R K M A V A D S E E **N W E T F**	551
S.m. McpT	G N G S A A V A R D **D W E E F**	665
S.m. McpU	T Q A A S Y Q A T S R R R A A	707
S.m. McpV	R L E E R G A Q P A Y G R A A	604
S.m. McpW	S T P S V T A S G E **N W E E F**	689
S.m. McpX	T S G A N A L A Q D **N W E E F**	788
S.m. McpY	S N L A L A P A A D **D W E N F**	593
S.m. McpZ	R L E P V A A A D H S Y R A A	841
S.m. IcpA	F G E V T S E R H L A G W R R	533

Figure 2.4 Sequence comparison of the 15 C-terminal amino acid residues in the NWETF-motif containing *E. coli* (E.c.) receptors Tar and Tsr and all eight *S. meliloti* (S.m.) chemoreceptors. The conserved pentapeptide sequence is marked in grey.

Chapter 3 Cellular stoichiometry of chemotaxis proteins in *Sinorhizobium meliloti*

TIMOFEY D. ARAPOV[1], RAFAEL CASTAÑEDA SALDAÑA[1a], AMANDA L. SEBASTIAN[1, b], W. KEITH RAY[2], RICHARD F. HELM[2], AND BIRGIT E. SCHARF[1]

[1]Department of Biological Sciences, Life Sciences I, Virginia Tech, Blacksburg, VA 24061, USA

[2]Department of Biochemistry, Virginia Tech, Steger Hall, Blacksburg, VA 24061, USA

Running title: *Sinorhizobium meliloti* chemotaxis protein stoichiometry

Key words: chemoreceptor methylation, flagellar motility, plant symbiont, rhizosphere, two-component system

*For correspondence:

E-mail bscharf@vt.edu

Tel (+1) 540 231 0757

Fax (+) 540 231 4043

Biological Sciences, Life Sciences I

Virginia Tech

Blacksburg, VA 24061, USA

[a]Present address: Department of Biology, Concord University, Vermillion Street, Athens, WV 24712; rcastaneda@concord.edu

[b]Present address: College of Veterinary Medicine, University of Florida, 2015 SW 16th Avenue, Gainesville, FL 32610; a.sebastian@ufl.edu

Attribution: TDA generated portions of Figure 3.1 pertaining to CheD, CheW1, CheY1 and purification of proteins required for quantification of CheY2 and CheT. RCS contributed to work shown in Figure 3.1 pertaining to CheB, CheR, CheY2, CheT and CheW2. WKR and RFH contributed to mass spectrometry quantification of CheS. Figure 3.2, Figure 3.3 and Figure 3.4 were generated by TDA. Data in Figure 3.4 were generated by ALS. Final manuscript was drafted by TDA, BES and WKR.

ABSTRACT

Chemotaxis systems enable microbes to sense their immediate environment and react by moving towards beneficial and away from harmful stimuli. *Sinorhizobium meliloti*, a symbiont of the legume alfalfa, possesses a chemotaxis system that exhibits deviations from the established paradigms. The cellular stoichiometries of all ten chemotaxis proteins in *S. meliloti* were determined by quantitative immunoblot analysis or mass spectrometry to gain a clear comparison to other characterized systems. Protein stoichiometries in the chemotaxis system of *S. meliloti* varied greatly from those in *E. coli* and *B. subtilis*. When compared to the central kinase CheA, all other proteins exhibited increased ratios to varying degrees. The ten-fold molar ratio of the adaptor proteins CheW1 and CheW2 to CheA might result in the formation of rings in the chemotaxis array that only consist of CheW instead of CheA and CheW in a 1:1 ratio. The higher ratio of CheA to the main response regulator CheY2 correlates with the presence of a speed-variable motor in *S. meliloti*, instead of a switch-type motor in *E. coli* and *B. subtilis*. Similarly, proteins involved in signal termination are far more abundant in *S. meliloti*, which utilizes a protein-interaction based phosphate-sink mechanism to inactivate the motor response regulator versus enzyme-catalyzed dephosphorylation as in *E. coli* and *B. subtilis*. Finally, CheB and CheR, which regulate chemoreceptor methylation and adaptation, were more highly abundant compared to CheA, indicative of variations in the adaptation system of *S. meliloti*. Collectively, these results mark significant differences in the composition of bacterial chemotaxis systems.

INTRODUCTION

Chemotaxis enables motile bacteria to perceive their immediate surroundings, which allows them to swim towards attractants or away from repellents (1-3). This ability to recognize chemical signals and react with an immediate physically response presents an evolutionary advantage (4). Chemotaxis aids in establishing several types of bacterial lifestyles including biofilm formation, symbiosis, and pathogenicity (5, 6). The enteric model organism *Escherichia coli* has been widely studied and has provided the foundational knowledge of bacterial chemotaxis mechanisms (3, 7). *E. coli* swims in a series of runs and tumbles (8, 9). In the course of a run, the peritrichous flagella rotate counter-clockwise (CCW) and synchronize into a flagellar bundle propelling the cell forward. Conversely, in a tumble, one or more of the flagella reverse the rotation to a clockwise (CW) direction, causing the flagellar bundle to splay apart, which allows reorientation of the cell in a new direction (10, 11). The amount of time spent in each swimming mode ultimately results in a biased random walk allowing a bacterial cell to swim away from repellents and towards attractants (12-14). Studies of the motility behavior in other flagellated bacterial species showed a variety of strategies leading to the biased random walk, influenced by variations in flagellar rotational speed and direction of rotation. In *Sinorhizobium meliloti*, the flagella rotate only CW but can vary their rotational speed. A tumble is achieved by the slowing down of one or more flagella, which perturbs the flagellar bundle and ultimately leads to a tumble (15-18). *Rhodobacter sphaeroides* initiates a tumble by pausing the rotation of its single, CW-rotating flagellum and continues its swimming path by resuming rotation (19, 20).

Bacterial chemotaxis, specifically in *E. coli* has been extensively investigated (for general chemotaxis reviews see Bren *et al.* (1), Porter *et al.* (2), Wadhams *et al*. (3), for more information specifically on MCPs see Bi *et al.* (21), Falke *et al.* (22), Parkinson *et al.*(23)). Chemical stimuli

are sensed by chemoreceptors, specifically named Methyl-accepting Chemotaxis Proteins (MCPs). An MCP is typically composed of a periplasmic ligand-binding domain (LBD), two membrane-spanning helices, and a cytoplasmic signaling domain. When a ligand binds to the LBD, the signal is transferred through the transmembrane helices to the cytoplasmic signaling domain, which controls the activity of a two-component system (3, 21-23). In *E. coli*, this system is composed of CheA, a dimeric histidine autokinase, which binds to the cytoplasmic domain of the MCPs via a coupling protein, CheW, and a response regulator, CheY, which interacts in its phosphorylated form directly with the flagellar motor complex to change direction of rotation. Attractant binding causes a conformational change in the MCP's cytoplasmic region that inhibits CheA autophosphorylation. In contrast, the binding of a repellent to an MCP results in increased CheA autophosphorylation. Phosphorylated CheA (CheA-P) transfers the phosphate group to a conserved aspartate residue in CheY (2, 3). CheY-P interacts with FliM, a cytoplasmic component of the flagellar motor, triggering a rotational switch to CW rotation, and, consequently, a tumble reaction. Inhibition of CheA autophosphorylation instigates a decrease in CheY-P concentration, thus reducing the frequency of rotational switching and hence tumbles. CheY-P can undergo self-catalyzed dephosphorylation, but the phosphatase CheZ greatly increases the dephosphorylation rate (24-26). An adaptation system involving CheR and CheB is utilized to maintain baseline activity and allow increased sensitivity. CheR is a constitutively active methyltransferase, which adds methyl groups to conserved glutamate residues on the cytoplasmic signaling domain of MCPs. This adaptation system is critical for effective chemotaxis because when an attractant is sensed CheA activity is rapidly reduced. For the chemotaxis system to continue responding to increasing concentration of stimuli the CheA the system. Methylation of the receptors allows for the return of CheA to the peristimulus state and reduces the affinity of the receptor to the attractant.

Due to the differences in time scale between methylation and the other reactions in the chemotaxis system the bacterium is able to compare its current state to the past. The antagonistic methylesterase CheB is phosphorylated and activated by CheA-P (27, 28). Addition and removal of methyl groups by CheR and CheB brings about the conformational change in the MCPs required for resetting and adaptation of the chemotaxis system (29-31).

Chemotaxis allows microorganisms not only to locate optimal environments for survival but to engage in a pathogenic or symbiotic relationship with their eukaryotic host organism. Chemotaxis-mediated plant-microbe interactions have been well documented for members of the *Rhizobiaceae* family including *S. meliloti* (32-35). Several studies revealed significant deviations of the chemotaxis systems from the well-studied enteric paradigm (17, 36). *S. meliloti* uses eight chemoreceptors for chemotactic responses, namely McpT-McpZ and IcpA (37, 38). We have demonstrated that McpU, McpX, and McpV play a role in chemotaxis towards the plant by sensing exuded amino acids, quaternary ammonium compounds, and short chain carboxylates, respectively (39-43). The function of the remaining five chemoreceptors is still under study. *S. meliloti* possesses two response regulators, CheY1 and CheY2, but is lacking a CheZ-type phosphatase. CheY2 is the main regulator of motor function, while CheY1 plays a role in signal termination (44-46). Specifically, phosphate groups from the response regulator CheY2 are shuttled back via CheA to CheY1 (46). An additional protein, CheS, enhances the phosphate transfer flow rate from CheA-P to CheY1 by increasing affinity between CheA-P and CheY1 100-fold (47). The one-kinase/two-response regulator system and the presence of an auxiliary protein allows the implementation of a tunable switch-like signal processing (48). The chemotaxis system of *S. meliloti* also contains a chemoreceptor deamidase, CheD, which has a homolog in *Bacillus subtilis* (49). It is yet unclear if CheD plays a similar function in *S. meliloti.* Finally, the role of a

protein encoded by the last gene in the *che1* chemotaxis operon, *cheT*, is currently under investigation.

A detailed understanding of bacterial chemotaxis requires a precise knowledge of the dynamics and protein stoichiometries within a variety of these systems. The total cellular quantities of chemotaxis proteins have been determined for *E. coli* and *B. subtilis*. These findings revealed that total protein amounts vary, depending on strain, growth conditions and nutrient availability, while cellular ratios of chemotaxis proteins are fairly robust. Additionally, the ratios between specific proteins, namely CheA and CheW, were equal in both species, while others, such as CheA and MCPs, varied greatly (50, 51). We used quantitative immunoblots to determine cellular amounts of chemotaxis proteins and to attain a sense of *S. meliloti*'s deviations from these two bacterial chemotaxis model systems. Together with previous work, in which we quantified cellular stoichiometries of *S. meliloti* chemoreceptors (52), the data will allow us to compare different chemotaxis systems and gain a better understanding of evolutionary developments and environmental adaptations. Ultimately, computational models can be employed to simulate the interactions of chemotaxis proteins within each system under various physiologically relevant conditions (53).

RESULTS

General quantification scheme of chemotaxis proteins in *S. meliloti*

Chemotaxis in *S. meliloti* is controlled by the *che1* operon, which encodes *icpA*, *cheS, cheY1, cheA, cheW, cheR, cheB, cheY2, cheD*, and *cheT.* The remaining chemoreceptors and two additional *cheW* genes are encoded in separate loci. A bicistronic operon encodes *cheW2* and chemoreceptor protein *mcpW.* The third *cheW* gene, *cheW3,* is located upstream of *mcpY* and separated by an IS element (38, 54). In previous work, we quantified the cellular amounts of chemoreceptors and the kinase CheA, to determine the receptor to kinase ratio, which left ten of the chemotaxis proteins remaining to be quantified (52).

S. meliloti chemotaxis proteins were overexpressed in *E. coli* and either purified using the IMPACT system or from inclusion bodies. Subsequently, polyclonal antibodies were raised against the purified proteins. Consistent results during quantification were maintained by collecting *S. meliloti* cell culture samples at a growth phase optimal for cell motility. All chemotaxis genes in *S. meliloti* are under a tight transcriptional control through a regulatory hierarchy of motility and chemotaxis gene expression including class IA and IB transcriptional regulators, VisNR and Rem (55). Harvesting of cells for immunoblots was therefore selected at an OD_{600} of 0.25, which represented a plateau for gene expression (38). Standard curves were established by adding varying amounts of each purified protein to cell extracts of corresponding deletion strains. Immunoblot signals were detected using film with different exposure times and band intensities were determined with ImageJ. We were unable to detect two proteins, CheS and CheW3, with this method. Therefore, we used mass spectrometry to detect and quantify CheS. CheW3 was not detected via mass spectrometry. Since deletion of the *cheW3* gene did not cause a chemotaxis defect, we excluded this protein in our analysis.

Quantifications of *S. meliloti* chemotaxis proteins via immunoblots

Eight *S. meliloti* chemotaxis proteins were quantified using immunoblot analysis. Representative examples for the quantification of each protein are given in Fig. 1. The representative blot for CheB (36.9 kDa) exhibited bands slightly below the 37-kDa marker as seen in lanes 2-4 of Fig. 1A comprising wild-type cell extracts. Lane 1 contains a *cheB* deletion cell extract and shows no CheB band. A cross-reacting band slightly below the CheB band is being detected in all lanes (Fig. 1A). The remaining lanes contain the standard curve created by mixing decreasing known amounts of purified CheB with *cheB* deletion cell extracts. CheD, CheR, CheT, CheW1, CheW2, CheY1, and CheY2 were quantified in a similar manner (Fig. 1 B-H). Notably, antibodies generated for CheY1 did not cross react with CheY2 and vice versa, despite high sequence homology. The same was true for the CheW1 and CheW2 antibodies, both of which were unable to detect CheW2 and 3 or CheW1 and 3, respectively (data not shown).

Quantification of *S. meliloti* CheS via immunoblot and mass spectrometry

Previously, our lab generated four different polyclonal antibodies from three vendors to detect CheS in immunoblots of *S. meliloti* wild-type cell extracts; however, none of the crude sera or affinity-purified CheS antibodies were able to provide the required sensitivity. The minimal amount of purified CheS that could be detected was approximately 10 ng. As a result, a remedial strategy using a combination of quantitative epitope-tag immunoblots and mass spectrometry was applied. We first created a strain that expressed 3xFLAG-CheS from its native chromosomal locus (BS265). The amount of cellular 3xFLAG-CheS was then determined by using a purified McpV-LBD-3xFLAG as standard (Fig. 2). We reported in an independent study that the fusion of epitope

tags can affect the stability of *S. meliloti* chemotaxis proteins, which would indicate non-physiological amounts of cellular protein (Arapov *et al.*,submitted for publication).To determine whether this was also the case for CheS with an N-terminal 3xFLAG-tag, we utilized mass spectrometry to measure the relative amounts of CheS and 3xFLAG-CheS in *S. meliloti* cell extracts by using two unique peptides obtained after tryptic digest. We found that the N-terminally tagged protein was 4.43 ± 2.38 times more abundant then wild-type CheS. Thus, the N-terminal epitope tag stabilized CheS, and the determined factor was incorporated in the final protein abundance calculation (Table 1).

Summary of chemotaxis protein quantification

We previously determined the number of *S. meliloti* cells in one ml of cell culture grown in minimal medium to an OD_{600} of 0.25 to be $2.56 \pm 0.31 \times 10^8$ cells (52). This number was used to calculate the number of chemotaxis proteins per cell. For each protein, the value was derived from the average of six immunoblots, with R^2 values above 0.95 for each standard curve. The abundance of the chemotaxis proteins ranged from 22 molecules of CheS and CheW1 to 853 molecules of CheY1 per cell (Table 1).

Bioinformatics analyses of *S. meliloti* CheW proteins

To gauge the relationship of the three *S. meliloti* CheW proteins to *E. coli* CheW and the two CheW proteins found in *A. tumefaciens*, we performed a relationship analysis. The two *cheW* genes in *A. tumefaciens*, *cheW1* and *cheW2*, are found in two separate loci distant from the major chemotaxis operon (56). A cladogram analysis and multiple sequence alignment revealed that the *S. meliloti* CheW3 peptide sequence shares the highest identity with *A. tumefaciens* CheW2

sequence. Interestingly, both genes are located upstream of an *mcp* gene. The *A. tumefaciens* CheW1 sequence shares the highest identity with *S. meliloti* CheW2 and slightly less with *S. meliloti* CheW1 (Fig. 3A). In *E. coli*, CheW interacts with the P5 domain of CheA. The P5 domain is not essential for autophosphorylation but is indispensable in coupling CheA activity to chemoreceptor control, and it contains residues mediating CheW binding (57, 58). Residues R117, E121 and F122 in *E. coli* CheW are critical to this interface (59). However, residues in these positions are not conserved in any of the *S. meliloti* or *A. tumefaciens* CheW proteins (Fig. 3B), which might indicate variations in the interaction of CheA and CheW in these alphaproteobacteria.

Motility assays of *S. meliloti cheW* mutant strains

To analyze the contribution of individual CheW proteins to chemotaxis, we created strains with in-frame deletions of single and multiple *cheW* genes by allelic exchange and determined their chemotaxis behavior on swim plates (Fig. 4). Significant impairment was observed in strains lacking either *cheW1* or *cheW2*, resulting in swim ring diameters of 29 % and 64 % of that produced by the wild type, respectively. In contrast, the deletion of *cheW3* had no effect on swim ring size. When both, *cheW1* and *cheW2*, were deleted, no additive effect on the swim ring diameter was detected. Furthermore, deletion of *cheW3* in a Δ*cheW1*, Δ*cheW2,* or Δ*cheW1*Δ*cheW2* background retained the swim ring diameter compared to each of the parental strains. Therefore, we can conclude that CheW1 is the main contributor to chemotaxis, CheW2 has a minor but significant role, and CheW3 does not contribute to chemotaxis under these conditions.

DISCUSSION

The chemotaxis system of *S. meliloti* is known to be divergent from other paradigm models that have been more extensively studied. Knowledge of the protein stoichiometries in model chemotaxis systems will contribute to a better understanding of protein function and dynamics within these systems, as well as to the evolution of their pathways. This study is concluding our previous work on *S. meliloti* chemoreceptors abundances by quantifying all remaining chemotaxis proteins (Table 1). The cellular numbers of the ten chemotaxis proteins fell within the range we reported for chemoreceptor proteins and the kinase CheA (52). As in our previous work, the total number of protein molecules was found to be lower than reported for other paradigm models. At this stage, we identified two factors contributing to the relatively low abundance of chemotaxis proteins. Firstly, *S. meliloti* cells are smaller than *E. coli*, and cell size is dependent on the cell cycle and nutrient availability (60). Secondly, while temporal expression of chemotaxis proteins is strictly growth-phase regulated, only part of the entire population expresses chemotaxis proteins, which suggests the existence of a bimodal population (52, 61). A cryotomographic analysis of chemoreceptor arrays in another alphaproteobacterium, *Caulobacter crescentus*, provided an estimate of 1,100 to 2,200 chemoreceptors per cell. This value is in close agreement with our reported value of 423 chemoreceptors per *S. meliloti* cell. Due to the smaller cell size of these two alphaproteobacterial species, the concentration of receptors appears to be similar to *E. coli*. In this study, we focused on the presentation and discussion of protein ratios, which were found to be robust (50).

CheW1 and CheW2 function in chemotaxis

S. meliloti possesses three *cheW* genes. According to behavioral studies of *cheW* deletion strains, CheW1 and CheW2 are the main contributors to chemotaxis, whereas *cheW3* is likely not expressed and deletion of *cheW3* has no effect on chemotactic performance (Fig. 4). CheW1 is nearly 10-fold more abundant than CheW2. Together with its dominant effect on chemotaxis, CheW1 can be considered the prevailing adaptor protein between chemoreceptors and the kinase CheA. CheW2 has a smaller but significant effect, and its co-expression with McpW suggests a potential specific role for select chemoreceptors. Similarly, both CheW proteins in *A. tumefaciens* contribute to chemotaxis with distinct capacities. In *A. tumefaciens*, CheW2, which is more closely related to *S. meliloti* CheW3, is the dominant CheW protein, while CheW1 appears to play a more minor role. Remarkably, both *A. tumefaciens cheW* genes can partially complement each other and interact with the same MCP (62). It would be interesting to see whether the same holds true for *S. meliloti*.

Protein ratios within the ternary core signaling complex

In our previous study, we established a CheA to chemoreceptor ratio of 1:23.5, which is similar to *B. subtilis* but different from the *E. coli* system. We made a small adjustment to this value due to rounding errors during our calculations (Table 1), which now results in a ratio of 1:22.3. In this work, we elucidated that the CheA dimer to CheW monomer ratio is highly divergent from that of *B. subtilis* and *E. coli.* The latter two organisms possess approximately two CheW monomers per CheA dimer, consistent with the formation of a ternary complex between one receptor dimer, one CheA dimer, and two CheW monomers (63). *S. meliloti* has over 20 CheW1 and CheW2 monomers per CheA dimer, which results in a ten-fold molar excess of adaptor proteins (Table 2,

Fig. 5). There is no indication that the majority of the CheW molecules would not be part of the chemoreceptor cluster (37), which then advocates the hypothesis that the organization of the core signaling complex in *S. meliloti* differs from the other two model systems. One hypothesis could involve the formation of rings composed of CheW1 and CheW2 alone. The presence of CheW rings has been observed in *E. coli*, where they are proposed to provide allosteric connections between core complexes (64). These rings are structurally analogous to the complex formed between the P5 domain of CheA and CheW, although they do not directly interact with CheA or CheW within the core complex. Additional evidence is provided from a structural analysis of *Vibrio cholerae* chemotaxis arrays, which are primarily composed of CheW rings without direct connection to the core signaling complex (65, 66). Our stoichiometry data suggests that CheW rings are more prevalent in the *S. meliloti* chemotaxis array as compared to *E. coli* and *V. cholerae.* Chemotaxis array models indicate that the ratio of a CheA dimer to coupling protein monomers in *E. coli* is approximately 1:4, assuming that all CheA-free rings are composed of CheW proteins. This ratio is much higher in *V. cholerae* with 1:14 (65) and *S. meliloti* with 1:22 (Table 2). Furthermore, *E. coli* CheW residues that are important to form the interface with CheA-P5, namely R117, E121, and F122 (59), are only partially conserved in *S. meliloti* and *A. tumefaciens* CheW1 and CheW2 (Fig. 3B), which may affect their affinity to CheA and CheA-CheW complex formation. It is apparent that CheW1 and CheW2 have distinct roles within the *S. meliloti* chemotaxis system, and it remains to be elucidated how both proteins contribute to the organization of the chemotaxis array in *S. meliloti*.

Protein ratios related to the adaptation system

The adaptation system in *S. meliloti* chemotaxis has not been characterized, but the function of at least three proteins encoded in the *che1* operon was deduced by bioinformatics (67). The two proteins that are mostly conserved in all systems are the methylesterase CheB and the methyltransferase CheR (68). In *S. meliloti*, both, CheB and CheR, are present at a higher ratio per CheA dimer, when compared to *B. subtilis* or *E. coli*, namely 6- and over a 100-fold for CheB, and 30- and nearly 500-fold for CheR (Table 2). Since no information is available about the mechanism of adaptation in *S. meliloti*, we can only speculate that these differences reflect variations in its adaptation system, such as alterations in the role of methylation in general or differences in specific enzymatic activities. However, when comparing the ratio of CheB to CheR in each species, the differences are not large, 0.4 in *S. meliloti* compared to 1.7 in *E. coli* and 1.9 in *B. subtilis*. The third protein presumed to be involved in adaptation is the receptor deamidase CheD. Its ratio to a CheA dimer is almost 50-fold higher in *S. meliloti* than in *B. subtilis.* In *B. subtilis*, in addition to its deamidase activity, CheD interacts with CheC to mediate CheY dephosphorylation (69). *S. meliloti* lacks CheC, but it is conceivable that CheD also interacts with other chemotaxis proteins and fulfills an additional role in chemotaxis. This is the case for CheD in the pathogen *Borrelia burgdoferi* (70). Finally, the protein encoded from the last gene in the *che1* operon, CheT, was identified at relatively low abundance. It has no homologues in *B. subtilis* or *E. coli*, but its gene has been described in chemotaxis operons of closely related alphaproteobacteria (35). Strains lacking *cheT* exhibit a chemotaxis defect (data not shown) but its function remains to be elucidated.

Response regulators, motor function, and signal termination

The main response regulator of *S. meliloti* motor function is CheY2 (44). It is present at a higher ratio per CheA dimer when compared to *B. subtilis* or *E. coli* CheY, approximately 20- and 40-fold, respectively. However, it is unclear whether this variation can be attributed to the presence of an exclusively CW-rotating, speed-regulated motor in *S. meliloti* versus the switch-type motors in *B. subtilis* or *E. coli*. Ratios of phosphatases involved in signal termination to their respective CheA dimer were similar for the CheZ dimer in *E. coli* and CheC in *B. subtilis* (0.5 and 0.3), while CheY1, the phosphate sink response regulator in *S. meliloti,* had a monomer ratio to the CheA dimer of 90. We hypothesize that these variations reflect the different mechanisms used for signal termination. *E. coli* and *B. subtilis* utilize an enzyme-catalyzed reaction mechanism (25, 71, 72), while *S. meliloti* uses a phosphate sink that acts as a protein-interaction based signal termination (47, 48). The phosphate sink may not be as efficient as a direct, enzyme-catalyzed reaction in signal termination, and hence requires a larger pool of CheY1 to match CheY2. An additional protein involved in signal termination in *S. meliloti* is CheS, which forms a tight complex with CheA and mediates interaction between CheA and CheY1 (47). CheS and CheA were determined to be present in a 1:1 ratio, which indicates that all CheA dimers are occupied by a CheS dimer.

Conclusions

Protein stoichiometries in the chemotaxis systems of *E. coli*, *B. subtilis*, and *S. meliloti* vary greatly. Here we showed that *S. meliloti* exhibits a more substantial deviation of chemotaxis protein ratios. Furthermore, it involves additional proteins, such as CheS and CheT, that are specifically present in closely related alpha-proteobacteria (73). Proteins with conserved functions

such as CheA and CheW appear in significantly altered stoichiometric ratios than those seen in other bacterial species. The reason for the increased abundance of proteins involved in adaptation is currently elusive due to the lack of experimental data for the chemotactic adaptation of *S. meliloti*. However, signal termination by a phosphatase mechanism versus an indirect sink mechanism marks a major difference between systems. Three response regulator proteins, CheB, CheY1, and CheY2 compete in receiving phosphate groups from CheA-P. Their phosphorylation and therefore activation is regulated by their affinities to CheA and auto-dephosphorylation activities. Thus, activation of the motor response regulator, termination of the signal, and receptor methylation/adaptation are intimately connected. Furthermore, the roles of CheD and CheT in *S. meliloti* are unexplored. Detailed studies of phosphotransfer reactions and receptor methylation are needed to gain a complete picture of this complex system.

The *S. meliloti* chemotaxis proteins quantified in this and the preceding study begin to give us an understanding of the diversity that exists between the chemotaxis systems in different bacterial species. Together with information on protein-protein interactions, enzymatic rate constants, and nature of chemoattractants and -repellents, this will enable us to develop a mathematical model of the chemotaxis behavior in *S. meliloti*. By varying chemotaxis ligand concentrations within the model, the behavior of *S. meliloti* in the soil or rhizosphere and during host interaction can be predicted.

MATERIALS AND METHODS

Bacterial strains and plasmids

Derivatives of *E. coli* K12 and *S. meliloti* MV II-I are listed in Table 3. The wild-type strain used in this study, RU11/001, is a spontaneous streptomycin-resistant derivative of MVII-1 (74).

Media and growth conditions

Lysogeny broth (LB) (75) was utilized in growing *E. coli* strains at specified temperatures. *S. meliloti* strains were grown in TYC (0.5 % tryptone, 0.3% yeast extract, 0.13 % $CaCl_2 6H_2O$ [pH 7.0] (76) or Sinorhizobium motility medium (SMM; RB [6.1 mM K_2HPO_4, 3.9 mM KH_2PO_4, 1 mM $MgSO_4$, 1 mM $(NH_4)_2SO_4$, 0.1 mM $CaCl_2$, 0.1 mM NaCl, 0.01 mM Na_2MoO_4, 0.001 mM $FeSO_4$, 2 µg/l biotin] (77) supplemented with 0.2 % mannitol, 2 % TY)(55) or Bromfield medium (0.04% tryptone, 0.01% yeast extract, 0.01% $CaCl_2$, $2H_2O$) at 30 ˚C. Antibiotics used to create the selective growth media in their final concentrations are as followed: for *E. coli*, 100 µg/ml ampicillin, 50 µg/ml kanamycin; for *S. meliloti* 120 µg/ml neomycin and 600 µg/ml streptomycin.

Motility Assays

Swim plates containing Bromfield medium and 0.3 % Bacto agar were inoculated with 3-µl droplets of the test culture and incubated at 30 °C for 4 days.

Genetic and DNA manipulations

Isolation and purification of *S. meliloti* DNA was described previously in Sourjik *et al* (1996) (44). Plasmid DNA, DNA fragments or PCR products were purified according to manufactures' instructions, and PCR amplification of chromosomal DNA was carried out according to published

protocols (44). Constructs containing mutations were cloned into the mobilizable suicide vector pK18*mobsacB*. The vector was used to transform *E. coli* S17-1 and transferred to *S. meliloti* by conjugation (78, 79). Allelic replacement was achieved by sequential selection on neomycin in TYC and 10 or 15 % sucrose in Bromfield medium(44). Gene-specific primer PCR and Sanger DNA sequencing was used to confirm mutations.

Purification of recombinant proteins

Proteins CheB (pBS93), CheR (pBS450), CheT (pBS359), CheW2 (pRU2553), CheY1 (pBS16) and CheY2 (pBS0018), and McpV-3xFLAG (pBS459) were overexpressed in *E. coli* ER2566 following established procedures (45). Cells were grown to an OD_{600} of 0.7 to 0.9 at 37 °C in LB supplemented with 100 µg/ml ampicillin. Protein expression was induced with 0.3 mM isopropyl-β-D-thiogalactopyranoside (IPTG) at 16 °C for 16 h. Cells were harvested by centrifugation and stored at -20 °C. Cell pellets were thawed and frozen three times on ice before being suspended in 20 ml of IMPACT buffer (0.5 M NaCl, 1 mM EDTA, 20 mM Tris/HCl, pH 8.0, 1 mM phenylmethylsulfonyl fluoride [PMSF], and 0.25 mg/liter DNase I) per liter culture harvested. Cells were lysed by three passages through a French pressure cell at 20,000 lb/in^2 (SLM Aminco, Silver Spring, MD). The lysate was centrifuged at 48,000 × g and 4 °C for 30 min, and the soluble, filtered fraction was loaded onto a chitin agarose column (2.6 x 5.0 cm) (NE Biolabs, Beverly MA, USA). Intein-mediated cleavage was elicited by equilibration of the column with IMPACT buffer containing 50 mM dithiothreitol (DTT) and incubation for 12 to 48 h at 4 °C. Proteins were eluted with IMPACT buffer, protein-containing fractions combined and concentrated to 10 ml by ultrafiltration using 10-kDa regenerated cellulose membranes in a 50 ml Amicon filter unit (Millipore, Bedford, MA). Proteins were further purified by (ÄKTA-prime plus or pure, GE

Healthcare) fast-performance liquid chromatography on a size exclusion column (HiPrep 26/60 Sephacryl S-300 HR). The column was equilibrated with PBS (100 mM NaCl, 80 mM Na_2HPO_4, 20 mM NaH_2PO_4, pH 7.5) with 5 % glycerol (v/v). Proteins were separated at a flow rate of 0.5 ml/min and protein-containing fractions were combined.

Proteins CheW1 (pBS481), CheD (pBS524), CheS (pBS173) were overexpressed in *E. coli* BL21(DE3). Cells were grown at 37 °C in LB containing 100 µg/ml ampicillin to OD_{600} of 0.7 – 0.9, and expression was induced by the addition of 1mM IPTG. Incubation continued for 4 h at 37 °C until harvest. Cell pellets from each 1-liter culture were suspended in 20 ml 0.5 mM EDTA, 20 mM Tris-HCl, pH 7.5 and lysed as described above. The lysate was centrifuged at 48,000 × g and 4 °C for 30 min. The soluble fraction was discarded and pellets were washed three times in wash solution (1% (vol/vol) Triton X-100, 1 mM EDTA). Inclusion bodies were dissolved by suspension in 10 ml denaturation buffer (8 M urea, 5 mM DTT, 50 mM Tris/HCl, pH 8.0) per liter culture harvested. Insoluble material was removed by centrifugation at 4 °C for 20 min at 48,000 x g and subsequent filtration through a 0.2-µm-pore-size cellulose acetate syringe filter. Further purification was performed by FPLC size exclusion chromatography (HiPrep 26/60 Sephacryl S-300 HR) in denaturation buffer. Appropriate protein containing fractions were combined.

Immunoblotting

Polyclonal antibodies raised against chemotaxis proteins were purified as described in Scharf *et al. (2001)* (76). In brief, one mg of purified protein was separated by SDS-PAGE and transferred to a nitrocellulose membrane (Amersham Protran 0.45 µm, GE HealthCare). A 1% Ponceau S solution was used to visualize blotted proteins, and protein-containing blot paper was cut out and sliced into smaller pieces (1 cm x 1 cm). Membrane pieces were transferred into 2 ml of crude

serum and incubated at 4 °C for 16 h under slow rotation. The blots were then consecutively washed thrice with PBS/0.1% bovine serum albumin (BSA), twice with PBS/0.1 % BSA/0.1 %/Nonidet P40, and thrice with PBS/0.1 % BSA for 5 min per wash step. Bound antibodies were eluted from the membrane by incubating with 750 µl of 0.2 M glycine/HCl, pH 2.5 for 1 min, immediately followed by neutralization with 375 µl of pre-chilled 1 M potassium phosphate, pH 9.0. The elution step was repeated once and the combined fractions were dialyzed three times against PBS at 4 °C.

Whole cell extracts for immunoblots were prepared as follows. Wild-type and deletion strains were grown in 50 ml of SMM to an OD_{600} of 0.250 ± 0.002. One milliliter aliquots were then sedimented by centrifugation at 13,000 × g for 10 min, suspended in approximately 15 µl of the supernatant and 15 µl of Laemmli buffer (4.5 % SDS, 18.7 mM Tris/HCl, pH 6.5, 43.5 % glycerol, 0.0125 % bromophenol blue, and 5 % β-mercaptoethanol). Samples were boiled for 10 min and stored at -20 °C. Defined amounts of purified protein were added to the appropriate deletion cell extract to create a standard curve.

Immunoblots were performed in the same manner as described in Zatakia *et al*. (2018) (52). In brief, cell extracts were separated by SDS-polyacrylamide gel electrophoresis and transferred onto 0.45 µm nitrocellulose membrane or 0.2 µm polyvinylidene fluoride (BIO-RAD, Sequiblot™) membrane in transfer buffer (20% v/v methanol, 50 mM Tris, 40 mM glycine). Membranes were blocked overnight with 5 % non-fat dry milk, 0.1 % Tween 20 in PBS. Blots were probed with 1:200 dilution of affinity-purified antibodies, 1:5,000 dilution of crude serum, or 1:20,000 dilution of monoclonal ANTI-FLAG® M2 antibody (Sigma-Aldrich) for 1.5 h. Blots were washed for 30 min with PBS/0.1 % Tween 20 with four buffer changes and then probed with a 1:1,500 dilution of donkey anti-rabbit or a 1:4,000 dilution of sheep anti-mouse horseradish peroxidase conjugated

antibodies. The blots were then washed for 30 min with PBS/0.1 % Tween 20 with four buffer changes. Detection was performed by chemiluminescence (Amersham ECL Western Blotting Detection Kit, GE Healthcare) using Hyperfilm ECL (GE Healthcare). Images were scanned with an Epson Perfection 160SU scanner, and pixel intensities were then quantified with ImageJ. The number of molecules per cell were calculated using the previously quantified number of cells per 1 ml volume for *S. meliloti* as described in Zatakia *et al.* (2018) (52), protein concentrations were first obtained by the standard Bradford Assay using Quick Start™ Bradford 1x Dye Reagent (BIO-RAD) and a bovine serum albumin standard curve as per manufacturer's protocol. The amounts of each protein standard as stated in the figure legends were calculated using this method. Accurate protein concentrations that were used to calculate final protein amounts were determined by quantitative amino acid analyses after total acid hydrolysis performed at the Protein Chemistry Lab, Texas A&M University.

Mass spectrometry

Wild type and mutant strain BS265 were grown in 50 ml of SMM to an OD_{600} of 0.250 ± 0.002. Twentyfive milliliter aliquots were then sedimented by centrifugation at 72411 × g and at 4 °C for 10 min. The supernatant was aspirated, cell pellets snap-frozen using liquid N_2, and lyophilized for two days. To each lyophilized cell pellet, 0.5 ml 2x S-Trap protein solubilization buffer (10 % (w/v) sodium dodecyl sulfate (SDS), 100 mM triethylammonium bicarbonate (TEAB), pH 8.5) was added and vortexed vigorously, followed by the addition of 0.5 ml water, and each sample was again vortexed vigorously. Samples were subjected to a total of 4 freeze/thaw cycles (30 min at -80 °C for 30 min followed by incubation at 37 °C for 30 min) with samples being vortexed vigorously after each thaw. Cell debris was removed by centrifugation (20 min at 3160 x g). The

solubilized supernatant was transferred to 1.5-ml microfuge tubes and protein concentration of each sample was determined by measurement of the absorbance at 280 nm. Samples were adjusted to a protein concentration of 1 mg/ml using 1x S-Trap solubilization buffer to protein. Five hundred microliters of each sample were reduced and alkylated by addition of 4.5 mM dithiothreitol (DTT) by addition of 10 mM iodoacetamide (IAA), respectively, and unreacted IAA was quenched using additional DTT (10 mM). Samples were then processed for digestion as described using mini S-Traps (Protifi). Briefly, samples were acidified by adding 1/10 volume 12 % (v/v) o-phosphoric acid and protein precipitated by adding 7 volumes of S-Trap protein binding buffer (90 % (v/v) LC-MS grade methanol, 100 mM TEAB, pH 8.5). Precipitated proteins were loaded onto a mini S-Trap by centrifugation for 1 min at 2000 x g followed by 4 washes with 150 µl of S-Trap protein binding buffer. Twenty micrograms of trypsin (Promega) in 125 µl 50 mM TEAB, pH 8.5, were added to each mini S-Trap and incubated overnight at 37 °C. Peptides were eluted sequentially using 80 µl 50 mM TEAB, pH 8.5, 80 µl 0.2 % (v/v) formic acid in LC-MS grade water, and 80 µl 50:50 LC-MS grade water: LC-MS grade acetonitrile supplemented with 0.2 % (v/v) formic acid. The three eluents were combined and concentrated to dryness using a centrifugal vacuum concentrator. Peptides were reconstituted in 40 µl solvent A (98:2 LC-MS grade water: LC-MS grade acetonitrile supplemented with 0.1 % (v/v) formic acid) by sonication. Peptide concentrations were determined by measuring the absorbance at 215 nm. Samples were diluted to 4 mg/ml using solvent A and duplicate injections of 9 µl were analyzed by liquid chromatography mass spectrometry.

Mass spectrometry analysis utilized an Orbitrap Fusion Lumos coupled to an Easy nLC 1200 UPLC/autosampler (Thermo Scientific). Samples were loaded onto a trap column (P/N 164564, Thermo Scientific) by flowing 21 µl solvent A at 500 bar. The flow path was then switched to

include an analytical column (P/N ES801A, Thermo Scientific), and peptides were eluted at a flow rate of 500 nl/min with a 110-min gradient from 98 % solvent A to 55 % solvent A. Solvent B was 20:80 LC-MS grade water: LC-MS grade acetonitrile supplemented with 0.1 % (v/v) formic acid. The analytical column was maintained at 55 °C and the ion transfer tube at 275 °C. Electrospray voltage was set to 3000 V and the RF lens set to 30 %. The MS1 scan utilized the orbitrap set to 240000 resolution (m/z 200) over the m/z range of 745 to 775 with an AGC target of 2e5, a maximum injection time of 50 ms in profile positive ion mode. If peaks corresponding to either of the two CheS peptides (750.4035 ± 10ppm (NTLMLAPVLDLNEATVLHER, z = +3) and 764.9238 ± 10ppm (TTQLIGADIGPLMAK, z = +2)) were detected with an intensity above 1e3, two MS2 scans were triggered. The first utilized quadrupole isolation of ±1.6 Da, the orbitrap detector set to 15000 resolution (m/z 200) and stepped HCD of 26, 30, and 3 4% with the first mass of the MS2 scan set to 150 and a default charge state of 3. The AGC target was 1e4 with a maximum injection time of 50 ms in profile positive ion mode. The second utilized quadrupole isolation of ±1.6 Da, the ion trap detector at normal scan speed using assisted CID of 26, 30, and 34 %. Activation Q was set to 0.25, CID activation time was 10 ms with an AGC target of 1e4, maximum injection time of 100 msec, again with data collected in the profile positive ion mode. Peptides were identified with Proteome Discoverer 2.2 (Thermo Scientific) using both Sequest HT and Mascot search engines. Data were searched against the *S. meliloti* reference proteome downloaded from UniProt on 6/14/19 and a database containing common lab contaminant proteins. All peptides were expected to be fully-specific for trypsin digestion with possibly two missed cleavages. MS1 tolerance was set to ± 20 ppm and MS2 tolerance was set to ± 0.5 Da. Carbamidomethylation of cysteine residues was set as a fixed modification while oxidation of methionine, deamidation of asparagine and glutamine, acetylation of the protein N-terminus and

formation of pyroglutamate from glutamine when at the N-terminus of a peptide were set as variable modifications. Quantitation of CheS utilized the maximum intensity of the sum of all expected MS2 ions (b and y type) for TTQLIGADIGPLMAK using HCD and detected using the orbitrap after normalization to the maximum intensity observed in the total ion chromatogram.

Bioinformatics analyses

Alignment of *E. coli K-12* CheW (NP_416401.1) and *A. tumefaciens* CheW1 (NP_355040.2) and CheW2 (NP_355554.2) and *S. meliloti* CheW1 (WP_014528989.1), CheW2 (WP_003536237.1), and CheW3 (WP_003528560.1) was generated by use of EMBL-EBI tool ClustalOmega (80).

ACKNOWLEDGMENTS

This study was supported by NSF grants MCB-1253234 and MCB-1817652 to Birgit Scharf and to the VT Multicultural Academics Opportunity Program Fellowship to Amanda Sebastian. We would like to thank Dr. Hardik Zatakia for purification of McpV-3xFLAG protein standard and all Scharf lab members for in the critical reading of the manuscript.

Table 3.1 Cellular content of chemotaxis proteins in *S. meliloti* strain RU11/001

Protein	Function	No. of molecules/cell[a]
Chemoreceptors total		422 ± 78[b]
CheA	Histidine autokinase	19 ± 5[b c]
CheB	Methylesterase	90 ± 17
CheD	Deamidase	404 ± 154
CheR	Methyltransferase	218 ± 60
CheS	Adaptor protein between CheA and CheY1	22 ± 7[d]
CheT	Chemotaxis protein of unknown function	32 ± 11
CheW1	Adaptor protein	189 ± 53
CheW2	Adaptor protein	22 ± 7
CheY1	Sink response regulator	853 ± 5
CheY2	Response regulator of motor function	811 ± 64

[a] Mean ± standard deviation. Values were obtained from six independent biological replicates.
[b] Zatakia *et al.*, 2018 (48)
[c] This value has been adjusted from 18 to 19 as compared to Zatakia et al., 2018, due to a rounding error during calculations.
[d] Values were obtained from six independent biological replicates for immunoblots and three independent biological replicates from mass spectrometry.

Table 3.2 Cellular stoichiometry of chemotaxis proteins normalized to a CheA dimer in *E. coli, B. subtilis,* and *S. meliloti*

Protein	***E. coli*[a]**	***B. subtilis*[b]**	***S. meliloti***
CheA[c]	1	1	1
CheB	0.08 ± 0.01	1.6 ± 0.5	9.1 ± 3.2
CheR	0.05 ± 0.01	0.8 ± 0.2	23.0 ± 6.4
CheD	N.A.	0.9 ± 0.3	42.6 ± 16.3
Coupling proteins (total)	1.6 ± 0.5[d]	7.4 ± 1.8[e]	22.4 ± 5.6[f]
CheY[g]/CheY2[h]	2.4 ± 0.4	5.5 ± 1.7	86 ± 7
CheY1	N.A.	N.A.	90 ± 17
CheZ[i]/ CheC[j]	0.5 ± 0.09	0.6 ± 0.3	N.A.
CheS[k]	N.A.	N.A.	1.2 ± 0.4
CheT	N.A.	N.A.	3.4 ± 1.2
MCPs dimer	3.4 ± 0.8	23.0 ± 4.5	22.3 ± 3.8
CheB:CheR	1.7	1.9	0.4

[a] Values from reference (50)
[b] Values from reference (51)
[c] CheA dimer
[d] CheW
[e] CheW and CheV
[f] CheW1 and CheW2
[g] *E. coli* and *B. subtilis*
[h] *S. meliloti*
[i] *E. coli* CheZ dimer
[j] *B. subtilis* CheC
[k] CheS dimer

Table 3.3 Bacterial strains and plasmids

Strain/Plasmid	Relevant Characteristics	Source or Reference
E. coli		
BL21(DE3)	*F− ompT hsdSB(rB− mB−) gal dcm λ (DE3)*	Novagen
ER2566	*ion ompT lacZ::T7*	New England Biolabs
M15/pREP4	Ap^r Km^r; F- ϕ80ΔlacM15 *thi lac- mtl- recA*$^+$	Qiagen
S17-1	Sm^r Tp^r; *recA endA thi hsdR* RP4-2 Tc::Mu::Tn7	(Simon *et al.*, 1986) (78)
S. meliloti		
BS195	Sm^r; Δ*cheW3*	This study
BS197	Sm^r; Δ*cheW2* Δ*cheW3*	This study
BS198	Sm^r; Δ*cheW1* Δ*cheW2* Δ*cheW3*	This study
BS265	Sm^r; 3xFLAG -CheS	This study
RU11/001	Sm^r; spontaneous streptomycin-resistant wild-type strain	(Pleier *et al.,* 1991) (81)
RU11/306	Sm^r; Δ*cheR*	This study
RU11/307	Sm^r; Δ*cheY2*	(Sourjik *et al*.,1996) (44)
RU11/312	Sm^r; Δ*cheB*	This study
RU11/319	Sm^r; Δ*cheT*	This study
RU11/411	Sm^r; Δ*cheD*	This study
RU11/414	Sm^r; Δ*cheW1*	This study
RU11/811	Sm^r; Δ*cheW2*	This study
RU11/816	Sm^r; Δ*cheY1*	This study
Plasmids		
pBS16	Ap^r; pTYB1-*cheY1*	This study
pBS18	Ap^r; pTYB1-*cheY2*	This study
pBS93	Ap^r; pTYB11-*cheB*	This study
pBS173	Km^r, 291-bp NcoI-BamHI fragment from pRU2804 containing *cheS* cloned into pET27bmod	(Dogra *et al.,* 2012) (47)
pBS359	Ap^r; pTYB11-*cheT*	This study
pBS450	Ap^r; pTYB1-*cheR*	This study
pBS459	Ap^r; pTYB11-*mcpV-LBD-3xFLAG*	This study
pBS481	Ap^r; pETDuet-*cheW1*	This study
pBS524	Km^r; pET27bmod-*cheD*	This study
pET27bmod	Km^r;derivative of pET27	R. Seidel, MPI Dortmund
pETDuet-1	Ap^r;	Novagen
pK18*mobsacB*	Km^r; *mob sacB*, vector used for homologous allelic exchange	(Schäfer *et al*., 1994) (82)

pRU2553	Ap^r; pTYB1-*cheW2*	This study
pTYB1	Ap^r; expression vector for Impact system	New England Biolabs
pTYB11	Ap^r; expression vector for Impact system	New England Biolabs

REFERENCES

1. Bren A, Eisenbach M. 2000. How signals are heard during bacterial chemotaxis: protein-protein interactions in sensory signal propagation. J Bacteriol 182:6865-6873.
2. Porter SL, Wadhams GH, Armitage JP. 2011. Signal processing in complex chemotaxis pathways. Nat Rev Microbiol 9:153-165.
3. Wadhams GH, Armitage JP. 2004. Making sense of it all: bacterial chemotaxis. Nat Rev Mol Cell Biol 5:1024-1037.
4. Miller LD, Russell MH, Alexandre G. 2009. Diversity in bacterial chemotactic responses and niche adaptation. Adv Appl Microbiol 66:53-75.
5. Duan Q, Zhou M, Zhu L, Zhu G. 2013. Flagella and bacterial pathogenicity. J Basic Microbiol 53:1-8.
6. Pratt LA, Kolter R. 1998. Genetic analysis of *Escherichia coli* biofilm formation: Roles of flagella, motility, chemotaxis and type I pili. Mol Microbiol 30:285-293.
7. Sourjik V. 2004. Receptor clustering and signal processing in *E. coli* chemotaxis. Trends Microbiol 12:569-576.
8. Spiro PA, Parkinson JS, Othmer HG. 1997. A model of excitation and adaptation in bacterial chemotaxis. Proc Natl Acad Sci U S A 94:7263-7268.
9. Berg HC, Brown DA. 1972. Chemotaxis in *Escherichia coli* analysed by three-dimensional tracking. Nature 239:500-504.
10. Berg HC. 2000. Constraints on models for the flagellar rotary motor. Philos Trans R Soc Lond B Biol Sci 355:491-501.
11. Turner L, Ryu WS, Berg HC. 2000. Real-time imaging of fluorescent flagellar filaments. J Bacteriol 182:2793-2801.
12. Paulick A, Sourjik V. 2018. FRET analysis of the chemotaxis pathway response, p 107-126, Bacterial Chemosensing. Springer.
13. Bi S, Sourjik V. 2018. Stimulus sensing and signal processing in bacterial chemotaxis. Curr Opin Microbiol 45:22-29.
14. Berg HC. 1993. Random walks in biology. Princeton University Press.
15. Attmannspacher U, Scharf B, Schmitt R. 2005. Control of speed modulation (chemokinesis) in the unidirectional rotary motor of *Sinorhizobium meliloti*. Mol Microbiol 56:708-718.
16. Platzer J, Sterr W, Hausmann M, Schmitt R. 1997. Three genes of a motility operon and their role in flagellar rotary speed variation in *Rhizobium meliloti*. J Bacteriol 179:6391-6399.
17. Scharf B, Schmitt R. 2002. Sensory transduction to the flagellar motor of *Sinorhizobium meliloti*. J Mol Microbiol Biotechnol 4:183-186.
18. Scharf B. 2002. Real-time imaging of fluorescent flagellar filaments of *Rhizobium lupini* H13-3: flagellar rotation and pH-induced polymorphic transitions. J Bacteriol 184:5979-5986.
19. Armitage JP, Macnab RM. 1987. Unidirectional, intermittent rotation of the flagellum of *Rhodobacter sphaeroides*. J Bacteriol 169:514-518.
20. Packer HL, Lawther H, Armitage JP. 1997. The *Rhodobacter sphaeroides* flagellar motor is a variable-speed rotor. FEBS Lett 409:37-40.

21. Bi S, Lai L. 2015. Bacterial chemoreceptors and chemoeffectors. Cell Mol Life Sci 72:691-708.
22. Falke JJ, Hazelbauer GL. 2001. Transmembrane signaling in bacterial chemoreceptors. Trends Biochem Sci 26:257-265.
23. Parkinson JS. 2010. Signaling mechanisms of HAMP domains in chemoreceptors and sensor kinases. Annu Rev Microbiol 64:101-122.
24. Scharf BE, Fahrner KA, Berg HC. 1998. CheZ has no effect on flagellar motors activated by CheY13DK106YW. J Bacteriol 180:5123-5128.
25. Blat Y, Eisenbach M. 1994. Phosphorylation-dependent binding of the chemotaxis signal molecule CheY to its phosphatase, CheZ. Biochemistry 33:902-906.
26. McEvoy MM, Bren A, Eisenbach M, Dahlquist FW. 1999. Identification of the binding interfaces on CheY for two of its targets the phosphatase CheZ and the flagellar switch protein FliM. J Mol Biol 289:1423-1433.
27. Djordjevic S, Goudreau PN, Xu Q, Stock AM, West AH. 1998. Structural basis for methylesterase CheB regulation by a phosphorylation-activated domain. Proc Natl Acad Sci U S A 95:1381-1386.
28. Anand GS, Goudreau PN, Stock AM. 1998. Activation of methylesterase CheB: evidence of a dual role for the regulatory domain. Biochemistry 37:14038-14047.
29. Parkinson JS, Hazelbauer GL, Falke JJ. 2015. Signaling and sensory adaptation in *Escherichia coli* chemoreceptors: 2015 update. Trends Microbiol 23:257-266.
30. Vladimirov N, Sourjik V. 2009. Chemotaxis: how bacteria use memory. Biol Chem 390:1097-1104.
31. Rao CV, Ordal GW. 2009. The molecular basis of excitation and adaptation during chemotactic sensory transduction in bacteria, p 33-64, Contrib Microbiol, vol 16. Karger Publishers.
32. Caetano-Anollés G, Wall LG, De Micheli AT, Macchi EM, Bauer WD, Favelukes G. 1988. Role of motility and chemotaxis in efficiency of nodulation by *Rhizobium meliloti*. Plant Physiol 86:1228-1235.
33. Miller LD, Yost CK, Hynes MF, Alexandre G. 2007. The major chemotaxis gene cluster of *Rhizobium leguminosarum* bv. viciae is essential for competitive nodulation. Mol Microbiol 63:348-362.
34. Gulash M, Ames P, Larosiliere R, Bergman K. 1984. *Rhizobia* are attracted to localized sites on legume roots. Appl Environ Microbiol 48:149-152.
35. Scharf BE, Hynes MF, Alexandre GM. 2016. Chemotaxis signaling systems in model beneficial plant–bacteria associations. Plant Mol Biol 90:549-559.
36. Schmitt R. 2002. *Sinorhizobial* chemotaxis: a departure from the enterobacterial paradigm. Microbiology 148:627-631.
37. Meier VM, Scharf BE. 2009. Cellular localization of predicted transmembrane and soluble chemoreceptors in *Sinorhizobium meliloti*. J Bacteriol 191:5724-5733.
38. Meier VM, Muschler P, Scharf BE. 2007. Functional analysis of nine putative chemoreceptor proteins in *Sinorhizobium meliloti*. J Bacteriol 189:1816-1826.
39. Webb BA, Karl Compton K, Castañeda Saldaña R, Arapov TD, Keith Ray W, Helm RF, Scharf BE. 2017. *Sinorhizobium meliloti* chemotaxis to quaternary ammonium compounds is mediated by the chemoreceptor McpX. Mol Microbiol 103:333-346.

40. Webb BA, Helm RF, Scharf BE. 2016. Contribution of individual chemoreceptors to S*inorhizobium meliloti* chemotaxis towards amino acids of host and nonhost seed exudates. Mol Plant Microbe Interact 29:231-239.
41. Webb BA, Hildreth S, Helm RF, Scharf BE. 2014. *Sinorhizobium meliloti* chemoreceptor McpU mediates chemotaxis toward host plant exudates through direct proline sensing. Appl Environ Microbiol 80:3404-3415.
42. Webb BA, Compton KK, del Campo JSM, Taylor D, Sobrado P, Scharf BE. 2017. *Sinorhizobium meliloti* chemotaxis to multiple amino acids is mediated by the chemoreceptor McpU. Mol Plant Microbe Interact 30:770-777.
43. Compton KK, Hildreth SB, Helm RF, Scharf BE. 2018. *Sinorhizobium meliloti* chemoreceptor McpV senses short-chain carboxylates via direct binding. J Bacteriol 200:e00519-18.
44. Sourjik V, Schmitt R. 1996. Different roles of CheY1 and CheY2 in the chemotaxis of *Rhizobium meliloti*. Mol Microbiol 22:427-436.
45. Riepl H, Maurer T, Kalbitzer HR, Meier VM, Haslbeck M, Schmitt R, Scharf B. 2008. Interaction of CheY2 and CheY2-P with the cognate CheA kinase in the chemosensory-signalling chain of *Sinorhizobium meliloti*. Mol Microbiol 69:1373-1384.
46. Sourjik V, Schmitt R. 1998. Phosphotransfer between CheA, CheY1, and CheY2 in the chemotaxis signal transduction chain of *Rhizobium meliloti*. Biochemistry 37:2327-2335.
47. Dogra G, Purschke FG, Wagner V, Haslbeck M, Kriehuber T, Hughes JG, Van Tassell ML, Gilbert C, Niemeyer M, Ray WK. 2012. *Sinorhizobium meliloti* CheA complexed with CheS exhibits enhanced binding to CheY1, resulting in accelerated CheY1 dephosphorylation. J Bacteriol 194:1075-1087.
48. Amin M, Kothamachu VB, Feliu E, Scharf BE, Porter SL, Soyer OS. 2014. Phosphate sink containing two-component signaling systems as tunable threshold devices. PLoS Comput Biol 10:e1003890-e1003890.
49. Glekas GD, Plutz MJ, Walukiewicz HE, Allen GM, Rao CV, Ordal GW. 2012. Elucidation of the multiple roles of CheD in *Bacillus subtilis* chemotaxis. Mol Microbiol 86:743-56.
50. Li M, Hazelbauer GL. 2004. Cellular stoichiometry of the components of the chemotaxis signaling complex. J Bacteriol 186:3687-94.
51. Cannistraro VJ, Glekas GD, Rao CV, Ordal GW. 2011. Cellular stoichiometry of the chemotaxis proteins in *Bacillus subtilis*. J Bacteriol 193:3220-7.
52. Zatakia HM, Arapov TD, Meier VM, Scharf BE. 2018. Cellular stoichiometry of methyl-accepting chemotaxis proteins in *Sinorhizobium meliloti*. J Bacteriol 200.
53. Levin MD, Morton-Firth CJ, Abouhamad WN, Bourret RB, Bray D. 1998. Origins of individual swimming behavior in bacteria. Biophys J 74:175-81.
54. Galibert F, Finan TM, Long SR, Pühler A, Abola P, Ampe F, Barloy-Hubler F, Barnett MJ, Becker A, Boistard P, Bothe G, Boutry M, Bowser L, Buhrmester J, Cadieu E, Capela D, Chain P, Cowie A, Davis RW, Dréano S, Federspiel NA, Fisher RF, Gloux S, Godrie T, Goffeau A, Golding B, Gouzy J, Gurjal M, Hernandez-Lucas I, Hong A, Huizar L, Hyman RW, Jones T, Kahn D, Kahn ML, Kalman S, Keating DH, Kiss E, Komp C, Lelaure V, Masuy D, Palm C, Peck MC, Pohl TM, Portetelle D, Purnelle B, Ramsperger U, Surzycki R, Thébault P, Vandenbol M, et al. 2001. The composite genome of the legume symbiont *Sinorhizobium meliloti*. Science 293:668-672.

55. Rotter C, Mühlbacher S, Salamon D, Schmitt R, Scharf B. 2006. Rem, a new transcriptional activator of motility and chemotaxis in *Sinorhizobium meliloti*. J Bacteriol 188:6932-6942.
56. Wood DW, Setubal JC, Kaul R, Monks DE, Kitajima JP, Okura VK, Zhou Y, Chen L, Wood GE, Almeida NF, Jr., Woo L, Chen Y, Paulsen IT, Eisen JA, Karp PD, Bovee D, Sr., Chapman P, Clendenning J, Deatherage G, Gillet W, Grant C, Kutyavin T, Levy R, Li MJ, McClelland E, Palmieri A, Raymond C, Rouse G, Saenphimmachak C, Wu Z, Romero P, Gordon D, Zhang S, Yoo H, Tao Y, Biddle P, Jung M, Krespan W, Perry M, Gordon-Kamm B, Liao L, Kim S, Hendrick C, Zhao ZY, Dolan M, Chumley F, Tingey SV, Tomb JF, Gordon MP, Olson MV, et al. 2001. The genome of the natural genetic engineer *Agrobacterium tumefaciens* C58. Science 294:2317-23.
57. Boukhvalova MS, Dahlquist FW, Stewart RC. 2002. CheW binding interactions with CheA and Tar importance for chemotaxis signaling in *Escherichia coli*. J Biol Chem 277:22251-22259.
58. Bourret RB, Davagnino J, Simon MI. 1993. The carboxy-terminal portion of the CheA kinase mediates regulation of autophosphorylation by transducer and CheW. J Bacteriol 175:2097-2101.
59. Piñas GE, Frank V, Vaknin A, Parkinson JS. 2016. The source of high signal cooperativity in bacterial chemosensory arrays. Proc Natl Acad Sci U S A 113:3335-3340.
60. Dai X, Shen Z, Wang Y, Zhu M. 2018. *Sinorhizobium meliloti*, a slow-growing bacterium, exhibits growth rate dependence of cell size under nutrient limitation. mSphere 3:e00567-18.
61. Grantcharova N, Peters V, Monteiro C, Zakikhany K, Römling U. 2010. Bistable expression of CsgD in biofilm development of *Salmonella enterica* serovar typhimurium. J Bacteriol 192:456-466.
62. Huang Z, Zhou Q, Sun P, Yang J, Guo M. 2018. Two *Agrobacterium tumefaciens* CheW proteins are incorporated into one chemosensory pathway with different efficiencies. Mol Plant Microbe Interact 31:460-470.
63. Bhatnagar J, Borbat PP, Pollard AM, Bilwes AM, Freed JH, Crane BR. 2010. Structure of the ternary complex formed by a chemotaxis receptor signaling domain, the CheA histidine kinase, and the coupling protein CheW as determined by pulsed dipolar ESR spectroscopy. Biochemistry 49:3824-3841.
64. Cassidy CK, Himes BA, Alvarez FJ, Ma J, Zhao G, Perilla JR, Schulten K, Zhang P. 2015. CryoEM and computer simulations reveal a novel kinase conformational switch in bacterial chemotaxis signaling. Elife 4:e08419.
65. Yang W, Alvarado A, Glatter T, Ringgaard S, Briegel A. 2018. Baseplate variability of *Vibrio cholerae* chemoreceptor arrays. Proc Natl Acad Sci U S A 115:13365-13370.
66. Yang W, Briegel A. 2019. Diversity of bacterial chemosensory arrays. Trends Microbiol.
67. Sourjik V, Sterr W, Platzer J, Bos I, Haslbeck M, Schmitt R. 1998. Mapping of 41 chemotaxis, flagellar and motility genes to a single region of the *Sinorhizobium meliloti* chromosome. Gene 223:283-290.
68. Wuichet K, Zhulin IB. 2010. Origins and diversification of a complex signal transduction system in prokaryotes. Sci Signal 3:ra50-ra50.
69. Rao CV, Glekas GD, Ordal GW. 2008. The three adaptation systems of *Bacillus subtilis* chemotaxis. Trends Microbiol 16:480-487.

70. Moon KH, Hobbs G, Motaleb MA. 2016. *Borrelia burgdorferi* CheD promotes various functions in chemotaxis and the pathogenic life cycle of the spirochete. Infect Immun 84:1743-1752.
71. Blat Y, Eisenbach M. 1996. Oligomerization of the phosphatase CheZ upon interaction with the phosphorylated form of CheY The signal protein of bacterial chemotaxis. J Biol Chem 271:1226-1231.
72. Park S-Y, Chao X, Gonzalez-Bonet G, Beel BD, Bilwes AM, Crane BR. 2004. Structure and function of an unusual family of protein phosphatases: the bacterial chemotaxis proteins CheC and CheX. Mol Cell 16:563-574.
73. Hauwaerts D, Alexandre G, Das SK, Vanderleyden J, Zhulin IB. 2002. A major chemotaxis gene cluster in *Azospirillum brasilense* and relationships between chemotaxis operons in α-proteobacteria. FEMS Microbiol Lett 208:61-67.
74. Krupski G, Götz R, Ober K, Pleier E, Schmitt R. 1985. Structure of complex flagellar filaments in *Rhizobium meliloti*. J Bacteriol 162:361-366.
75. Bertani G. 1951. Studies on lysogenesis I.: the mode of phage liberation by lysogenic *Escherichia coli*. J Bacteriol 62:293.
76. Scharf B, Schuster-Wolff-Bühring H, Rachel R, Schmitt R. 2001. Mutational analysis of the R*hizobium lupini* H13-3 and *Sinorhizobium meliloti* flagellin genes: importance of flagellin A for flagellar filament structure and transcriptional regulation. J Bacteriol 183:5334-5342.
77. Götz R, Limmer N, Ober K, Schmitt R. 1982. Motility and chemotaxis in two strains of *Rhizobium* with complex flagella. Microbiology 128:789-798.
78. Simon R, O'connell M, Labes M, Pühler A. 1986. Plasmid vectors for the genetic analysis and manipulation of rhizobia and other gram-negative bacteria, p 640-659, Methods Enzymol, vol 118. Elsevier.
79. Simon R, Priefer U, Pühler A. 1983. A broad host range mobilization system for in vivo genetic engineering: transposon mutagenesis in gram negative bacteria. Bio/technology 1:784-791.
80. Sievers F, Wilm A, Dineen D, Gibson TJ, Karplus K, Li W, Lopez R, McWilliam H, Remmert M, Soding J, Thompson JD, Higgins DG. 2011. Fast, scalable generation of high-quality protein multiple sequence alignments using Clustal Omega. Mol Syst Biol 7:539.
81. Pleier E, Schmitt R. 1991. Expression of two *Rhizobium meliloti* flagellin genes and their contribution to the complex filament structure. J Bacteriol 173:2077-2085.
82. Schäfer A, Tauch A, Jäger W, Kalinowski J, Thierbach G, Pühler A. 1994. Small mobilizable multi-purpose cloning vectors derived from the *Escherichia coli* plasmids pK18 and pK19: selection of defined deletions in the chromosome of *Corynebacterium glutamicum*. Gene 145.

FIGURES

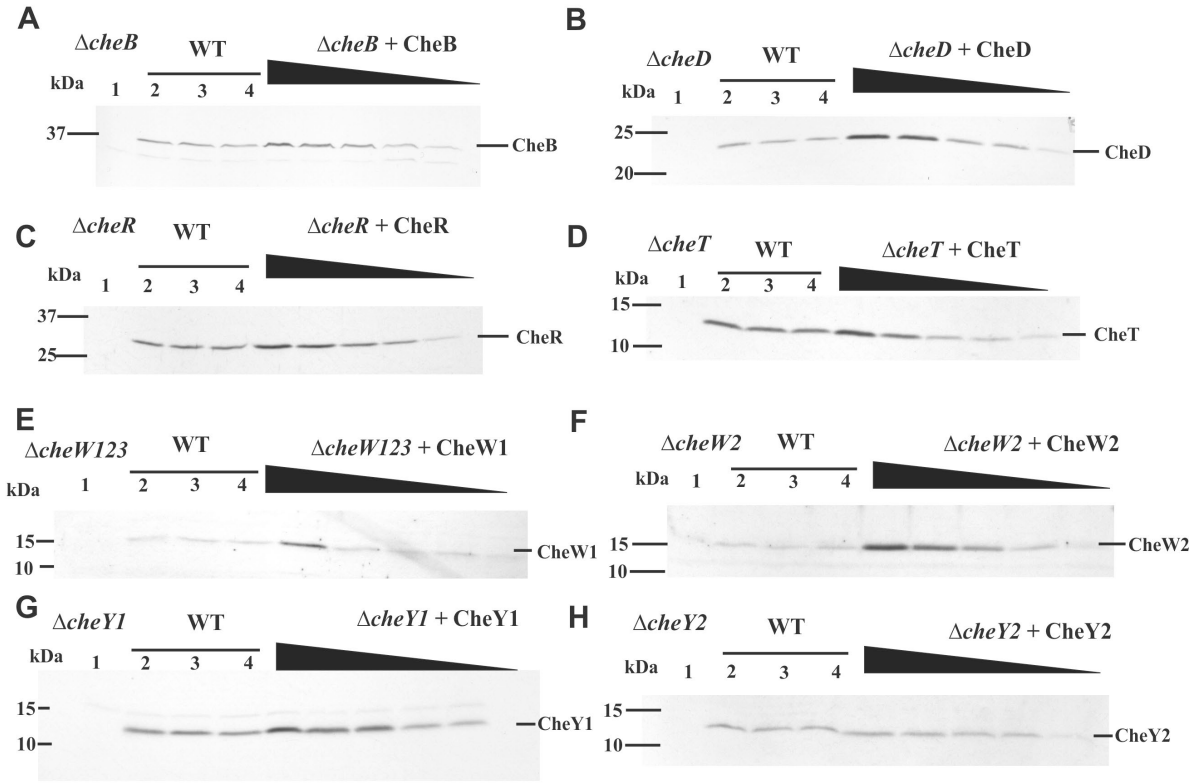

Figure 3.1 Representative immunoblots used to quantify chemotaxis proteins. For each panel, lane 1 contains cell lysate of the respective deletion strain from 1 ml culture at OD_{600} 0.25, lanes 2 – 4 contain RU11/001 (WT) cell lysates from 1 ml of culture at an OD_{600} of 0.25, and lanes 5 – 9 contain different amounts of purified protein to be quantified mixed with cell lysates of the respective deletion strain, as indicated. **A.** (3, 2.5, 1.5, 1, and 0.5 ng CheB mixed with RU11/312 cell lysates. **B.** 16, 13, 9, 6, and 3 ng CheD mixed with RU11/312 cell lysates **C.** 7.5, 6, 4.5, 3, and 1.5 ng CheR mixed with RU11/306 cell lysates. **D.** 7, 5, 3, 1, and 0.5 ng McpV-LBD-3xFLAG mixed with RU11/001 cell lysates. **E.** 0.3, 0.2, 0.1, 0.075, and 0.050 ng CheT mixed with RU11/319 cell lysates. **F.** 2, 1.5, 1, 0.5, and 0.25 ng CheW1 mixed with BS198 cell lysates.

G. 0.9, 0.7, .5, 0.3, and 0.17 ng CheW2 mixed with RU11/811 cell lysates. **H.** 12, 10.5, 7.8, 6.4, and 5 ng CheY1 mixed with RU11/816 cell lysates. **I.** 12, 9.6, 6.4, 5.1, and 3.2 ng CheY2 mixed with RU11/307 cell lysates.

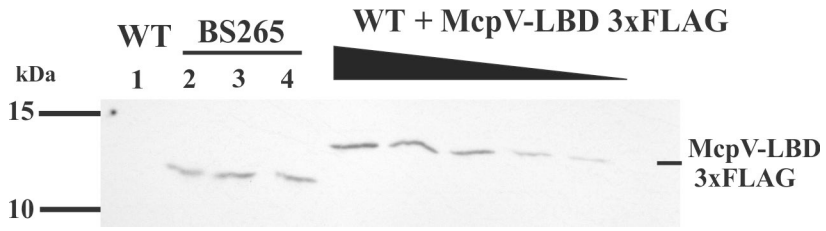

Figure 3.2 Representative immunoblot used to quantify 3xFLAG-CheS . Lane 1 (WT) contains RU11/001 cell lysate from 1 ml culture at an OD_{600} of 0.25. Lanes 2 - 4 contain BS265 cell lysates from 1 ml of culture at an OD_{600} of 0.25. WT + McpV-LBD 3xFLAG lanes contain purified McpV-LBD-3xFLAG (7, 5, 3, 1, and 0.5 ng) mixed with RU11/001 cell lysates.

A

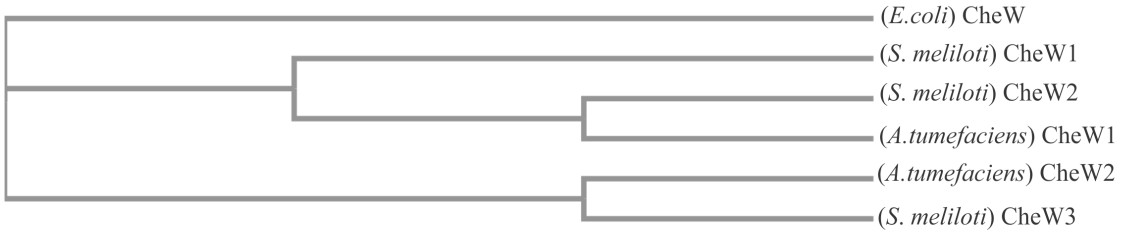

B

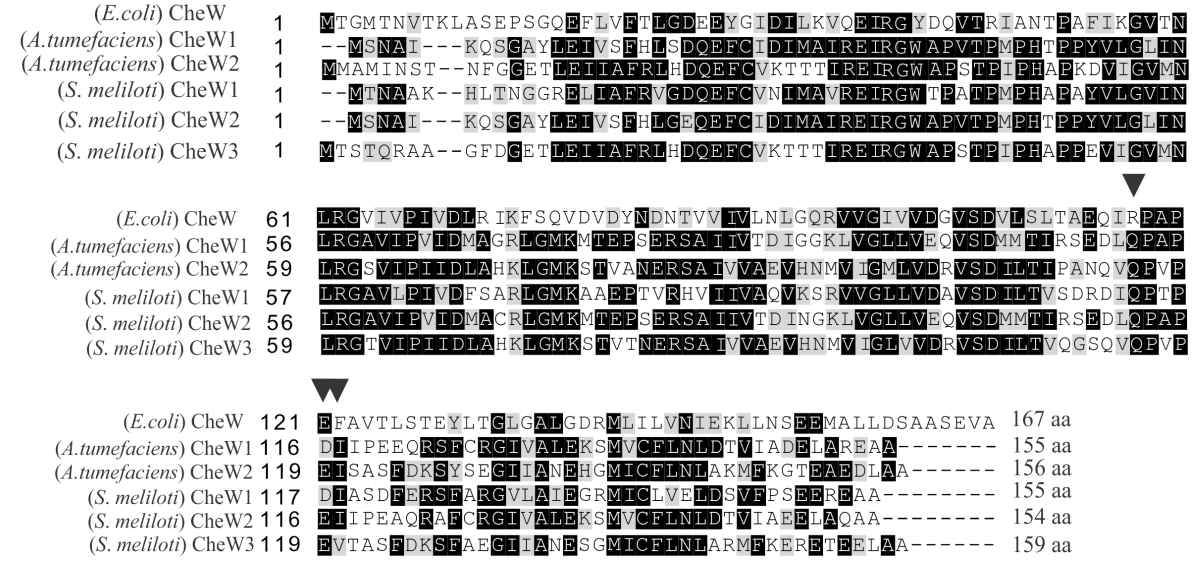

Figure 3.3 Relationship analysis and sequence alignment of CheW proteins from various bacterial species . **A.** Cladogram illustrating the relationship between *E. coli* K-12 CheW (NP_416401.1), *A. tumefaciens* CheW1 (NP_355040.2) and CheW2 (NP_355554.2), and *S. meliloti* CheW1 (WP_014528989.1), CheW2 (WP_003536237.1), and CheW3 (WP_003528560.1). **B.** Multiple sequence alignment of *E. coli* CheW, *A. tumefaciens* CheW1, CheW2, and *S. meliloti* CheW1, CheW2, and CheW3. Arrows denote residues involved in the interaction with the P5 domain of CheA using *E. coli* as paradigm model. White, light grey, black shading indicates identity among zero, two and three or more sequences respectively.

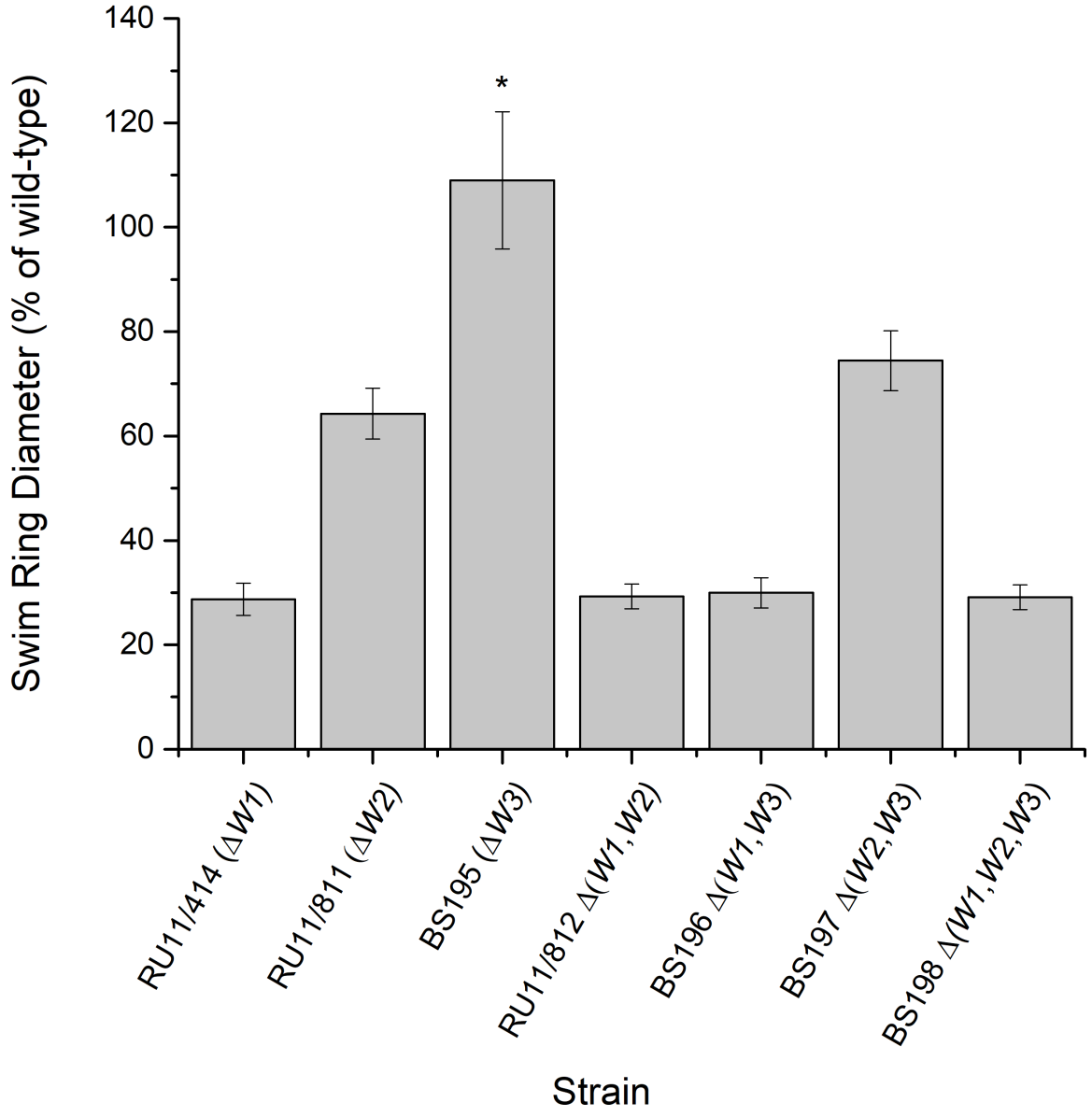

Figure 3.4 Chemotactic responses of various *S. meliloti cheW* mutant strains in a quantitative swim plate assay compared to the wild-type strain . Strain designation: ΔW1 in-frame deletion of *cheW1* (RU11/414), ΔW2 in-frame deletion of *cheW2* (RU11/811), ΔW3 in-frame deletion of *cheW3* (BS195), Δ(W1, W2) in-frame deletions of *cheW1* and *cheW2* (RU11/812), Δ(W1 W3)

in-frame deletions of *cheW1* and *cheW3*, (BS196), Δ(W2 W3) in-frame deletions of *cheW2* and *cheW3* (BS197), Δ(W1, W2, W3) in-frame deletions of *cheW1*, *cheW2,* and *cheW3 (*BS198). Percentages of the wild-type swim diameter on 0.3% Bromfield agar are the means of seven replicates. Error bars represent the standard deviations from the mean. Statistical significance was determined by a two-tailed Student's T-test ($p < 0.05$). Asterisk symbol denotes no statistically significant difference from the wild-type.

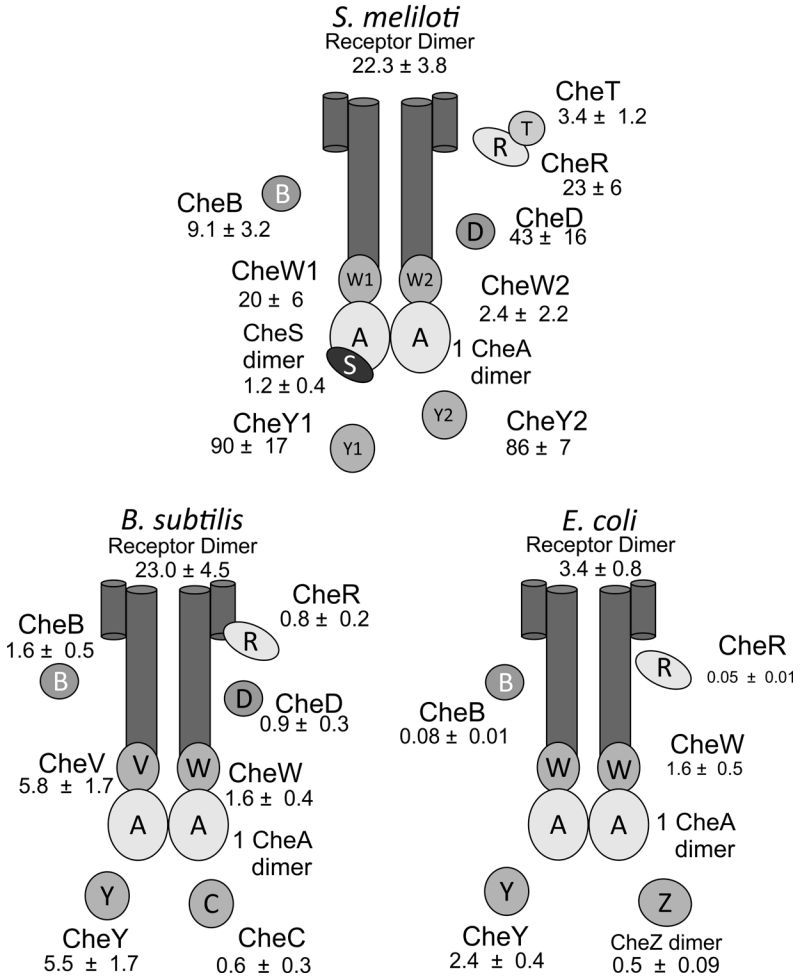

Figure 3.5 Cartoon of *in vivo* stoichiometries in *S. meliloti, B*. *subtilis*, and *E*. *coli* signaling complexes . Shown are the cellular stoichiometries of the chemotaxis signaling proteins in this

study, receptor ratios previously published for *S. meliloti*, and previously reported ratios from *E. coli* and *B. subtilis* (50-52) .Models are normalized to show the cellular ratios to a CheA dimer in each species.

Chapter 4 Features in the C-terminal region control McpU degradation in *Sinorhizobium meliloti*

TIMOFEY D. ARAPOV[1], JIWOO KIM[2], RACHEL M. CRONIN[a], MAYA PAHIMA[b], BIRGIT E. SCHARF[1]

[1]Department of Biological Sciences, Life Sciences I, Virginia Tech, Blacksburg, VA 24061, USA

[2]Department of Biochemistry, Virginia Tech, Blacksburg, VA 24061, USA

Running title: C-terminal extension prevents degradation of McpU

Key words: alphaproteobacteria, cell cycle, chemotaxis, ClpXP protease, epitope tags

*For correspondence:

E-mail bscharf@vt.edu

Tel (+1) 540 231 0757

Fax (+1) 540 231 4043

Biological Sciences, Life Sciences I

Virginia Tech

Blacksburg, VA 24061, USA

[a]Present Address: Department of Biological Sciences, University of Notre Dame, 100 Galvin Life Science Center, Notre Dame, IN 46556; rcronin1@nd.edu

[b]Present Address: Icahn School of Medicine at Mount Sinai, NY 10029; maya.pahima@icahn.mssm.edu

Attribution: TDA was responsible for design of expirements and generated Figure 4.1, Figure 4.4 and Figure 4.5. JK, RMC, MP contributred to data in Figure 4.2 and Figure 4.3 and summarized in Figure 4.4. JK generated data in Figure 4.6. TDA and BES generated. Final manuscript was draft by TDA and BES.

ABSTRACT

Chemotaxis and motility are important traits supporting bacterial survival in various ecological niches and in pathogenic and symbiotic host interaction. Chemotactic stimuli are sensed by chemoreceptors or Methyl-accepting Chemotaxis Proteins (MCPs), which direct the swimming behavior of the bacterial cell. In this study, we present evidence that the cellular abundance of chemoreceptors in the plant-symbiont *Sinorhizobium meliloti* can be altered by the addition of several to as little as one amino acid residue, and including common epitope tags such as 3xFLAG and 6xHis to their C-termini. To further dissect this phenomenon and its underlying molecular mechanism, we focused on a detailed analysis of the amino acid sensor McpU. We hypothesized that enhanced stability is due to interference with protease binding, thus affecting proteolytic efficacy. We defined the location of the protease recognition site through McpU stability measurements in a series of deletion and amino acid substitution mutants. Deletions in the putative protease recognition site had similar effects on McpU abundance than extensions at the C-terminus. Controlled proteolysis is important for the maintenance of an appropriate stoichiometry of chemoreceptors and between chemoreceptors and chemotactic signaling proteins, which is essential for an optimal chemotactic response. In addition, our work revealed that C-terminal fusions of epitope tags, which are often used for protein quantification, resulted in stabilization. This inevitably affects accurate quantification and could yield false results, not only in *S. meliloti* but also in other bacterial systems. Thus, researchers are warned to take precautionary measurement when using epitope tags for protein quantification.

INTRODUCTION

A number of bacterial species can transition between motile and sessile life styles. Factors that influence this behavior include nutrient availability, cell density, the presence of solid surfaces or their eukaryotic hosts (1-5). Many bacteria use flagella for motility to travel within their environment. By controlling flagellar rotational mode, bacteria can move towards beneficial attractants and away from detrimental repellents, a process called chemotaxis (6).

Sinorhizobium meliloti is a soil dwelling alphaproteobacterium that has the ability to live freely in the soil, in a biofilm on the surface of plants roots, or as differentiated bacteroid within specialized root organs called nodules (7, 8). The symbiosis of *S. meliloti* with select legumes involves multiple developmental changes, leading to the final development of nitrogen-fixing bacteroids (8-10). Biological nitrogen fixation provides the host plant with ammonia, which greatly promotes plant growth. Before the symbiotic relationship can be initiated, the bacterial symbiont uses chemotaxis to sense chemical compounds exuded by the host, moves towards host roots and colonizes them (11). The chemotaxis process is mediated by a two-component signaling system using Methyl-accepting Chemotaxis Proteins (MCPs) as chemoreceptors (for recent reviews see Wadhams *et al*. (6), Porter *et al.* (12) ,Hazelbaur *et al.*(13) and Salah Ud-Din *et al.* (14)). Typically, MCPs are integral membrane proteins with a periplasmic ligand binding domain (LBD), two transmembrane helices, and a cytoplasmic signaling domain. The LBDs are highly variable between receptors, which is reflected in a diverse set of ligands (14, 15). In contrast, the cytoplasmic domains are highly conserved allowing them to interact with the same set of proteins in the cytoplasm. MCPs assemble into a highly organized array architecture at the cell poles that allows for cooperativity between receptors within the chemotaxis system (16, 17). Binding of a ligand to the LBD changes the conformation of the MCP thereby altering the activity of the

histidine autokinase CheA. Phosphorylated CheA transfers its phosphate group to the response regulator CheY, which interacts with components of the flagellar motor. This alters its rotational mode, resulting in a change in swimming behavior.

Since the motility and chemotaxis machinery is not required during sessile life or *in planta*, protein production and degradation in *S. meliloti* are strictly regulated (18-20). One of the most important regulators in this transcriptional hierarchy is Rem. This OmpR-like protein is a class IB regulator, controlled by the LuxR-type master regulator VisNR (class IA) and is only synthesized during the exponential growth phase (18, 19). Rem controls expression of class II motility genes, which dictate if class III genes are expressed. Class III genes are responsible for assembly of the flagellum and the chemotaxis machinery (11, 19). It is vital for bacterial survival that cellular differentiation processes and cell cycle regulation are closely linked. Thus, the cell cycle master regulator CtrA indirectly regulates the majority of genes involved in chemotaxis and motility, and also directly controls four MCPs and three flagellin-encoding genes (21).

Involvement of the cell cycle regulatory network in cell differentiation and expression of motility genes appears to be manifested in alphaproteobacteria (22-25). For *S. meliloti*, proper timing of the cell cycle is critical to its symbiosis (26-28). CtrA is present at high levels in free-living *S. meliloti* cells, but at very low levels in bacteroids. Since CtrA is a key protein in cell cycle progression, its cellular abundance is not only regulated on the transcriptional level but also post-translationally through proteolysis. While *ctrA* is an essential gene in *S. meliloti*, mutations prohibiting CtrA proteolysis are also lethal (29, 30). In *Caulobacter crescentus,* a fresh-water alphaproteobacterium with a motile and a sessile lifestyle, CtrA is regulated through targeted proteolysis upon the onset of DNA replication by ClpXP (31). In addition, CtrA-dependent proteins in *C. crescentus* such as the chemoreceptors McpA and McpB are also targets of ClpXP

and are degraded during the course of the cell cycle (32, 33). Furthermore, the degradation of proteins in *C. crescentus* is spatially organized through the regulatory protein CpdR, which controls polar localization of the protease (26, 34).

The protease ClpXP is strictly required for growth and normal cell division in *C. crescentus*, and ClpX has been shown to also be essential in *S. meliloti* (20, 26, 35). This ubiquitous AAA+ protease uses ATP binding and hydrolysis to degrade proteins within the cell. ClpX targets unstructured peptide tags also called degrons, unfolds the target protein into a useable substrate, and delivers it to ClpP, which hydrolyzes the unfolded chain. ClpXP is studied as model for other AAA+ proteases like ClpAP, ClpCP, and HslUV (36). Degrons for ClpXP can be found on both the N- and C-terminus of mature proteins. One well-characterized degron is the SsrA tag in *Escherichia coli*, which is 11 amino acids in length. Two C-terminal alanine residues in the SsrA-degron allow for binding of ClpX (36, 37). Several bacterial species use ClpXP to degrade chemotaxis-related proteins, such as CtrA, McpA, and McpB in *C. crescentus*, and CheW in *E. coli* and *Bacillus subtilis* (38-40). *C. crescentus* McpA and McpB both possess hydrophobic regions characterized by alanine residues near the C-terminus, which are commonly found in degrons (32, 33, 41). However, little is known about the degradation of chemotaxis and flagellar proteins by ClpXP in *S. meliloti*, with the exception of one study that has identified flagellar proteins associated with ClpXP through coimmunoprecipitation experiments. The same study reported a link between CtrA and the protease HslUV (20).

In this work, we provide evidence that chemotaxis proteins in *S. meliloti* undergo proteolysis through protease recruitment by specific recognition sites near their C-terminus. Using a combinatory approach of quantitative immunoblot assays and targeted mutagenesis, we showed that the C-terminal fusion of epitope tags frequently used for protein detection as well as the

addition of single amino acid residues enhance the stability of chemotaxis proteins. Focusing on the amino acid receptor McpU, we further dissected and defined the protease recognition site near the C-terminus. Knowledge accrued from this study will aid in a better understanding of the regulation of the chemotaxis machinery and inform future research using epitope tags for cellular protein quantification in alphaproteobacteria.

RESULTS

C-terminal fusion of commonly used epitope tags increases the abundance of McpU in *S. meliloti*

During our analysis of chemoreceptor stoichiometry in *S. meliloti* (42), we attempted to utilize epitope tags for the assisted quantification of individual MCPs. However, we observed that the fusion of a 3xFLAG-tag to the C-terminus of McpU, which adds 22 amino acid residues, substantially increased its abundance. To determine whether this phenomenon was specific to the 3xFLAG-tag, we constructed two more epitope tag strains, one expressing McpU with a 1xFLAG-tag (8 aa; BS222) and one with another commonly used tag, the 6xhistidine (6xhis)-tag (6 aa; BS220) (Fig. 1). In each case, abundance of McpU bearing a C-terminal epitope tag was greater than native McpU in the wild-type strain (RU11/001). Next, we used comparative immunoblotting with purified anti-McpU polyclonal antibodies to quantify the amount of McpU in each mutant strain. The McpU band intensity was either compared directly to the intensity of native McpU or mutant strain lysates were added to lysates of an *mcpU* deletion strain (RU11/828) in known ratios (Figs. 2, 3). This experimental approach kept the amount of cellular material in each cell lysate constant, which prevented the overestimation of McpU in mutant strains (43). The increase in McpU abundance was expressed as a fold change compared to the amount of McpU in wild type (Fig. 4). All three tags significantly increased the amount of McpU; the 3xFLAG and 6xhis-tag increased abundance 6.0-fold and the 1xFLAG-tag caused an 8.2-fold increase over that of the wild type.

Addition of the single amino acid residues histidine or alanine but not glycine increases McpU abundance

To test if less extensive modifications such as single amino acid additions would elicit an increase in McpU abundance, three mutant strains were constructed that added a single histidine (BS252), alanine (BS257), or glycine residue (BS258) to the C-terminus of McpU (Fig. 1). BS252 and BS257 both exhibited a significant increase in McpU abundance, by 4.7- and 3.2-fold, respectively (Fig. 3). Contrary, BS258 displayed no significant difference in McpU abundance (Fig. 2). In conclusion, changes of the C-terminus as minor as the addition of an individual amino acid residue can increase McpU stability. However, it appears that the size and/or nature of the modification is important, as the addition of an amino acid without side chain did not alter McpU abundance.

Deciphering the putative protease recognition site in the C-terminal domain of McpU

Evidence from McpU epitope-tag fusions and single amino acid additions suggested that the C-terminus of McpU is critical in controlling its abundance, which determined that the protein is specifically targeted by a protease. To decipher the mechanism of target recognition, we identified three potential protease recognition sites based on evidence from McpA and McpB in *C. crescentus* and known *E. coli* degrons (44). In *C. crescentus* McpA and McpB, a short, alanine-rich motif is required for its degradation by ClpXP (32, 33). We found two such putative protease recognition motifs in the C-terminal domain of McpU, namely motif I (AAL) and motif II (AAS) (Fig. 1). In analogy to Tsai & Alley (2001) (33), both motifs were mutated to 'ELD', resulting in mutant strains BS268 and BS270. A third motif, named Motif III (AA) encompassing the last two residues, was mutated to 'DD' (BS272) (Fig. 1). While motif I and II variants were less (0.2-fold) or equally (1.5-fold) stable than wild-type McpU, the motif III variant exhibited a small, but significant

increase in protein abundance by about 2.2-fold (Fig. 2A). However, the increase was about three times smaller than that of the maximally stabilizing tag-fusion variants (Fig. 3). Finally, we tested whether a combination of the motif III variant with the 3xFLAG-epitope fusion had an additive effect on McpU stability (BS273), but this was not the case. The di-alanine mutation in combination with the 3xFLAG-tag increased McpU stability approximately to the same level as the 3xFLAG-epitope fusion alone (Fig. 3). In conclusion, the C-terminal di-alanine (di-ala peptide) is involved in McpU degradation, while the two other putative protease recognition sites are not.

Identifying regions in the C-terminal domain affecting McpU stability

Since specific mutations in the three protease recognition sites had no or only a moderate effect on McpU stability, we hypothesized that additional residues within these regions contribute to protease recognition. To test this theory, we deleted regions within the C-terminal domain of McpU. In analogy to the *C. crescentus* MS-ring protein FliF, regions were chosen to encompass the three di-alanine containing motifs putatively associated with proteolysis (32, 33, 45). Initially, three mutant strains were created expressing variants of McpU that were C-terminally truncated by 9 (Δ aa 699-707; BS266), 25 (Δ aa 683-707; BS267), or 39 (Δ aa 668-707; BS269) amino acid residues (Fig. 1). The abundance of McpU truncated by 9 aa (BS266) was 6.6-fold increased, which was comparable to that of epitope-tagged mutants. However, truncating McpU by 25 aa increased its abundance by only 3.2-fold, while a 39-aa truncation yielded a protein that was just 1.8-fold more abundant than wild-type McpU (Figs. 2, 4). These results indicate that the last 9 residues play a central role in McpU stability. To further decipher the putative protease recognition site, we deleted 16 aa preceding the 9 most C-terminal aa (Δ aa 683-698; BS271). Interestingly, the modification resulted in a 0.14-fold decrease in McpU abundance. (Figs. 2, 3). It is conceivable

to speculate that this 16-aa region contains features supporting McpU stability, which would explain the gradually decreased stability of McpU lacking the most C-terminal 25 or 39 aa, compared to a 9-aa truncation. However, it cannot be excluded that the internal 16-aa deletion disrupted secondary structure elements and thus proper folding of the mutated protein leading to its instability. To summarize, deleting the 9 most C-terminal residues including motif III (di-ala peptide) induced the most dramatic increase in McpU abundance suggesting that important determinants of the protease recognition site are contained in this region.

Effect of C-terminal 3xFLAG-tag fusions on the abundance of four additional chemoreceptors and the coupling protein CheW1

We next asked the question whether the positive effect of epitope-tags on protein stability was unique to the *S. meliloti* chemoreceptor McpU. Therefore, we chose two cytosolic chemoreceptors, McpY and IcpA, the high-abundance receptor McpV, and a receptor that was below the limit of detection, McpT (42), as well as the major receptor-CheA coupling protein CheW1, for stability assays. We constructed strains through allelic exchange that encode proteins with C-terminal 3xFLAG-tag fusions in their native, chromosomal locus and quantified protein abundance in cell extracts as described above (Fig. 5A-D). Table 1 lists molecules per cell and the ratio between native and tagged proteins. Four of the five proteins were more abundant with the C-terminal epitope tag, with ratios varying from 2- to 45-fold. The change in abundance of McpT could only be estimated to be at least 210-fold because the amount of untagged protein was below the limit of detection (Table 1) (42). In contrast, a direct comparison of band intensities in cell extracts from strains expressing McpV or McpV-3xFLAG indicated the presence of very similar protein

amounts (Fig. 5E). In conclusion, the fusion of a C-terminal 3xFLAG-tag increases the *in vivo* abundance of at least four *S. meliloti* chemoreceptors and one chemotaxis protein.

Chemotaxis in strains with increased McpU abundance is unaltered

To investigate whether increased McpU abundance due to the addition of epitope-tags alters *S. meliloti* chemotaxis, we used low percentage agar swim plate assays with tryptone/yeast extract (Bromfield) and with defined Rhizobium Basal (RB) medium containing 10^{-4} M lysine. Lysine was chosen as carbon source as it is known to be a ligand for McpU (46, 47). As previously described, the deletion of *mcpU* (RU11/828) resulted in a reduced swim ring diameter (46, 48). Although McpU abundance increased 6- to 8-fold with C-terminal 3xFLAG and 6xHis-epitope tags (Fig. 3), swim ring diameters were either slightly reduced (BS207) or similar to wild type (BS220) (Fig. 6). The slight decrease in chemotaxis of BS207 with 3xFLAG-tagged McpU versus BS220 with 6xHis-tagged McpU might be due to the larger size of the 3xFLAG tag (22 aa). We had observed previously that a C-terminal fusion of EGFP to McpU caused a small reduction in swim ring size (49). In conclusion, abundance of McpU does not correlate with chemotactic performance.

DISCUSSION

Engineered peptide epitope tags are sensitively and specifically recognized by commercially available antibodies to facilitate the detection, localization, and purification of proteins (50). Although epitope tags typically do not disrupt normal protein functions, our study showed that they can alter protein stability in the chemotaxis system of *S. meliloti*. Proteolysis is an important process in all living cells, which allows for a fast but irreversible response to a changing environment. As a result, it is tightly controlled. Contributing proteases are known to bind and degrade only a subset of protein substrates (51). We documented that introduction of epitope tags to the C-terminus of several *S. meliloti* chemotaxis proteins effectively disrupted normal *in vivo* proteolysis.

The role of the C-terminal domain in McpU degradation

Addition of charged epitope tags and single aa residues to the C-terminus of McpU increased abundance of the protein up to 8-fold. Larger and charged tags had a greater effect on abundance than single aa, and larger and charged aa greater than smaller ones (+ his>ala>gly). A similar effect has been described for *C. crescentus* FliF (52). We therefore hypothesize that charged amino acids abolish degradation by blocking access of the protease to the hydrophobic degradation signal. This is supported by the fact that the addition of glycine, which lacks a side chain, did not stabilize McpU (Fig. 2). The presence of a hydrophobic degradation signal containing an AAL or AVA motif has been reported for *C. crescentus* McpA and McpB (32, 33). Of the three putative motifs in McpU, only mutations of the C-terminal di-ala peptide affected McpU stability (Figs. 2, 3). The importance of this motif for protein stability in conjunction with residues in the preceding region allowed the conclusion that a protease recognition site exists in the C-terminal domain of McpU.

Yet, it is unclear which exact residues are critical for recognition. Deletion of the di-ala peptide together with the preceding 7-aa region is sufficient to promote protein stability, a result that is in agreement with the degradation scheme of *C. crescentus* FliF (52). However, we cannot dismiss the possibility that additional residues in the larger aliphatic C-terminal region of McpU are contributing to an extended protease recognition site. Analyses of targeted protein degradation in *E. coli* and *C. crescentus* suggest that the terminal di-ala peptide in McpU could be part of a larger SsrA-degron like motif (37, 53). ClpXP as well as other proteases such as HslUV are known to bind to the 11-aa SsrA motif (20, 54). A di-ala peptide motif is present in the C-terminal domain of *S. meliloti* and *C. crescentus* CtrA and is important for its ClpXP-dependent proteolysis (27, 45). The nature of the degradation signal does not seem to be based on a distinct primary sequence. Rather, ClpXP appears to recognize short clusters of aliphatic residues in the hydrophobic, disordered C-terminal domain of McpU, similar to *C. crescentus* FliF (52).

Effect of epitope tags on other *S. meliloti* chemotaxis proteins

The presence of C-terminal epitope-tags impacted not only the stability of McpU but four of the five *S. meliloti* chemotaxis proteins assayed. The abundance of McpT, McpY, IcpA, and CheW1 was increased to varying degrees between 2-fold (CheW1) and an estimated 210-fold (McpT) when a 3xFLAG-tag was fused to their respective C-termini (Fig. 5, Table 2). An alignment of the C-terminal domains revealed that only CheW1 possesses a C-terminal di-ala peptide that was determined to mediate degradation of McpU (Fig. 7). However, the C-terminal domain of all analyzed proteins are rich in aliphatic residues (Fig. 7), which could explain their tendency to targeted proteolytic degradation. Additionally, we identified putative protease recognition sites near the C-terminus of McpY and McpT, analogous to *C. crescentus* McpA and McpB (Fig. 7). It

would be interesting to assess the molecular mechanisms for the differential degree of degradation of these *S. meliloti* chemotaxis proteins.

S. meliloti McpV stability and cell-cycle control

The only chemotaxis protein in our assay that did not significantly increase in abundance as a C-terminal 3xFLAG-tag fusion was McpV (Fig. 5, Table 1), although it terminates in a di-ala peptide and its C-terminal domain contains several other putative degradation motifs (Fig. 7). Interestingly, McpV is the most abundant MCP within the *S. meliloti* cell, accounting for approximately 70% of all MCPs (42). A study by Pini *et al.* (2015) (21) indicated that transcription of *mcpV* is not regulated by CtrA, while other chemoreceptor genes (*icpA*, *mcpT*, *mcpU*, *mcpX*, *mcpZ*) are under direct or indirect control of CtrA (21, 29). Commonly, proteins, which are encoded by genes in a regulon, under control of the same transcriptional regulator, are also degraded by a shared protease (44). For instance, *E. coli ftsZ*, *dps*, *katE*, and *glpD* are all transcribed under the control of σ^S, and their gene products, including σ^S are degraded by ClpXP (44). It is conceivable to propose that the lack of cell-cycle related control of *mcpV* transcription by CtrA exempts it from the proteolytic mechanism governing the other receptors, which would explain its high abundance. In *C. crescentus* and related alphaproteobacteria, a complex proteolytic hierarchy exists allowing for targeted degradation of proteins (55). In *S. meliloti*, motility and chemotaxis are limited to early exponential growth. Thus, transcriptional and post-translational regulatory controls are in place to negatively regulate the chemotaxis machinery at later stages of growth (18, 49). We envision a mechanism in the *S. meliloti* chemotaxis system to selectively target a subset of receptors for proteolysis. At this point, however, it is challenging to make predictions based on primary sequences alone.

General conclusions on the use of epitope-tag fusions

Our present study asserts that the presence of C-terminal epitope tags disrupts cell-cycle regulated proteolysis in the chemotaxis system of *S. meliloti* and induces an accumulation of the tagged proteins. These results are supported by similar findings in another alphaproteobacterium, *C. crescentus* specifically the flagellar protein FliF (52). The *C. crescentus* receptor McpA has been widely used as a model substrate for protein degradation during the course of the *C. crescentus* cell cycle (34, 56, 57). Researchers interested in pursuing similar cell cycle experiments in *S. meliloti* or other alphaproteobacteria should be aware of the possible effect of epitope tags on their experimental outcomes. This could be particularly important when studying transient, spatiotemporal processes such as CpdR-mediated proteolysis (26, 56). Furthermore, we presented evidence that C-terminal fusion of a 3xFLAG-tag had differential effects on protein stability, spanning from no effect, to a several-fold and up to a several hundred-fold increase (Table 1). Our studies revealed the presence of a SsrA-like signal sequence in McpU. However, the prediction of specific protease recognition sites in other chemotaxis proteins appeared challenging. Therefore, we caution researchers on the use of epitope tags for the *in vivo* protein quantifications without the implementation of appropriate controls.

MATERIALS AND METHODS

Bacterial strains and plasmids

Derivatives of *E. coli* K12 and *S. meliloti* MV II-1 and the plasmids used are listed in Table 1. RU11/001 is a spontaneous streptomycin-resistant derivative of MVII-1 (58).

Media and growth conditions

E. coli strains were grown in lysogeny broth (LB) (59) at indicated temperatures. *S. meliloti* strains were grown in TYC (0.5 % tryptone, 0.3 % yeast extract, 0.13 % $CaCl_2$ $6xH_2O$ [pH 7.0]) (60) or SMM (*Sinorhizobium* motility medium; RB [6.1 mM K_2HPO_4, 3.9 mM KH_2PO_4, 1 mM $MgSO_4$, 1 mM $(NH_4)_2SO_4$, 0.1 mM $CaCl_2$, 0.1 mM NaCl, 0.01 mM Na_2MoO_4, 0.001 mM $FeSO_4$, 2 µg/l biotin, 10 µg/l thiamine] (61), 0.2 % mannitol, 2 % TY) or Bromfield medium (0.04% tryptone, 0.01% yeast extract, 0.01% $CaCl_2$ $2xH_2O$) (18). Motile cells for immunoblots were grown in SMM for two days, diluted to an OD_{600} of 0.02 and incubated at 30 °C to an OD_{600} of 0.25. The following antibiotics were used in their final concentrations: for *E. coli*, ampicillin at 100 µg/ml and kanamycin at 50 µg/ml; for *S. meliloti*, neomycin at 120 µg/ml and streptomycin at 600 µg/ml. *S. meliloti* cell culture used within the motility assays was grown in 3 ml TYC for two days at 30 °C.

Motility Assays

Swim plates (0.3% Bacto agar) containing Bromfield medium or RB minimal medium supplemented with lysine (10^{-4} M) were inoculated with 3 µl bacterial cell culture grown in TYC. Bromfield plates were incubated for three days and RB/lysine plates for 5 days, respectively, at 30 °C.

Genetic and DNA manipulations

S. meliloti mutants listed in Table 2 were created by allelic replacement essentially as laid out (42, 62, 63).

Purification of recombinant McpV-LBD-3xFLAG

McpV-LBD-3xFLAG was purified using the IMPACT (NEB) system. McpV-LBD-3xFLAG was expressed from pBS0459 in *E. coli* ER2566 essentially as described in *Zatakia et al.* (42). Expression was induced at an OD_{600} of 0.6 to 0.8 by addition of 0.3 mM isopropyl-β-D-thiogalactopyranoside (IPTG) and growth was continued at 16 °C for 16 hours. Cells were harvested, and suspended in IMPACT buffer (500 mM NaCl, 1 mM EDTA, 1 mM phenylmethylsulfonyl fluoride, 20 mM Tris-HCl, pH 8.0) and lysed by three passages through a French pressure cell at 20,000 lbs./in^2 (SLM Aminco, Silver Spring, MD). The cleared lysate was loaded on a chitin-agarose (New England Biolabs) column (6 cm x 5 cm), and Intein-mediated cleavage was induced by addition of IMPACT buffer with 50 mM dithiothreitol and incubation overnight at 4 °C. The protein was eluted with IMPACT buffer. Pooled protein fractions were then subject to size exclusion chromatography using a HiPrep 26/60 Sephacryl S-200 HR column (GE Healthcare). The column was developed in phosphate buffered saline (PBS; 100 mM NaCl, 80 mM Na_2HPO_4, 20 mM NaH_2PO_4, pH 7.5) with 5 % (vol/vol) glycerol. Protein concentrations were obtained by quantitative amino acid analyses after total acid hydrolysis performed at the Protein Chemistry Lab, Texas A&M University.

Immunoblotting

Polyclonal antibodies were raised against the ligand binding domain of McpU or McpV (McpU-LBD or McpV-LBD) and then subsequently purified as described in Scharf *et al.* (42, 60). Cell extracts were prepared as follows. Wild-type and deletion strains were grown in SMM to an OD_{600} of 0.25 ± 0.05. One ml aliquots were then pelleted by centrifugation at 21,000 x g for 10 min, suspended in approximately15 µl of the supernatant and 15 µl of Laemmli buffer (4.5 % SDS, 18.75 mM Tris/HCl pH 6.5, 43.5 % glycerol, 0.0125 % Bromophenol Blue, and 5 % β-mercaptoethanol). Samples were boiled for 10 min and stored at -20 °C. For the relative quantification of McpU abundance, mutant and deletion strains were grown to an OD_{600} of 0.25 ± 0.05, mixed in specified ratios prior to centrifugation and then treated as described above. Relative differences in abundance were derived from three biological replicates for each mutant. For the quantification of IcpA-3xFLAG, McpT-3xFLAG, McpY-3xFLAG, CheW1-3xFLAG in cell extracts, defined amounts of purified McpV-LBD-3xFLAG were added to wild-type extracts to create a standard curve. Means were derived from six biological replicates.

Blotting was performed in the same manner as described by Zatakia *et al.* (42). Cell extracts were separated by SDS-polyacrylamide gel electrophoresis and transferred onto 0.45 µm nitrocellulose membranes. Membrane were blocked overnight or for 2 h with 5 % non-fat dry milk in PBS/0.1 % Tween 20. Blots were probed with a 1:200 dilution of affinity-purified antibodies or a 1:20,000 dilution of monoclonal ANTI-FLAG® M2 antibody (Sigma-Aldrich). Blots were washed for 30 min with PBS/0.1 % Tween 20 with four buffer changes and then probed with a 1:1,500 dilution of donkey anti-rabbit polyclonal antibodies linked to horseradish peroxidase or a 1:4,000 dilution of sheep anti-mouse antibodies linked to horseradish peroxidase. The blots were then washed for 30 min with PBS/0.1 % Tween 20 with four buffer changes. Detection was performed by

chemiluminescence (Amersham ECL Western Blotting Detection Kit, GE Healthcare) using Hyperfilm ECL (GE Healthcare). Images were scanned with an Epson Perfection 160SU scanner, and pixel intensities were then quantified with ImageJ. The number of molecules per cell were calculated using the quantified number of cells per volume for *S. meliloti* previously determined in Zatakia *et al.* (42).

ACKNOWLEDGMENTS

This study was supported by NSF grants MCB-1253234 and MCB-1817652 to Birgit Scharf, the VT Fralin Summer Undergraduate Research Fellowship to Jiwoo Kim, and the VT Multicultural Academics Opportunity Program Fellowship to Maya Pahima. We are indebted to Dr. Hardik Zatakia for purification of McpV-LBD-3xFLAG, to Rafael Castañeda Saldaña for quantification of CheW1-3xFLAG, and all of the members of the Scharf lab for critical reading and comments.

Table 4.1 Absolute protein abundance of chemotaxis proteins with C-terminal 3xFLAG epitope

Protein	**Molecules per cell**	**Protein**	**Molecules per cell**	**Fold increase**
CheW1	189[a]	CheW1-3xFLAG	367	1.9
IcpA	17[b]	IcpA-3xFLAG	468	27
McpT	<0.36 (B.D.L.[b, c])	McpT-3xFLAG	76	210
McpU	47[b]	McpU-3xFLAG	291	6.2
McpV	299[b]	McpV-3xFLAG	314[d]	1.05[d]
McpY	0.33[b]	McpY-3xFLAG	15	45

[a] Value from Arapov *et al.* (64)
[b] Value from Zatakia *et al.* (42)
[c] Value is representing the maximum amount of McpT (Zatakia *et al.* (42)*)*. This value was deduced from the minimal amount of EGFP required for detection, 5 pg or the equivalent of 0.36 molecules per cell, detected in immunoblot assays performed under standardized conditions compared to the lack of an McpT-EGFP band in cell extracts.
[d] Value is derived from direct comparison of band intensities between native McpV and McpV-3xFLAG (Fig. 5E) and does not a represent a statistically significant change. Molecules per cell are based on this value.

Table 4.2 Bacterial strains and plasmids

Strain/Plasmid	Relevant Characteristics	Source or Reference
E. coli		
ER2566	*ion ompT lacZ::T7*	New England Biolabs
S17-1	Tp^r Sm^r; *recA endA thi hsdR* RP4-2 Tc::Mu::Tn7	(Simon *et al*, 1986) (65)
S. meliloti		
RU11/001	Sm^r; spontaneous streptomycin-resistant wild-type strain	(Pleier *el al.,* 1991)(58)
RU11/828	Sm^r; Δ*mcpU*	(Meier *et al,* 2007*)* (46)
BS193	Sm^r; McpT-3xFLAG	This work
BS194	Sm^r; McpY-3xFLAG	This work
BS201	Sm^r; CheW1-3xFLAG	This work
BS203	Sm^r; IcpA-3xFLAG	This work
BS207	Sm^r; McpU-3xFLAG	This work
BS220	Sm^r; McpU-6xHis	This work
BS221	Sm^r; McpV-3xFLAG	This work
BS222	Sm^r; McpU-1xFLAG	This work
BS252	Sm^r; McpU-1xHis	This work
BS256	Sm^r; McpU-2xHis	This work
BS257	Sm^r; McpU-1xAla	This work
BS258	Sm^r; McpU-1xGly	This work
BS266	Sm^r; McpU Δ aa 699-707	This work
BS267	Sm^r; McpU Δ aa 683-707	This work
BS268	Sm^r; McpU aa 679-681 AAL mutated to ELD	This work
BS269	Sm^r; McpU, Δ aa 668-707	This work
BS270	Sm^r; McpU aa 695-697 AAS mutated to ELD	This work
BS271	Sm^r; McpU Δ aa 683-698	This work
BS272	Sm^r; McpU aa 706-707 AA mutated to DD	This work
BS273	Sm^r; McpU-3xFLAG, aa 706-707 AA mutated to DD	This work
Plasmids		
pK18*mobsacB*	Km^r; *mob sacB*, vector used for homologous allelic exchange	(Schäfer *et al*., 1994) (66)
pBS459	pTYB11-McpV-LBD-3xFLAG	This work

REFERENCES

1. Pratt LA, Kolter R. 1998. Genetic analysis of *Escherichia coli* biofilm formation: roles of flagella, motility, chemotaxis and type I pili. Mol Microbiol 30:285-293.
2. Locke JCW. 2013. How bacteria choose a lifestyle. Nature 503:476-477.
3. Davey ME, O'Toole G A. 2000. Microbial biofilms: from ecology to molecular genetics. Microbiol Mol Biol Rev 64:847-67.
4. Raina J-B, Fernandez V, Lambert B, Stocker R, Seymour JR. 2019. The role of microbial motility and chemotaxis in symbiosis. Nat Rev Microbiol 17:284-294.
5. Oliveira NM, Foster KR, Durham WM. 2016. Single-cell twitching chemotaxis in developing biofilms. Proc Natl Acad Sci U S A 113:6532-7.
6. Wadhams GH, Armitage JP. 2004. Making sense of it all: bacterial chemotaxis. Nat Rev Mol Cell Biol 5:1024-1037.
7. Amaya-Gómez CV, Hirsch AM, Soto MJ. 2015. Biofilm formation assessment in *Sinorhizobium meliloti* reveals interlinked control with surface motility. BMC Microbiol 15:58-58.
8. van Rhijn P, Vanderleyden J. 1995. The Rhizobium-plant symbiosis. Microbiol Rev 59:124-42.
9. Van de Velde W, Zehirov G, Szatmari A, Debreczeny M, Ishihara H, Kevei Z, Farkas A, Mikulass K, Nagy A, Tiricz H, Satiat-Jeunemaitre B, Alunni B, Bourge M, Kucho K, Abe M, Kereszt A, Maroti G, Uchiumi T, Kondorosi E, Mergaert P. 2010. Plant peptides govern terminal differentiation of bacteria in symbiosis. Science 327:1122-6.
10. Brewin NJ. 1991. Development of the legume root nodule. Annu Rev Cell Biol 7:191-226.
11. Scharf BE, Hynes MF, Alexandre GM. 2016. Chemotaxis signaling systems in model beneficial plant–bacteria associations. Plant Molecular Biology 90:549-559.
12. Porter SL, Wadhams GH, Armitage JP. 2011. Signal processing in complex chemotaxis pathways. Nat Rev Microbiol 9:153-165.
13. Hazelbauer GL, Falke JJ, Parkinson JS. 2008. Bacterial chemoreceptors: high-performance signaling in networked arrays. Trends Biochem Sci 33:9-19.
14. Salah Ud-Din AIM, Roujeinikova A. 2017. Methyl-accepting chemotaxis proteins: a core sensing element in prokaryotes and archaea. Cell Mol Life Sci 74:3293-3303.
15. Falke JJ, Hazelbauer GL. 2001. Transmembrane signaling in bacterial chemoreceptors. Trends Biochem Sci 26:257-65.
16. Briegel A, Ladinsky MS, Oikonomou C, Jones CW, Harris MJ, Fowler DJ, Chang YW, Thompson LK, Armitage JP, Jensen GJ. 2014. Structure of bacterial cytoplasmic chemoreceptor arrays and implications for chemotactic signaling. Elife 3:e02151.
17. Yang W, Briegel A. 2019. Diversity of bacterial chemosensory arrays. Trends Microbiol doi:https://doi.org/10.1016/j.tim.2019.08.002.
18. Rotter C, Mühlbacher S, Salamon D, Schmitt R, Scharf B. 2006. Rem, a new transcriptional activator of motility and chemotaxis in *Sinorhizobium meliloti*. J Bacteriol 188:6932-6942.
19. Sourjik V, Muschler P, Scharf B, Schmitt R. 2000. VisN and VisR are global regulators of chemotaxis, flagellar, and motility genes in *Sinorhizobium (Rhizobium) meliloti*. J Bacteriol 182:782-8.

20. Ogden AJ, McAleer JM, Kahn ML. 2019. Characterization of the *Sinorhizobium meliloti* HslUV and ClpXP Protease Systems in Free-Living and Symbiotic States. J Bacteriol 201:e00498-18.
21. Pini F, De Nisco NJ, Ferri L, Penterman J, Fioravanti A, Brilli M, Mengoni A, Bazzicalupo M, Viollier PH, Walker GC, Biondi EG. 2015. Cell cycle control by the master regulator CtrA in *Sinorhizobium meliloti*. PLoS Genetics 11:e1005232.
22. Hallez R, Bellefontaine AF, Letesson JJ, De Bolle X. 2004. Morphological and functional asymmetry in alpha-proteobacteria. Trends Microbiol 12:361-5.
23. Bird TH, MacKrell A. 2011. A CtrA homolog affects swarming motility and encystment in *Rhodospirillum centenum*. Arch Microbiol 193:451-9.
24. Francis N, Poncin K, Fioravanti A, Vassen V, Willemart K, Ong TA, Rappez L, Letesson JJ, Biondi EG, De Bolle X. 2017. CtrA controls cell division and outer membrane composition of the pathogen *Brucella abortus*. Mol Microbiol 103:780-797.
25. Curtis PD, Brun YV. 2010. Getting in the loop: regulation of development in *Caulobacter crescentus*. Microbiology and Molecular Biology Reviews 74:13-41.
26. Kobayashi H, De Nisco NJ, Chien P, Simmons LA, Walker GC. 2009. *Sinorhizobium meliloti* CpdR1 is critical for co-ordinating cell cycle progression and the symbiotic chronic infection. Mol Microbiol 73:586-600.
27. Xue S, Biondi EG. 2019. Coordination of symbiosis and cell cycle functions in *Sinorhizobium meliloti*. Biochim Biophys Acta Gene Regul Mech 1862:691-696.
28. Hallez R, Delaby M, Sanselicio S, Viollier PH. 2017. Hit the right spots: cell cycle control by phosphorylated guanosines in alphaproteobacteria. Nat Rev Microbiol 15:137-148.
29. De Nisco NJ, Abo RP, Wu CM, Penterman J, Walker GC. 2014. Global analysis of cell cycle gene expression of the legume symbiont *Sinorhizobium meliloti*. Proc Natl Acad Sci U S A 111:3217-24.
30. Barnett MJ, Hung DY, Reisenauer A, Shapiro L, Long SR. 2001. A homolog of the CtrA cell cycle regulator is present and essential in *Sinorhizobium meliloti*. J Bacteriol 183:3204-10.
31. Smith SC, Joshi KK, Zik JJ, Trinh K, Kamajaya A, Chien P, Ryan KR. 2014. Cell cycle-dependent adaptor complex for ClpXP-mediated proteolysis directly integrates phosphorylation and second messenger signals. Proc Natl Acad Sci U S A 111:14229-34.
32. Potocka I, Thein M, Østerås M, Jenal U, Alley MRK. 2002. Degradation of a *Caulobacter* soluble cytoplasmic chemoreceptor is ClpX dependent. J Bacteriol 184:6635-6641.
33. Tsai JW, Alley MR. 2001. Proteolysis of the *Caulobacter* McpA chemoreceptor is cell cycle regulated by a ClpX-dependent pathway. J Bacteriol 183:5001-7.
34. Iniesta AA, McGrath PT, Reisenauer A, McAdams HH, Shapiro L. 2006. A phospho-signaling pathway controls the localization and activity of a protease complex critical for bacterial cell cycle progression. Proc Natl Acad Sci U S A 103:10935-10940.
35. Vass RH, Nascembeni J, Chien P. 2017. The essential role of ClpXP in *Caulobacter crescentus* requires species constrained substrate specificity. Front Mol Biosci 4:28-28.
36. Baker TA, Sauer RT. 2012. ClpXP, an ATP-powered unfolding and protein-degradation machine. Biochim Biophys Acta Mol Cell Res 1823:15-28.

37. Gottesman S, Roche E, Zhou Y, Sauer RT. 1998. The ClpXP and ClpAP proteases degrade proteins with carboxy-terminal peptide tails added by the SsrA-tagging system. Genes Dev 12:1338-47.
38. Alexander RP, Zhulin IB. 2007. Evolutionary genomics reveals conserved structural determinants of signaling and adaptation in microbial chemoreceptors. Proc Natl Acad Sci U S A 104:2885-2890.
39. Gerth U, Kock H, Kusters I, Michalik S, Switzer RL, Hecker M. 2008. Clp-dependent proteolysis down-regulates central metabolic pathways in glucose-starved *Bacillus subtilis*. J Bacteriol 190:321-331.
40. Joshi KK, Chien P. 2016. Regulated proteolysis in bacteria: *Caulobacter*. Annu Rev Genet 50:423-445.
41. Flynn JM, Levchenko I, Seidel M, Wickner SH, Sauer RT, Baker TA. 2001. Overlapping recognition determinants within the ssrA degradation tag allow modulation of proteolysis. Proc Natl Acad Sci U S A 98:10584-10589.
42. Zatakia HM, Arapov TD, Meier VM, Scharf BE. 2018. Cellular Stoichiometry of Methyl-Accepting Chemotaxis Proteins in *Sinorhizobium meliloti*. J Bacteriol 200.
43. Scharf BE, Fahrner KA, Turner L, Berg HC. 1998. Control of direction of flagellar rotation in bacterial chemotaxis. Proc Natl Acad Sci U S A 95:201-206.
44. Flynn JM, Neher SB, Kim Y-I, Sauer RT, Baker TA. 2003. Proteomic discovery of cellular substrates of the ClpXP protease reveals five classes of ClpX-recognition signals. Mol Cell 11:671-683.
45. Ryan KR, Judd EM, Shapiro L. 2002. The CtrA response regulator essential for *Caulobacter crescentus* cell-cycle progression requires a bipartite degradation signal for temporally controlled proteolysis. J Mol Biol 324:443-455.
46. Meier VM, Muschler P, Scharf BE. 2007. Functional analysis of nine putative chemoreceptor proteins in *Sinorhizobium meliloti*. J Bacteriol 189:1816-26.
47. Webb BA, Compton KK, del Campo JSM, Taylor D, Sobrado P, Scharf BE. 2017. *Sinorhizobium meliloti* chemotaxis to multiple amino acids is mediated by the chemoreceptor McpU. Mol Plant Microbe Interact 30:770-777.
48. Webb BA, Helm RF, Scharf BE. 2016. Contribution of individual chemoreceptors to *Sinorhizobium meliloti* chemotaxis towards amino acids of host and nonhost seed exudates. Mol Plant Microbe Interact 29:231-9.
49. Meier VM, Scharf BE. 2009. Cellular localization of predicted transmembrane and soluble chemoreceptors in *Sinorhizobium meliloti*. J Bacteriol 191:5724-5733.
50. Jarvik JW, Telmer CA. 1998. EPITOPE TAGGING. Annu Rev Genet 32:601-618.
51. Gur E, Biran D, Ron EZ. 2011. Regulated proteolysis in Gram-negative bacteria — how and when? Nat Rev Microbiol 9:839-848.
52. Grünenfelder B, Tawfilis S, Gehrig S, Østerås M, Eglin D, Jenal U. 2004. Identification of the protease and the turnover signal responsible for cell cycle-dependent degradation of the *Caulobacter* FliF Motor Protein. J Bacteriol 186:4960-4971.
53. Herman C, Thevenet D, Bouloc P, Walker GC, D'Ari R. 1998. Degradation of carboxy-terminal-tagged cytoplasmic proteins by the *Escherichia coli* protease HflB (FtsH). Genes Dev 12:1348-55.
54. Sundar S, McGinness KE, Baker TA, Sauer RT. 2010. Multiple sequence signals direct recognition and degradation of protein substrates by the AAA+ protease HslUV. Journal J Mol Biol 403:420-429.

55. Mahmoud SA, Chien P. 2018. Regulated proteolysis in bacteria. Annu Rev Biochem 87:677-696.
56. Lau J, Hernandez-Alicea L, Vass RH, Chien P. 2015. A phosphosignaling adaptor primes the AAA+ protease ClpXP to drive cell cycle-regulated proteolysis. Mol Cell 59:104-16.
57. Duerig A, Abel S, Folcher M, Nicollier M, Schwede T, Amiot N, Giese B, Jenal U. 2009. Second messenger-mediated spatiotemporal control of protein degradation regulates bacterial cell cycle progression. Genes Dev 23:93-104.
58. Pleier E, Schmitt R. 1991. Expression of two *Rhizobium meliloti* flagellin genes and their contribution to the complex filament structure. J Bacteriol 173:2077-2085.
59. Bertani G. 1951. Studies on lysogenesis. I. The mode of phage liberation by lysogenic *Escherichia coli*. J Bacteriol 62:293-300.
60. Scharf B, Schuster-Wolff-Bühring H, Rachel R, Schmitt R. 2001. Mutational analysis of the *Rhizobium lupini* H13-3 and *Sinorhizobium meliloti* flagellin genes: Importance of flagellin A for flagellar filament structure and transcriptional regulation. J Bacteriol 183:5334.
61. Götz R, Limmer N, Ober K, Schmitt R. 1982. Motility and chemotaxis in two strains of *Rhizobium* with complex flagella. J Gen Microbiol 128:789-798.
62. Sourjik V, Schmitt R. 1996. Different roles of CheY1 and CheY2 in the chemotaxis of *Rhizobium meliloti*. Mol Microbiol 22:427-36.
63. Compton KK, Hildreth SB, Helm RF, Scharf BE. 2018. *Sinorhizobium meliloti* chemoreceptor McpV senses short-chain carboxylates via direct binding. J Bacteriol 200.
64. Arapov TD, Castaneda Saldana R, Sebastian AL, Keith Ray W, Helm RF, Scharf B, E. 2020. Cellular stoichiometry of chemotaxis proteins in *Sinorhizobium meliloti*. In preparation
65. Simon R, O'connell M, Labes M, Pühler A. 1986. Plasmid vectors for the genetic analysis and manipulation of rhizobia and other gram-negative bacteria, p 640-659, Methods Enzymol, vol 118. Elsevier.
66. Schäfer A, Tauch A, Jäger W, Kalinowski J, Thierbach G, Pühler A. 1994. Small mobilizable multi-purpose cloning vectors derived from the *Escherichia coli* plasmids pK18 and pK19: selection of defined deletions in the chromosome of *Corynebacterium glutamicum*. Gene 145.

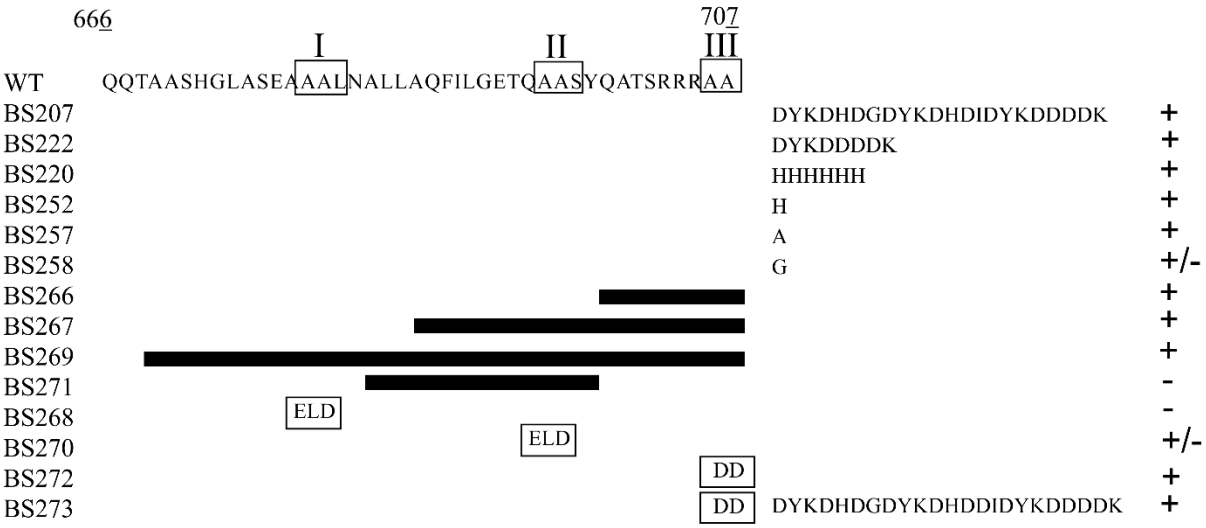

Figure 4.1 Mutational analysis of the C-terminal region of McpU and its results on stability. Depicted is a diagram of the C-terminal region of McpU (aa 666-707) and the extensions, deletions, and substitutions made in its native chromosomal locus (Table 1). Boxes in the wild-type sequence and the respective mutants indicate specific motifs and their substitutions, respectively. Black bars represent extent of deletions. The column on the right symbolizes McpU abundance relative to wild type; plus: increase, minus: decrease; plus/minus: no change.

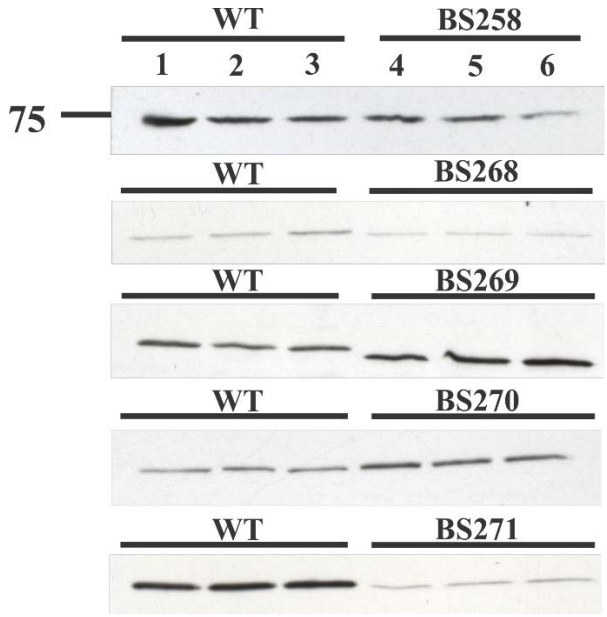

Figure 4.2 Representative immunoblots for direct comparison of McpU abundance in cell lysates of wild type compared to mutant strains. Each lane contains cell lysates from 1 ml of culture at OD_{600} 0.25. Each panel is the result of different film exposures, therefore, comparisons can only be made within a panel.

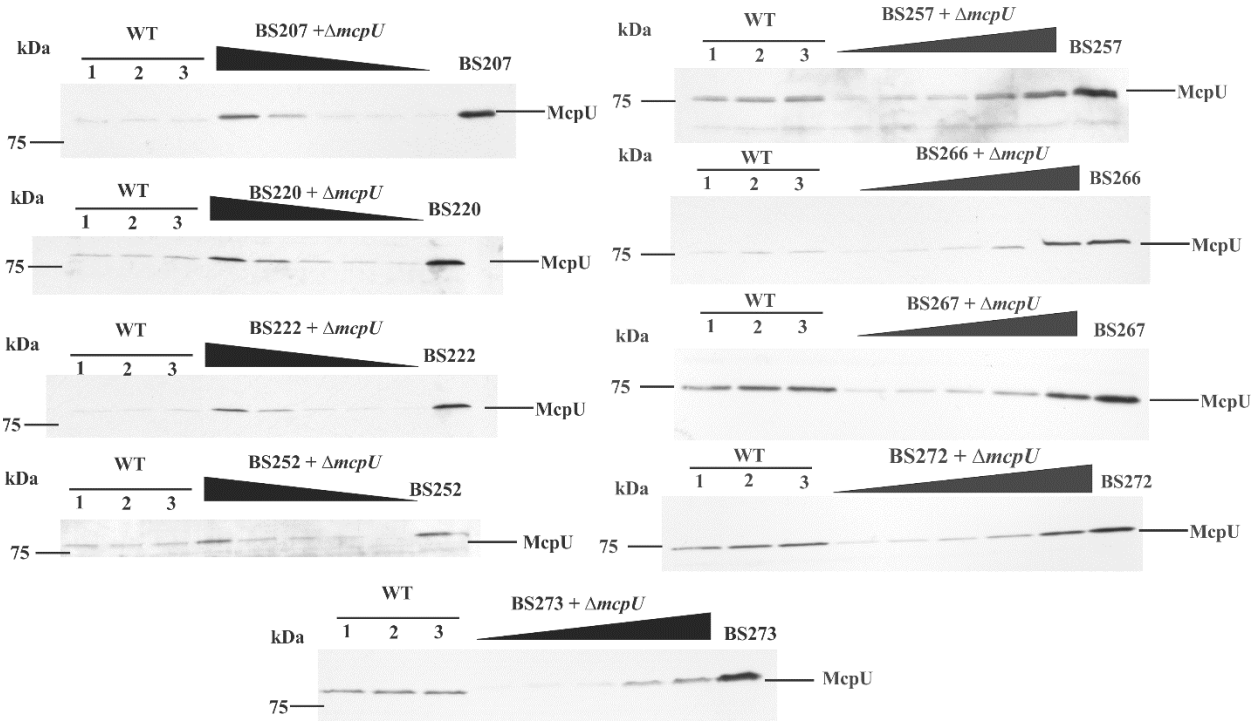

Figure 4.3 Representative immunoblots used to quantify the relative abundance of McpU in cell lysates of wild type compared to mutant strains. Lanes 1-3 contain RU11/001 lysates (WT) from 1 ml of culture at an OD_{600} of 0.25. Lanes denoted by the wedge shape contain a mix of each mutant strain and RU11/828 (Δ*mcpU*) at ratios of 1:1, 3:1, 5.7 :1, 7:1, 9:1 yielding a total volume of 1 ml of culture at OD_{600} 0.25. The last lane in each panel contains lysates from 1 ml of culture of the respective mutant strain at an OD_{600} of 0.25.

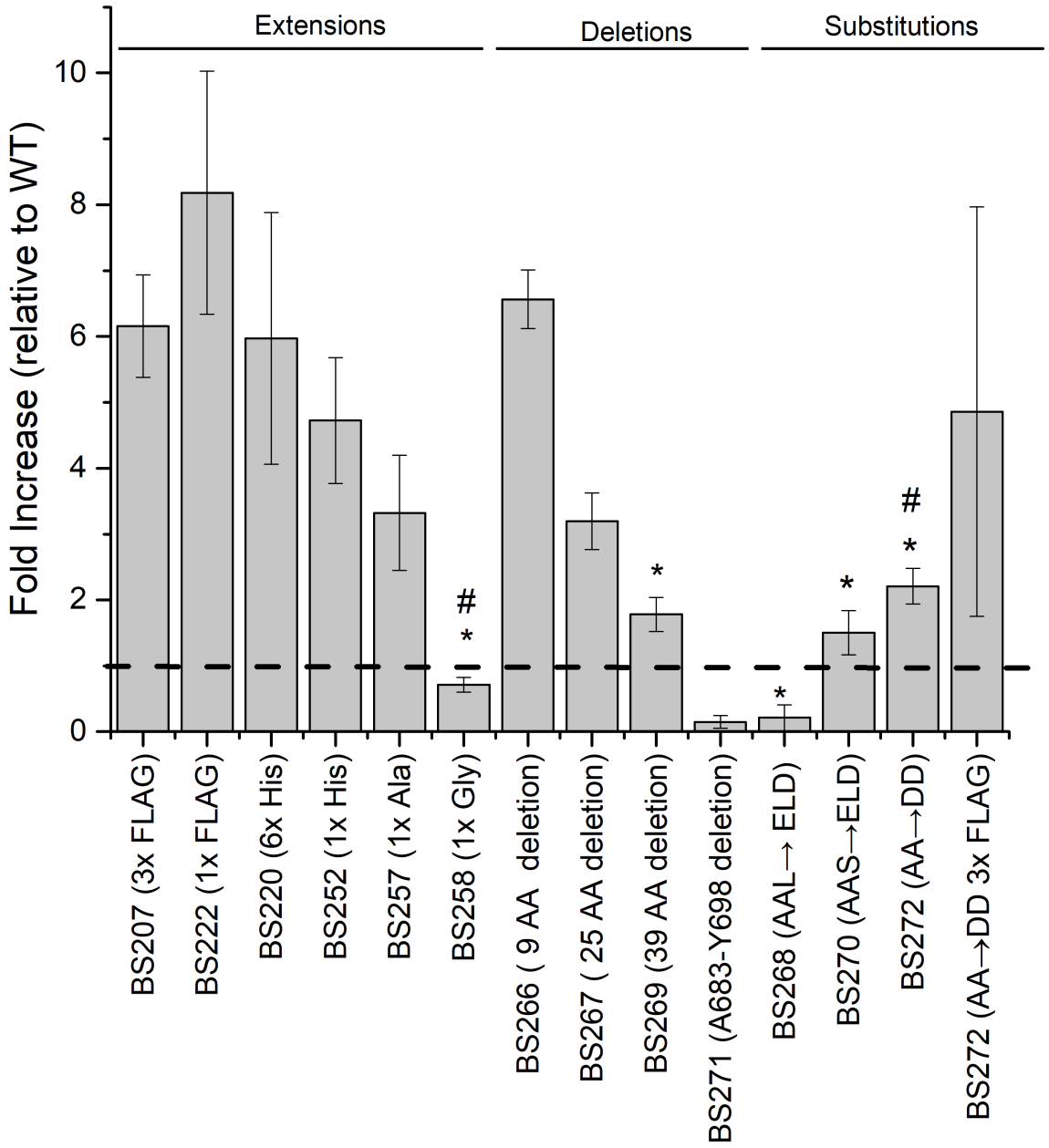

Figure 4.4 Relative abundance of McpU in mutant strains compared to wild type. Asterisks indicate quantifications obtained through direct comparison (Fig. 4.2); all other values were obtained through generation of a standard curve (Fig. 4.3). The dashed line represents wild-type abundance of McpU. Values and error bars are the mean and standard deviation of three

biological replicates. Statistical significance was determined by a two-tailed Student's T-test ($p < 0.05$). All values but those marked by octothorpe symbols denote statistically significant differences from the wild type.

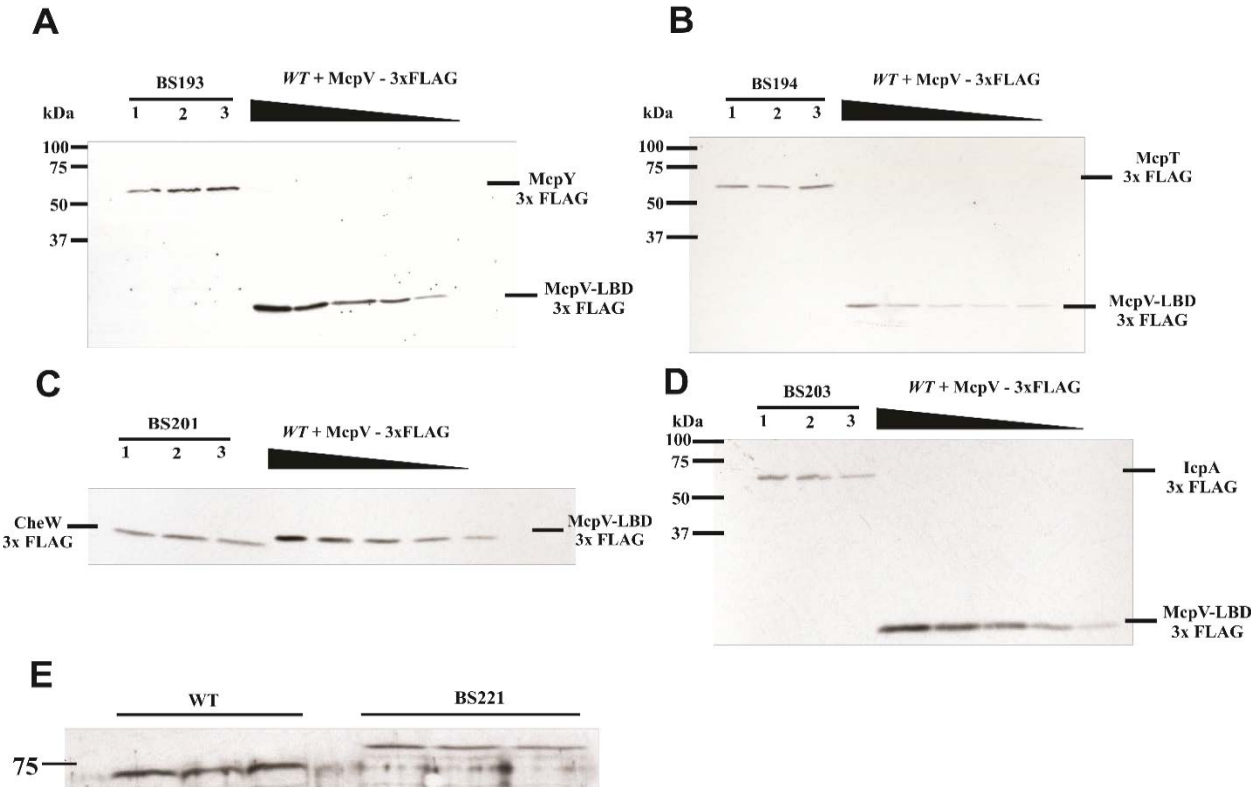

Figure 4.5 Representative immunoblots used to quantify chemotaxis proteins with C-terminal 3xFLAG fusions. **A.** Lanes 1-3 contain BS193 (McpY-3xFLAG expressing strain) cell lysate from 1 ml of culture at an OD_{600} of 0.25, WT + McpV-3xFLAG lanes contain RU11/001 (WT) cell lysate from 1 ml of culture at an OD_{600} of 0.25 with McpV-LBD-3xFLAG (0.4, 0.3, 0.2, 0.01, 0.05, 0 ng). **B.** Lanes 1-3 contain BS194 (McpT-3xFLAG expressing strain) cell lysate from 1 ml of culture at an OD_{600} of 0.25, WT + McpV-3xFLAG lanes contain RU11/001 (WT) cell lysate from 1 ml of culture at an OD_{600} of 0.25 with McpV-LBD-3xFLAG (1.8, 1.5, 1, 0.5, 0.3, 0 ng). **C** Lanes 1-3 contain BS201 (CheW1-3xFLAG expressing strain) cell lysate from 1 ml

of culture at an OD_{600} of 0.25, WT + McpV-3xFLAG lanes contain RU11/001 (WT) cell lysate from 1 ml of culture at an OD_{600} of 0.25 with McpV-LBD-3xFLAG (8, 6.5, 5.2, 4, 2.6, 0 ng). **D.** Lanes 1-3 contain BS203 (IcpA-3xFLAG expressing strain) cell lysate from 1 ml of culture at an OD600 of 0.25, WT + McpV-3xFLAG lanes contain RU11/001 (WT) cell lysate from 1 ml of culture at an OD600 of 0.25 with McpV-LBD-3xFLAG (10, 8, 6, 4, 2, 0 ng). **E.** Representative immunoblot for direct comparison of McpV abundance in cell lysates of wild type compared to BS221. Each lane contains cell lysates from 1 ml of culture at OD_{600} 0.25.

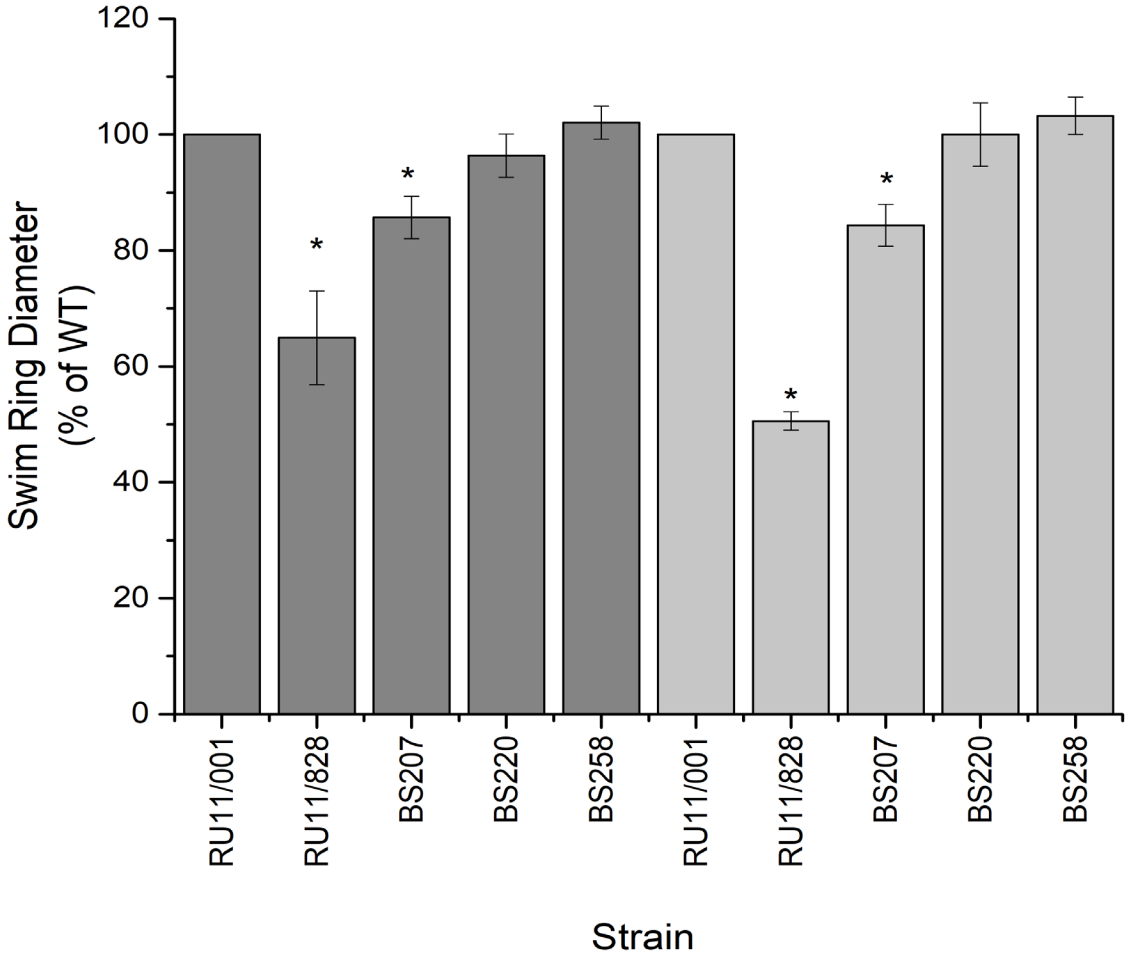

Figure 4.6 Relative swim ring diameter of *S. meliloti* mutant strains in Bromfield and Rhizobium Basal medium containing 10^{-4} M lysine. Plates containing 0.3 % agar were inoculated with 3 µl stationary phase TYC culture and incubated for 3 and 5 days, respectively, at 30 °C. Dark and light grey bars represent results obtained in Bromfield and Rhizobium Basal medium, respectively. Values are the mean and error bars reflect the standard deviation from five replicates. Statistical significance was determined by a two-tailed Student's T-test ($p < 0.05$). Asterisk symbols denote statistically significant differences from the wild type.

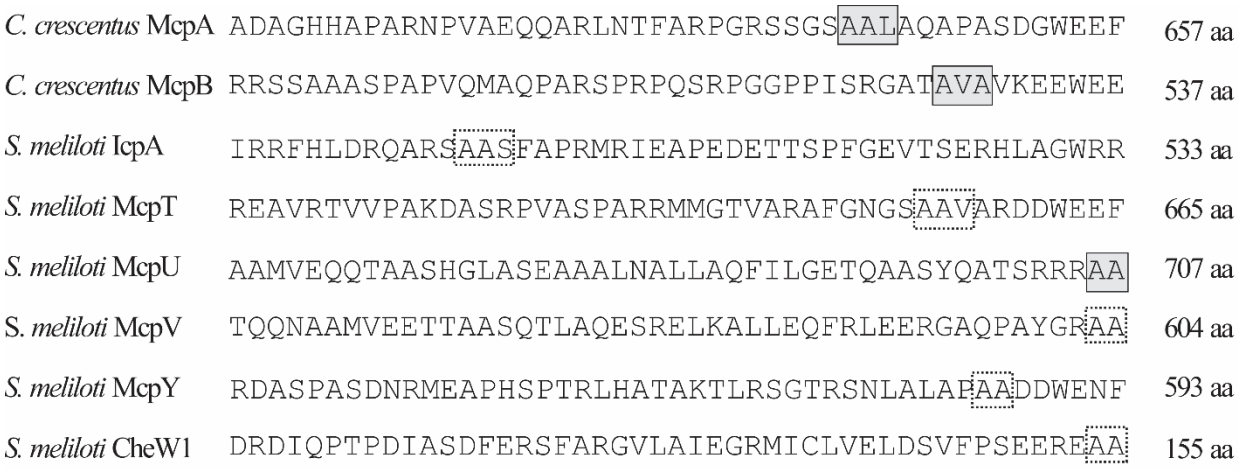

Figure 4.7 Comparison of the region comprising 47 amino acid residues proximal to the carboxy-terminus of *C. crescentus* McpA and McpB, five *S. meliloti* MCPs and *S. meliloti* CheW1. Residues critical for correct proteolysis are indicated by boxes shaded in grey according to Tsai *et al.* (2001) (33), Potocka *et al.* (2002) (32), and this work. Putative residues important for proteolysis are marked by unshaded boxes. Numbers at the end of each sequence reflect overall protein length.

Chapter 5 CheT, a novel chemotaxis protein in the legume symbiont *Sinorhizobium meliloti*, is part of the adaptation system

TIMOFEY D. ARAPOV[1], WING-CHEUNG LAI[2], GERALD L. HAZELBAUER[2] AND BIRGIT E. SCHARF[1]

[1] Department of Biological Sciences, Life Sciences I, Virginia Tech, Blacksburg, VA 24061, USA

[2] Department of Biochemistry, University of Missouri-Columbia, Columbia, MO 65211, USA

Running title: CheT, a novel *Sinorhizobium meliloti* chemotaxis protein

Key words: carboxyl methylation, sensory adaptation, transmembrane receptors, speed-variable flagellar motor, two-component system

*For correspondence:
E-mail bscharf@vt.edu
Tel (+1) 540 231 0757
Fax (+) 540 231 4043
Biological Sciences, Life Sciences I
Virginia Tech
Blacksburg, VA 24061, USA

Attribution: TDA was responsible for design of expirements and generated Figure 5.1, portions of Figure 5.2A, Figure 5.2B and Figure 5.4 – 5.7 . Final manuscript was drafted by TDA and BES.

ABSTRACT

Motility and chemotaxis are important traits for various bacterial species in diverse ecological niches. Therefore, it is critical to establish chemotaxis paradigms beyond the enteric archetypes. Bacteria utilize chemoreceptors or Methyl-Accepting Chemotaxis Proteins (MCP) to sense external signals and communicate with the internal two-component regulatory system. Their basic composition is conserved, but variations are present in bacterial species living in more complex environments. The plant symbiont *Sinorhizobium meliloti* can exist freely in the soil or as endosymbiont with host legumes. Most chemotaxis genes in *S. meliloti* are located in the *che1* operon, which encodes for a chemoreceptor, two-component system proteins, and proteins involved in adaptation. However, no function is assigned to the last gene in the *che1* operon, although homologs are present in the chemotaxis operons of closely related alphaproteobacteria. Deletion of *cheT* resulted in a chemotaxis-defective phenotype, with cells swimming at a higher velocity. The rotational speed of the *S. meliloti* flagellar motor is negatively regulated through binding of the phosphorylated response regulator CheY2-P. This notion suggested that the CheY2-P pool is depleted in the absence of CheT. Using an *in-vitro* chemical crosslinking assay, as well as co-expression in *E. coli* and co-purification, we established that CheT interacts with the methyltransferase CheR. An *in-vitro* methylation assay of McpX in membrane vesicles indicated its methylation by CheR, but revealed no effect of CheT on methylation. Together, these data suggest that CheT is part of the adaptation system in *S. meliloti* chemotaxis, although its exact function is not yet understood.

INTRODUCTION

Sinorhizobium meliloti is a soil dwelling alphaproteobacterium best known for its ability to engage in an endosymbiotic relationship with various legume species. Free-living *S. meliloti* cells use rotating flagella to move through the soil and chemotaxis to localize to its host plant roots (1, 2). Chemotaxis is the ability to sense chemical signals and respond through movement towards an attractant or away from a repellent. Flagellated bacteria are able to alternate between straight swimming paths or runs and random reorientations or tumbles. By altering the length of a run, cells move up an attractant or down a repellent concentration gradient. This phenomenon is known as a biased random walk (3). Within the cell, this behavior is mediated by a two-component signal transduction system, which is best studied in the gammaproteobacterium *Escherichia coli* (for recent reviews, see Wadhams *et al*. (4) , Porter *et al. (5)* Sourjik *et al* (6)). *E. coli* and *S. meliloti* share the basic chemotaxis system architecture but also exhibit notable differences. Both species have a repertoire of chemoreceptor proteins or Methyl-accepting Chemotaxis Proteins (MCPs) (4, 6). MCPs are dimers, which form a stable, ternary complex with two CheW adaptor protein monomers and a histidine kinase CheA dimer. Theses complexes build larger hexagonal arrays that allow for cooperativity between different receptor types (7, 8). Chemoreceptors control the activity of the histidine autokinase CheA, which autophosphorylates in an ATP-dependent reaction. CheA-P then transfers phosphoryl groups to a conserved aspartate residue of the response regulator CheY. Phosphorylated *E.coli* CheY (CheY-P) interacts with the flagellar motor protein FliM, altering flagellar rotation from counterclockwise (CCW) to clockwise (CW) resulting in a tumble reaction (9-11). In *S. meliloti*, the phosphorylated motor response regulator causes a reduction of flagellar rotary speed (12-15). Response regulators spontaneously dephosphorylate, but *E. coli* utilizes a phosphatase, CheZ, which accelerates dephosphorylation and therefore signal

termination. *S. meliloti* and other related alphaproteobacteria such as *Agrobacterium tumefaciens, Azospirillum brasilense,* and *Caulobacter crescentus* possess more than one response regulator species and lack a CheZ homologue (13, 16). In *S. meliloti*, CheY2 serves as main response regulator of motor function, while CheY1 does not interact with the flagellar motor but instead acts as a phosphate sink. Signal termination is mediated by retrophosphorylation from CheY2-P to CheA, which in turn transfers phosphate groups to CheY1 (13-15, 17, 18). CheS, a small protein that has no counterpart in *E. coli*, promotes interaction between CheA and CheY1, which allows for the drainage of the phosphate sink (18).

To enable sensitivity to a wide range of stimuli concentrations, bacteria return to pre-stimulus behavior in the continued presence of a signal. This process, known as adaptation, has been intensely studied in *E. coli* (for a recent reviews, see Vladimirov *et al.*(19) Tu *et al.* (20)). The *E. coli* adaptation system is based on reversible methylation of conserved glutamate residues in the cytoplasmic signaling domain of MCPs (21-23). Receptor methylation is carried out by CheR, a constitutively active methyltransferase, while the activated methylesterase CheB serves as an antagonist to CheR (4, 19). The adaptation enzymes are tethered to the chemoreceptor cluster via a canonical pentapeptide motif at the C-terminus of MCPs (24). Additionally, CheB is only able to demethylate glutamate residues when it is activated through phosphorylation by CheA (9, 25). Upon binding of an attractant to an MCP, the rate of CheA autophosphorylation is reduced. As a result, the amount of CheB-P is reduced, causing an increase in MCP methylation. A second activity of CheB-P is the deamidation of conserved glutamine residues in the signaling domain of MCPs, converting them into glutamate residues, which then become substrates for methylation (26, 27). This function is important for the accurate signaling function of chemoreceptors.

The adaptation system through receptor methylation is present and appears to be conserved in *S. meliloti*; however, its function has not been experimentally characterized. In addition to CheB and CheR, *S. meliloti* expresses another receptor-modifying enzyme, CheD, which is homologous to the deamidase CheD in *Bacillus subtilis*. In *B. subtilis*, CheD also promotes autokinase activity of CheA when bound to chemoreceptors. The second function of CheD is regulated through CheC, one of two phosphatases in *B. subtilis*. The receptor-bound pool of CheD can be depleted via CheC-CheD interaction. This feedforward regulatory mechanism reduces both, the rate of CheA autophosphorylation and the amount of CheY-P present. As CheY-P levels decrease, more CheD becomes bound to the chemoreceptors, thus restoring CheA autokinase activity (28, 29).

Studies in *E. coli* and *B. subtilis* have revealed differences in the impact of receptor methylation on histidine kinase activity. In *E. coli*, net levels of receptor methylation increase with attractant concentration (30). Contrary, the net level of receptor methylation in *B. subtilis* remains unchanged, but methylation patterns at conserved glutamate residues are altered (29, 31, 32). Thus, although CheB and CheR functions are conserved in both species, the output of receptor methylation is distinct. At this point, one can only speculate about the function and regulation of the adaptation system in *S. meliloti*, which shares similarities with both model systems. The presence of a pentapeptide motif at the C-terminus of four of eight *S. meliloti* chemoreceptors, which could serve as tether for CheB and CheR, is alike the *E. coli* system, while the presence of a deamidase CheD is similar to *B. subtilis* (33, 34). These variations profoundly justify further studies of the *S. meliloti* chemotaxis in general and the adaptation system in particular. In this work, we investigated the function of a chemotaxis protein encoded by the last gene adjacent to *cheD* in the chemotaxis operon *che1* in *S. meliloti* (34). The corresponding protein, CheT, has no

homology to other characterized chemotaxis proteins. Here, we present evidence for a function of CheT in the adaptation system of *S. meliloti*.

RESULTS

Bioinformatics analysis of *S. meliloti* CheT

The major chemotaxis operon *che1* in *S. meliloti* contains a gene of unknown function, which is the last gene in the operon downstream of *cheD*. The deduced primary sequence of the gene product is a protein with 124 amino acid residues (13.4 kDa), which we named CheT. It has no apparent homologues in paradigm models of bacterial chemotaxis, but *cheT* is similar to genes found in other, closely related alphaproteobacteria such as *Sinorhizobium medicae, Agrobacterium tumefaciens, Caulobacter crescentus, Rhizobium leguminosarum* and *Hoeflea sp 108* (Fig.1). Gene synteny of these orthologs is highly conserved, as they are the last gene in the major chemotaxis operons of each species, with the exception of *C. crescentus* that has two additional chemotaxis genes in the operon proceeding the *cheT* homologue. Their primary sequences exhibit varied identity of 81 % (*S. medicae),* 70 % (*A. tumefaciens*), 67 % (*R. leguminosarum)*, 28 % (*Hoeflea sp. 108)* and 20 % (*C. crescentus)* (Fig. 1). PSIPRED predicts the secondary structure of CheT to contain four alpha helices accounting for 56 % of the primary sequence with the remainder of the sequence being composed of unstructured linkers (35). Across all genomes surveyed, the position of and distance between two residues, asp-57 and gln-61, were highly conserved. The DXXXQ sequence has been previously implicated as a phosphatase motif on the catalytic surface of CheZ (36, 37) suggesting that CheT is a CheZ-like phosphatase.

Phenotypic analysis of an *S. meliloti* strain lacking *cheT*

To gauge the function of CheT in chemotaxis, an in-frame deletion was introduced into the *S. meliloti* wild-type strain (RU11/001), and the chemotactic ability of the resulting mutant strain (RU11/319) was assessed and compared to mutants lacking six single chemotaxis genes (Fig. 2).

The Δ*cheT* mutant strain exhibited a 50 % reduction in swim ring diameter on Bromfield soft agar plates compared to the wild type. This chemotaxis defect could be fully restored by complementation with a *cheT*-expressing plasmid. Deletions of *cheA, cheD, cheR,* and *cheY2* were more detrimental than deletion of *cheT*, while the deletion of *cheY1* was less severe. The *cheB* deletion strain displayed the most similar reduction in swim ring size to the Δ*cheT strain.*

To further assess how chemotaxis is affected by the deletion of *cheT*, we used computerized motion analysis to quantify the average free-swimming velocity of a population of cells. In *S. meliloti*, the swimming speed varies depending on the fraction of phosphorylated CheY2 (CheY2-P) (14). A low swimming speed is indicative of high levels of CheY2-P, whereas a high swimming speed is the result of low levels of CheY2-P. Therefore, deletion of *cheA* or *cheY2* induced an increased swimming speed. Contrary, the swimming speed of *cheB* or *cheY1* deletion strains was decreased, because CheB and CheY1 compete with CheY2 in phosphotransfer from CheA (14) (Fig. 3A). The *cheT* deletion strain exhibited an increased swimming speed, similar to that of the Δ*cheD* and Δ*cheR* strains (Fig. 3A). Bioinformatics analysis identified two conserved residues in CheT that are critical for phosphatase activity in *E. coli* CheZ and other homologues (Fig. 1) (36, 37). To test whether these residues are important for CheT function, we created two mutant strains with asp-57 (BS190) and gln-61 (BS170) each replaced with an alanine residue. When these strains were tested in a swim plate motility assay, they behaved like wild type (Fig. 3B). In conclusion, deletion of *cheT* caused a chemotaxis defect in *S. meliloti* resulting in a fast swimming phenotype, which is likely not due to phosphatase activity of CheT.

In-vitro crosslinking assay to screen for CheT interaction partners

The observed phenotype of the *cheT* deletion strain indicated a role in *S. meliloti* chemotaxis by directly or indirectly affecting CheY2-P levels. However, the exact function and placement of CheT in the chemotactic signal transduction system is unclear. To test protein-protein interactions *in vitro*, we overexpressed CheT in *E. coli* ER2566 and purified it with the IMPACT system. A chemical crosslinking assay was used to examine putative interactions between CheT and selected chemotaxis proteins. Equimolar amounts of CheT and the target proteins were crosslinked by 1 % glutaraldehyde and separated electrophoretically. Subsequent detection was achieved via an anti-CheT antibody. From the banding pattern on the immunoblot we can infer that CheT migrates according to its predicted molecular weight at 13.4 kDa and has a strong tendency to dimerize despite the presence of a reducing agent (Fig. 4A, lane 1). The crosslinking agent further promoted dimerization and completely depleted the monomer pool (Fig. 4A, lane 2). Out of eight chemotaxis proteins tested, only the addition of CheR (34 kDa) to the crosslinking reaction resulted in a significant change in banding pattern. Two new major bands emerged, migrating at approximately 45 and 90 kDa, which concurred with a reduction in CheT-dimer band intensity (Fig. 4A, lane 6). Both bands are indicative of the formation of a 1:1 and a 2:2 CheR/CheT complex, respectively. To confirm the presence of CheR in these bands, we probed blots of similarly preformed cross-linking reactions with an anti-CheR antibody (Fig. 4B). While a 95-kDa band was detected, verifying the formation of a CheR/CheT complex, the 45-kDa band was absent (Fig. 4B, lane 3). Thus, this band might correspond to a CheT tetramer and its formation was promoted in the presence CheR. It should also be noted that a 75-kDa band in the anti-CheR blot indicated dimerization of CheR even in the presence of a reducing agent (Fig. 4B, lane 1). This finding is contrary to data from *Salmonella typhimurium* and *Pseudomonas putida,* which indicated a

monomeric nature of CheR-type methyltransferases (38, 39). In conclusion, data obtained from these crosslinking experiments revealed a putative interaction between CheT and CheR.

CheT can be copurified with CheR

In-vitro crosslinking experiments indicated that CheT likely interacts with CheR. To collect further evidence, we coexpressed CheR and CheT to determine if a stable complex could be purified. We used the pETDuet-1 system to express His_6-CheR and CheT both under control of the T7 promoter in *E. coli* strain BL21(DE3). Protein expression was induced for four hours at 25 °C, and cells were harvested and lysed. The cleared cell lysate was applied to a Ni-NTA column and bound proteins were eluted using a linearly increasing gradient of imidazole. Protein-containing fractions were separated by SDS-PAGE and visualized by Coomassie Brilliant Blue staining (Fig. 5A). As depicted in Fig. 5A, CheR and CheT co-eluted in the imidazole gradient from the Ni-NTA column. Next, CheR- and CheT-containing fractions were pooled and subjected to size exclusion chromatography (SEC). The chromatogram showed two main, protein-containing fractions (Fig. 5B), which were analyzed by SDS-PAGE (Fig. 5C). The first peak was comprised of CheR and CheT, while the latter only contained CheR. This result indicated that CheR and CheT form a complex, and that the eluant from the Ni-NTA column consisted of CheR and the CheR/CheT complex. We also performed the same experiment with coexpressed CheR and His_6-CheT. Both proteins coeluted from a Ni-NTA column, however, a larger amount of CheR eluted in the wash fractions indicating weaker protein interaction. Since CheR and His_6-CheT coeluted during SEC, protein interaction was not completely abolished by the His_6-tag (data not shown). In summary, chromatography of CheR and CheT confirmed the *in-vitro* crosslinking analysis.

CheR methylation of McpX is unaltered by CheT

To test whether CheT affects methyltransferase activity of CheR, we applied a tritium-based *in-vitro* methylation assay as developed for *E. coli* chemoreceptors (40). We chose McpX, which detects quaternary ammonium compounds, as substrate for methylation. McpX was overexpressed in *E. coli* strain Lemo21 (DE3) and McpX-containing membrane vesicles were isolated. These were then incubated with CheR in the presence of [^{3}H]-S-adenosyl-L-methionine (SAM[^{3}H]) and aliquots withdrawn at different time points. Samples were separated via SDS-gel electrophoresis and the release of ^{3}H-methanol from alkali-hydrolyzed gel fragments containing McpX was determined. Over a time course of 15 min, McpX methylation increased linearly. Yet, the addition of CheT had no significant effect on CheR methylation activity (Fig. 6.) Next, we analyzed methylation of McpX in the presence of one of its ligands, choline (41, 42). In analogy to *E. coli* MCPs, the addition of a ligand should increase receptor methylation *in vitro* (43). Nonetheless, this was not the case for McpX (Fig. 7). We also tested whether divalent cations, reducing (DTT) or chelating (EDTA) agents were required for CheT function; however, no change in McpX methylation was observed, with the exception of the addition of 5 mM magnesium that slightly reduced activity (Fig. 7). It has been reported that cyclic-di-GMP (c-di-GMP) is an activator for the CheR-binding protein MapZ in *Pseudomonas aeruginosa* (44, 45). Therefore, we assayed McpX methylation by CheR in the presence of CheT and c-di-GMP but found no significant impact. Finally, the methyltransferase activity of copurified CheR/CheT was compared to that of CheR, again without observing any difference in McpX methylation (data not shown). To assay a different CheR substrate, we purified membrane vesicles containing McpU. Yet, we were unsuccessful to determine conditions at which McpU was methylated by CheR (data not shown). In conclusion, CheT had no effect on McpX methylation by CheR under these assay conditions.

DISCUSSION

Investigations of the chemotaxis signaling pathway in *S. meliloti* had focused on the function of chemoreceptors, phosphotransfer reactions, and the stoichiometry of chemotaxis proteins (13, 14, 17, 18, 41, 46-48). In contrast, no direct experimental evidence of receptor methylation and its role in adaptation is available. However, information can be gleamed through a comparison of enzymes involved in adaptation across species. The canonical adaptation system in *E. coli* employs CheR and CheB to modify conserved glutamate residues in the signaling domains of MCPs (38). Both proteins bind to high-abundance MCPs in *E. coli* via a C-terminal pentapeptide motif that serves as a tether in the chemoreceptor array (49). In *S. meliloti*, four of the eight chemoreceptors (including McpX) possess a conserved pentapeptide motif (50, 51). However, different from *E. coli*, these MCPs are not present at high abundance, but only represent 13 % of the total receptor pool (33). Furthermore, *S. meliloti* CheR varies from *E. coli* CheR in lacking all residues required for pentapeptide binding in the beta-subdomain, a characteristic shared with closely related alphaproteobacteria (Fig. 1) (50). In addition, the CheR/receptor ratio is particularly high with one CheR monomer per receptor dimer. Lastly, the presence of CheD in the absence of a cognate phosphatase differentiates the *S. meliloti* system from that of *B. subtilis* (52). CheT, as described in this study, appears to only further set apart the adaptation system of *S. meliloti* and other alphaproteobacteria from the enteric model.

CheT is part of the chemotaxis system in *S. meliloti*

Initial bioinformatics analyses suggested that CheT functions as phosphatase due to the presence of a CheZ-like phosphatase motif. However, mutations of two conserved residues, asp-57 and gln-61, in the putative phosphatase motif of CheT failed to induce any chemotaxis defect (Fig. 2B).

We thus infer that CheT is not acting as a phosphatase. The deletion of *cheT* results in a chemotaxis defect due to an increased swimming velocity of mutant cells (Fig. 3). In the absence of key signal transduction proteins such as CheA and CheY2, the flagellar motors in *S. meliloti* always rotate at a fast speed, because the cells lack of phosphorylated CheY2 (14). Therefore, an increased swimming speed as a result of the *cheT* deletion points to a low cellular concentration of CheY2-P. Chemical crosslinking experiments suggest no direct interaction between CheT and any chemotaxis proteins other than CheR (Fig. 4), which let us to propose that CheT is part of the adaptation system. An adaption defect due to the absence of CheT likely results in inhibition of CheA autophosphorylation, which ultimately leads to a decreased pool of CheY2-P. This conclusion is also supported by the increased swimming speed of the *cheR* deletion strain (Fig. 3). However, *in-vitro* methylation assays suggest that the absence of CheT does not inhibit the net methylation of receptors as exemplary analyzed for McpX.

CheT forms a complex with CheR

Crosslinking and co-purification experiments indicate that CheT directly interacts with CheR to form a heterodimer (Figs. 4, 5). In addition, immunoblot analyses indicate that CheT, and to a certain degree CheR, form homodimers in the absence of a chemical crosslinking agent (Fig. 4). Contrary, there is no experimental evidence that CheR forms a homodimer in *E. coli* (38). At this point, we can only speculate whether a CheT dimer forms a complex with a CheR dimer or two CheR monomers. We observed that the N-terminal fusion of a his_6-tag to CheT weakens binding to CheR as referenced by a lower yield of a CheR/his_6-CheT complex after Ni-NTA chromatography, although binding is not completely abolished as both proteins co-elute during

SEC (data not shown). This suggests that the N-terminal region of CheT may be important in forming the CheR/CheT binding interface.

A proposed role of CheT in chemoreceptor methylation by CheR

The complex formation of CheT and CheR suggests that CheT affects CheR activity or the interaction of CheR with chemoreceptors. However, we observed no change in net methylation of McpX by CheR in the presence of CheT, despite various conditions tested. Furthermore, the addition of the McpX-ligand choline had no influence on methylation rate either in the presence or absence of CheT (Figs. 6, 7) (41, 42). There are a number of reasons for the lack of an observable effect of CheT on McpX methylation: (i) it is possible that McpX needs to be deamidated prior to methylation by the CheR/CheT complex. This would require the pre-treatment of McpX vesicles with CheB and/or CheD before performing methylation experiments; (ii) CheT may alter the order at which sites on McpX are being methylated. It is known for *E. coli* MCPs that CheR transfers methyl groups to different sites at different rates (53, 54). At this point, methylation sites in the signaling domain of McpX have only been annotated through homology with *E. coli* MCPs but not been verified experimentally. In *E. coli*, MCPs change their electrophoretic mobility, when different sites are methylated (55). However, we did not observe a change in the mobility of McpX upon methylation in the absence or presence of CheT (data not shown); (iii) it is feasible to propose that McpX cannot bind its ligand in membrane vesicles and, consequently, is not activated by choline, which might be a requirement for CheT function; (iv) It is possible that CheT only acts on a subset of receptors and that McpX is not the substrate of choice for the CheR/CheT complex. Unfortunately, we were unable to show methylation of McpU in membrane vesicles by CheR; (v) finally, CheT might need an additional signaling molecule for activation. In *P. aeruginosa*, the

CheR1-binding protein MapZ requires the presence of c-di-GMP to down-regulate CheR1 methylation activity (44, 45). Although CheT has no homology to MapZ or a putative c-di-GMP binding domain, we tested the activity of the CheR/CheT complex in the presence of c-di-GMP without observing a significant effect (Fig. 7). However, it is imaginable that a different signaling molecule or even another protein is required for CheT activity.

Conclusions

Here, we have shown that the CheT is part of the adaptation system of *S. meliloti* chemotaxis, which was a rather unexpected result. At this point, few conclusions can be made regarding its role without significant exploration of chemoreceptor methylation and the functions of CheB, CheR, and CheD in adaptation. However, we can assume that the adaptation system in *S. meliloti* exhibits unexpected departures from mechanisms in previously described species.

MATERIALS AND METHODS

Bacterial strains and plasmids

E. coli K12 and *S. meliloti* MV II-I derivatives used are listed in Table 1. The wild-type *S. meliloti* strain RU11/001, is a spontaneous streptomycin-resistant derivative of MVII-1 (56).

Genetic and DNA manipulations

S. meliloti mutants listed in Table 1 were created by allelic replacement essentially as laid out in Sourjik *et al.* and Zatakia *et al.* (14, 33).

Media and growth conditions

S. meliloti strains were grown in TYC (0.5 % tryptone, 0.3 % yeast extract, 0.13 % $CaCl_2$ x 6 H_2O [pH 7.0]) at 30 °C for 2 days. For motility and tracking experiments, cultures were subsequently diluted 1:100 in 10 ml RB minimal medium [6.1 mM K_2HPO_4, 3.9 mM KH_2PO_4, 1 mM $MgSO_4$, 1 mM $(NH_4)_2SO_4$, 0.1 mM $CaCl_2$, 0.1 mM NaCl, 0.01 mM Na_2MoO_4, 0.001 mM $FeSO_4$, 20 µg/l biotin, 100 µg/l thiamine], which was added as liquid layer on top of Bromfield medium (0.04 % tryptone, 0.01 % yeast extract, 0.01 % $CaCl_2H_2O$) agar plates and incubated at 30 °C to an optical density at 600 nm (OD_{600}) of 0.1. *E. coli* strains were grown at 37 °C in lysogeny broth (LB). Antibiotics were used at the following concentration: for *S. meliloti,* streptomycin at 600 µg/ml, neomycin 120 µg/ml, for *E. coli*, ampicillin at 100 µg/ml and chloramphenicol at 30 µg/ml.

Swim plate assays

Bromfield medium swim plates containing 0.3 % (wt/vol) Bacto agar were inoculated with 3 µl of *S. meliloti* cultures grown in TYC and incubated at 30 °C for 3 to 4 days.

Computerized motion analysis of free-swimming cells

The speed of free-swimming cells at an OD_{600} of 0.1 was determined with a Zeiss standard 14 phase-contrast microscope (magnification, × 400) at 22 °C using the computerized motion analysis of the Hobson BacTracker system (Hobson Tracking Systems, Sheffield, United Kingdom) as previously described in Meier *et al.,* 2007 (51). Mean and standard deviation were calculated from five separate biological replicates. Statistical significance was determined by a two-tailed Student's *T-test* in relation to the wild-type strain speed.

Expression and purification of CheR and CheT

CheT and CheR were overexpressed in *E. coli* ER2566 from pBS359 and pBS450, respectively. Cells were grown at 37 °C in LB containing 100 µg/ml ampicillin to an OD_{600} of 0.7-0.9 and gene expression was induced with 0.3 mM IPTG (isopropyl-β-d-thiogalactopyranoside). Cultivation of the cells continued for 16-20 h at 16 °C until cells harvest by centrifugation. The cells were suspended in IMPACT buffer (20 mM Tris/HCl [pH 8.0], 500 mM NaCl, 1 mM EDTA). Cells were then lysed by three passages through a French pressure cell (SLM Aminco, Silver Spring, MD) at 20,000 psi and centrifuged 48,000 x g at 4 °C for 1 h to remove insoluble material and unlysed cells. The soluble fraction was passed through a 0.2 µm filter and loaded on a chitin agarose (NE Biolabs, Beverly MA, USA) column (2.6 x 5.0 cm) equilibrated with IMPACT buffer. The column was washed with 10-20 bed volumes of IMPACT buffer at 4 °C. Intein-mediated cleavage was induced by equilibration of the column with two bed volumes of IMPACT buffer containing 50 mM dithiothreitol, followed by 12-36 h incubation at 4 °C. The protein was eluted with IMPACT buffer and protein-containing fractions were collected. Fractions were pooled,

concentrated to 10 ml and subjected to size exclusion chromatography (SEC) on a HiPrep^{TM} 26/60 Sephacryl^{TM} S-200 HR column (GE Healthcare Life Sciences). CheR and CheT were co-expressed in *E. coli* BL21(DE3) from pBS1097 or pBS1108. For both constructs cells were grown at 37 °C in lysogeny broth (LB) containing 100 µg/ml ampicillin to an OD_{600} of 0.7- 0.9 and gene expression was induced with 0.5 mM IPTG. Cultivation of the cells continued for 4 h at 37˚ C until cells harvest by centrifugation. Cells were suspended in Ni-NTA binding buffer (500 mM NaCl, 20 mM imidazole, 1 mM PMSF, 20 mM $NaPO_4$ [pH 7.0]), lysed by three passages through a French pressure cell (SLM Aminco, Silver Spring, MD), and centrifuged for 1 h at 48,000 x g and 4 °C. The soluble fraction was passed through a 0.2 µm filter and loaded onto a charged 5-ml Ni-NTA column (GE Healthcare Life Sciences). Proteins were eluted using a linear gradient of elution buffer (500 mM NaCl, 500 mM imidazole, 1 mM PMSF, 20 mM $NaPO_4$ [pH 7.0]). Protein-containing elution fractions were pooled, concentrated and further purified through SEC on a HiPrepTM 26/60 Sephacryl^{TM} S-200 HR column (GE Healthcare Life Sciences).

Expression and purification of other chemotaxis proteins

Expression and purification of CheA, CheY1, CheY2, and CheS was performed as described in Dogra *et al.*, 2012 (18). Expression and purification of CheB, CheD, and CheW1 was accomplished essentially as described in Arapov *et al.* (57).

***In-vitro* crosslinking assays**

Freshly prepared glutaraldehyde (Sigma-Aldrich) at a final concentration of 1 % (wt /vol) was used for protein crosslinking experiments essentially as previously described (17, 18). Proteins were used at a concentration of 1 µM in a buffer containing 20 mM NaCl, 1 mM EDTA, 20 mM

$NaPO_4$, pH 7.5. Reactions were stopped after an incubation of 30 min at room temperature by the addition of an equal volume of 2x Laemmli buffer.

Immunoblots

Cross-linked samples were separated by gel electrophoresis on a 4-20 % Criterion TGX gradient gel (Biorad) and transferred to a 0.45 µm nitrocellulose membrane in transfer buffer (20 % methanol, 50 mM Tris, 40 mM glycine). Membranes were blocked overnight with 5 % non-fat dry milk with 0.1 % Tween 20 in phosphate buffered saline (PBS, 100 mM NaCl, 80 mM Na_2HPO_4, 20 mM NaH_2PO_4, pH 7.5). Blots were then probed with anti-CheT or anti-CheR affinity-purified antibodies at a 1:400 dilution for 1.5 h at room temperature. Blots were subsequently washed for 30 min with PBS/0.1 % Tween 20 with four buffer changes and probed with donkey anti-rabbit conjugated with horseradish peroxidase at a 1:1,500 dilution for 1.5 h. The blots were then washed for 30 min with PBS/0.1 % Tween 20 with four buffer changes. Detection was performed by chemiluminescence (Amersham ECL Western Blotting Detection Kit, GE Healthcare) using Hyperfilm ECL (GE Healthcare).

Isolation of McpX-containing membrane vesicles

Preparation of membrane vesicles was done essentially as previously described in Osborne and Munson (58) and Gegner *et al.* (59). An overnight culture of *E. coli* Lemo21(DE3) with pBS1096 expressing McpX grown in LB containing ampicillin and chloramphenicol as well as 500 µM L-rhamnose was diluted to a final OD_{600} of 0.05. To ensure proper aeration, cultures were placed in flasks with the volume of the growth medium not exceeding 15 % of the maximum volume of each flask. Cells were grown at 37 °C to an OD_{600} of 0.4-0.5, gene expression was induced by 0.4 mM

IPTG and cultivation continued for 4 h at 37 °C. Cells were harvested by centrifugation and suspended in 10 mM Tris/HCl (pH 7.5), 20 % sucrose (wt/wt). Lysozyme and EDTA were subsequently added to a final concentration of 100 µg/ml and 5mM, respectively. Cells were incubated on ice for 5 min under gentle agitation. Two volumes of 5 mM EDTA, 1 mM PMSF and 1 mM 1,10 phenanthroline (Phe) were then slowly added with a glass pipette. Cells were lysed by the addition of four volumes of ice-cold H_2O and subsequent vigorous agitation for 1 min. DNase and $MgCl_2$ were added to a final concentration of 10 µg/ml and 3mM, respectively. The lysate was centrifuged for 1.5 h at 27,485 x g and 4 °C. The insoluble fraction was suspended in 50 mM Tris/HCl [pH 7.5], 5 mM $MgCl_2$, 50 mM KCl, 0.5 mM PMSF, 1 mM Phe, and subsequently dialyzed for 14 h at 4 °C against the same buffer.

***In-vitro* methylation assays**

In-vitro methylation assays were carried out essentially as described in Barnakov *et al.*, 1998 (40). Isolated membrane vesicles with and without McpX, CheT, and CheR were dialyzed against TGD buffer (50 mM Tris/HCl [pH 7.5], 10 % glycerol, 5 mM dithiothreitol). McpX in membrane vesicles and CheR were used at 1.2 µM and 0.2 µM, respectively, in the absence and in the presence of 4.6 µM CheT, and reactions were initiated by addition of adenosyl-L-methionine S-[methyl-^{3}H] (SAM) (PerkinElmer) (0.9 Ci/mmole) at a final concentration of 50 µM. At indicated time points, 20-µl samples were added to 20 µl 2x Laemmli buffer and boiled for 1 min to terminate the reactions. Twenty microliter aliquots were analyzed by electrophoresis on a 10 % acrylamide SDS-gel. Bands corresponding to McpX were excised from Coomassie-stained dry gels. The excised bands were subjected to alkali hydrolysis in 200 µl 1 M NaOH for 24 h. Quantification of

released radiolabeled methanol was enabled by vapor-phase equilibrium of volatile methanol and ECONO-SAFE scintillation cocktail.

ACKNOWLEDGMENTS

This study was supported by NSF grants MCB-1253234 and MCB-1817652 to Birgit Scharf. We would like to thank Andrea Brücher (Department of Genetics, University Regensburg. Germany) for *S. meliloti* velocity measurements, Victor Sourjik for constructing strains RU11/306, RU11/312, RU11/319, Paul Muschler for constructing strain RU11/411, and all Scharf lab members for in the critical reading of the manuscript.

Table 5.1.Bacterial strains and plasmids

Strain/Plasmid	Relevant Characteristics	Source or Reference
E. coli		
BL21(DE3)	*F− ompT hsdSB(rB− mB−) gal dcm λ (DE3)*	Novagen
ER2566	*ion ompT lacZ::T7*	New England Biolabs
Lemo21(DE3)	*fhuA2* [*lon*] *ompT gal* (λDE3) *dcm* Δ*hsdS*/pLemo(Cm^r)	New England Biolabs
M15/pREP4	Ap^r Km^r; F- ϕ80ΔlacM15 *thi lac- mtl- recA*$^+$	Qiagen
S17-1	Sm^r Tp^r; *recA endA thi hsdR* RP4-2 Tc::Mu::Tn7	(60)
S. meliloti		
RU11/001	Sm^r; Spontaneous streptomycin-resistant wild-type strain	(61)
RU11/306	Δ*cheR*	Arapov *et al.* (57)
RU11/307	Δ*cheY2*	(14)
RU11/308	Δ*cheY1*	(14)
RU11/310	Δ*cheA*	(14)
RU11/312	Δ*cheB*	Arapov *et al.* (57)
RU11/319	Δ*cheT*	Arapov *et al.*(57)
RU11/411	Δ*cheD*	Arapov *et al.*(57)
BS170	Sm^r; *cheT* with codon 61 changed from CAG to GCC (Q61A)	This study
BS190	Sm^r; *cheT* with codon 57 changed from GAC to GCC (D57A)	This Study
Plasmids		
pBBR1-MCS2	Km^r; broad host-range vector	(62)
pBS16[a]	Ap^r; pTYB1-*cheY1*	(17)
pBS18[a]	Ap^r; pTYB1-*cheY2*	(17)
pBS57[a]	Ap^r; pTYB1-*cheA*	(17)
pBS93	Ap^r; pTYB11-*cheB*	This study
pBS173	Km^r; 291-bp NcoI-BamHI fragment from pRU2804 containing *cheS* cloned into pET27bmod	(18)
pBS189	Km^r; pBBR1MCS2-*lacI*^{q}	(47)
pBS331	Ap^r; pTYB11-*cheD*	This study
pBS359	Ap^r; pTYB11-*cheT*	This study
pBS445	Km^r; pBS189-*cheT*	This study
pBS450	Ap^r; pTYB1-*cheR*	This study
pBS567	Ap^r; pQE60-*cheW1*	This study
pBS1095	Ap^r; pET22B(+)-*mcpU*	This study
pBS1096	Ap^r; pET22B(+)-*mcpX*	This study
pBS1097	Ap^r; pETDuet-MCS1-*cheR* MCS2-*cheT*	This study
pBS1108	Ap^r; pETDuet-MSC1-*cheT* MSC2-*cheR*	This study
pET27bmod	Km^r; expression vector	Novagen
pETDuet-1	Ap^r; expression vector	Novagen
pK18*mobsacB*	Km^r; *mob sacB*, vector used for homologous allelic exchange	(63)
pQE60	Ap^r;	Qiagen

pTYB1	Ap^r; expression vector for Impact system	New Biolabs	England
pTYB11	Ap^r; expression vector for Impact system	New Biolabs	England

[a]Equivalent to pRU2312, pRU2313, and pRU2326, respectively, as described in Riepl *et al.*, 2008 (17).

REFERENCES

1. Scharf BE, Hynes MF, Alexandre GM. 2016. Chemotaxis signaling systems in model beneficial plant–bacteria associations. Plant Mol Biol 90:549-559.
2. Raina J, Fernandez V, Lambert B, Stocker R, Seymour JR. 2019. The role of microbial motility and chemotaxis in symbiosis. Nat Rev Microbiol 17:284-294.
3. Berg HC. 1993. Random walks in biology. Princeton University Press.
4. Wadhams GH, Armitage JP. 2004. Making sense of it all: bacterial chemotaxis. Nat Rev Mol Cell Biol 5:1024-1037.
5. Porter SL, Wadhams GH, Armitage JP. 2011. Signal processing in complex chemotaxis pathways. Nat Rev Microbiol 9:153-165.
6. Sourjik V, Wingreen NS. 2012. Responding to chemical gradients: bacterial chemotaxis. Curr Opin Cell Biol 24:262-268.
7. Yang W, Briegel A. 2020. Diversity of bacterial chemosensory arrays. Trends Microbiol 28:68-80.
8. Briegel A, Ladinsky MS, Oikonomou C, Jones CW, Harris MJ, Fowler DJ, Chang YW, Thompson LK, Armitage JP, Jensen GJ. 2014. Structure of bacterial cytoplasmic chemoreceptor arrays and implications for chemotactic signaling. Elife 3:e02151.
9. Borkovich KA, Kaplan N, Hess JF, Simon MI. 1989. Transmembrane signal transduction in bacterial chemotaxis involves ligand-dependent activation of phosphate group transfer. Proc Natl Acad Sci U S A 86:1208-1212.
10. Lukat GS, Lee BH, Mottonen JM, Stock AM, Stock JB. 1991. Roles of the highly conserved aspartate and lysine residues in the response regulator of bacterial chemotaxis. J Biol Chem 266:8348-54.
11. Welch M, Oosawa K, Aizawa S, Eisenbach M. 1993. Phosphorylation-dependent binding of a signal molecule to the flagellar switch of bacteria. Proc Natl Acad Sci U S A 90:8787-8791.
12. Schmitt R. 2002. *Sinorhizobial* chemotaxis: a departure from the enterobacterial paradigma. Microbiology 148:627-631.
13. Scharf BE, Schmitt R. 2002. Sensory transduction to the flagellar motor of *Sinorhizobium meliloti*. J Mol Microbiol Biotechnol 4:183-6.
14. Sourjik V, Schmitt R. 1996. Different roles of CheY1 and CheY2 in the chemotaxis of *Rhizobium meliloti*. Mol Microbiol 22:427-36.
15. Attmannspacher U, Scharf B, Schmitt R. 2005. Control of speed modulation (chemokinesis) in the unidirectional rotary motor of *Sinorhizobium meliloti*. Mol Microbiol 56:708-18.
16. Miller LD, Russell MH, Alexandre G. 2009. Diversity in bacterial chemotactic responses and niche adaptation. Adv Appl Microbiol 66:53-75.
17. Riepl H, Maurer T, Kalbitzer HR, Meier VM, Haslbeck M, Schmitt R, Scharf BE. 2008. Interaction of CheY2 and CheY2-P with the cognate CheA kinase in the chemosensory-signalling chain of *Sinorhizobium meliloti*. Mol Microbiol 69:1373-1384.
18. Dogra G, Purschke FG, Wagner V, Haslbeck M, Kriehuber T, Hughes JG, Van Tassell ML, Gilbert C, Niemeyer M, Ray WK, Helm RF, Scharf BE. 2012. *Sinorhizobium meliloti* CheA complexed with CheS exhibits enhanced binding to CheY1, resulting in accelerated CheY1 dephosphorylation. J Bacteriol 194:1075-87.

19. Vladimirov N, Sourjik V. 2009. Chemotaxis: how bacteria use memory. Biol Chem 390:1097-104.
20. Tu Y. 2013. Quantitative modeling of bacterial chemotaxis: signal amplification and accurate adaptation. Annual review of biophysics 42:337-359.
21. Hazelbauer GL, Falke JJ, Parkinson JS. 2008. Bacterial chemoreceptors: high-performance signaling in networked arrays. Trends Biochem Sci 33:9-19.
22. Morgan DG, Baumgartner JW, Hazelbauer GL. 1993. Proteins antigenically related to methyl-accepting chemotaxis proteins of *Escherichia coli* detected in a wide range of bacterial species. J Bacteriol 175:133-140.
23. Weis RM, Koshland DE. 1988. Reversible receptor methylation is essential for normal chemotaxis of *Escherichia coli* in gradients of aspartic acid. Proc Natl Acad Sci U S A 85:83-87.
24. Lai W-C, Barnakova LA, Barnakov AN, Hazelbauer GL. 2006. Similarities and differences in interactions of the activity-enhancing chemoreceptor pentapeptide with the two enzymes of adaptational modification. J Bacteriol 188:5646.
25. Hess JF, Oosawa K, Kaplan N, Simon MI. 1988. Phosphorylation of three proteins in the signaling pathway of bacterial chemotaxis. Cell 53:79-87.
26. Kehry MR, Bond MW, Hunkapiller MW, Dahlquist FW. 1983. Enzymatic deamidation of methyl-accepting chemotaxis proteins in *Escherichia coli* catalyzed by the cheB gene product. Proc Natl Acad Sci U S A 80:3599-3603.
27. Djordjevic S, Goudreau PN, Xu Q, Stock AM, West AH. 1998. Structural basis for methylesterase CheB regulation by a phosphorylation-activated domain. Proc Natl Acad Sci U S A 95:1381-1386.
28. Rosario ML, Ordal GW. 1996. CheC and CheD interact to regulate methylation of *Bacillus subtilis* methyl-accepting chemotaxis proteins. Mol Microbiol 21:511-518.
29. Rao CV, Glekas GD, Ordal GW. 2008. The three adaptation systems of *Bacillus subtilis* chemotaxis. Trends Microbiol 16:480-7.
30. Krembel A, Colin R, Sourjik V. 2015. Importance of multiple methylation sites in Escherichia coli chemotaxis. PloS one 10.
31. Glekas GD, Cates JR, Cohen TM, Rao CV, Ordal GW. 2011. Site-specific methylation in *Bacillus subtilis* chemotaxis: effect of covalent modifications to the chemotaxis receptor McpB. Microbiology 157:56-65.
32. Walukiewicz HE, Tohidifar P, Ordal GW, Rao CV. 2014. Interactions among the three adaptation systems of *Bacillus subtilis* chemotaxis as revealed by an in vitro receptor-kinase assay. Mol Microbiol 93:1104-18.
33. Zatakia HM, Arapov TD, Meier VM, Scharf BE. 2018. Cellular stoichiometry of methyl-accepting chemotaxis proteins in *Sinorhizobium meliloti*. J Bacteriol 200:e00614-17.
34. Sourjik V, Sterr W, Platzer J, Bos I, Haslbeck M, Schmitt R. 1998. Mapping of 41 chemotaxis, flagellar and motility genes to a single region of the *Sinorhizobium meliloti* chromosome. Gene 223:283-290.
35. Buchan DW, Jones DT. 2019. The PSIPRED protein analysis workbench: 20 years on. Nucleic Acids Res 47:W402-W407.
36. Zhao R, Collins EJ, Bourret RB, Silversmith RE. 2002. Structure and catalytic mechanism of the *E. coli* chemotaxis phosphatase CheZ. Nat Struct Biol 9:570-5.

37. Liu X, Liu W, Sun Y, Xia C, Elmerich C, Xie Z. 2018. A cheZ-like gene in *Azorhizobium caulinodans* is a key gene in the control of chemotaxis and colonization of the host plant. Appl Environ Microbiol 84:e01827-17.
38. Simms SA, Stock AM, Stock JB. 1987. Purification and characterization of the S-adenosylmethionine:glutamyl methyltransferase that modifies membrane chemoreceptor proteins in bacteria. J Biol Chem 262:8537-43.
39. García-Fontana C, Reyes-Darias J, Muñoz-Martínez F, Alfonso C, Morel B, Ramos J, Krell T. 2013. High specificity in CheR methyltransferase function: CheR2 of *Pseudomonas putida* is essential for chemotaxis, whereas CheR1 is involved in biofilm formation. J Biol Chem 288:18987-18999.
40. Barnakov AN, Barnakova LA, Hazelbauer GL. 1998. Comparison *In Vitro* of a high- and a low-abundance chemoreceptor of *Escherichia coli*: similar kinase activation but different methyl-accepting activities. J Bacteriol 180:6713-6718.
41. Webb BA, Karl Compton K, Castaneda Saldana R, Arapov TD, Keith Ray W, Helm RF, Scharf BE. 2017. *Sinorhizobium meliloti* chemotaxis to quaternary ammonium compounds is mediated by the chemoreceptor McpX. Mol Microbiol 103:333-346.
42. Shrestha M, Compton KK, Mancl JM, Webb BA, Brown AM, Scharf BE, Schubot FD. 2018. Structure of the sensory domain of McpX from *Sinorhizobium meliloti*, the first known bacterial chemotactic sensor for quaternary ammonium compounds. Biochem J 475:3949-3962.
43. Spiro PA, Parkinson JS, Othmer HG. 1997. A model of excitation and adaptation in bacterial chemotaxis. Proc Natl Acad Sci U S A 94:7263-7268.
44. Yan X, Xin L, Yen J, Zeng Y, Jin S, Cheang Q, Fong R, Chiam K, Liang Z, Gao Y. 2018. Structural analyses unravel the molecular mechanism of cyclic di-GMP regulation of bacterial chemotaxis via a PilZ adaptor protein. J Biol Chem 293:100-111.
45. Orr MW, Lee VT. 2016. A PilZ domain protein for chemotaxis adds another layer to c-di-GMP–mediated regulation of flagellar motility. Sci Signal 9:fs16-fs16.
46. Sourjik V, Schmitt R. 1998. Phosphotransfer between CheA, CheY1, and CheY2 in the chemotaxis signal transduction chain of *Rhizobium meliloti*. Biochemistry 37:2327-2335.
47. Webb BA, Hildreth SB, Helm RF, Scharf BE. 2014. *Sinorhizobium meliloti* chemoreceptor McpU mediates chemotaxis toward host plant exudates through direct proline sensing. Appl Environ Microbiol 80:3404-3415.
48. Compton KK, Hildreth SB, Helm RF, Scharf BE. 2018. *Sinorhizobium meliloti* chemoreceptor McpV senses short-chain carboxylates via direct binding. J Bacteriol 200:e00519-18.
49. Wu J, Li J, Li G, Long DG, Weis RM. 1996. The receptor binding site for the methyltransferase of bacterial chemotaxis is distinct from the sites of methylation. Biochemistry 35:4984-4993.
50. Perez E, Stock AM. 2007. Characterization of the *Thermotoga maritima* chemotaxis methylation system that lacks pentapeptide-dependent methyltransferase CheR:MCP tethering. Mol Microbiol 63:363-78.
51. Meier VM, Muschler P, Scharf BE. 2007. Functional analysis of nine putative chemoreceptor proteins in *Sinorhizobium meliloti*. J Bacteriol 189:1816-1826.
52. Yuan W, Glekas GD, Allen GM, Walukiewicz HE, Rao CV, Ordal GW. 2012. The importance of the interaction of CheD with CheC and the chemoreceptors compared to its enzymatic activity during chemotaxis in *Bacillus subtilis*. PLoS One 7:e50689.

53. Li M, Hazelbauer GL. 2020. Methyltransferase CheR binds to its chemoreceptor substrates independent of their signaling conformation yet modifies them differentially. Protein Sci 29:443-454.
54. Chalah A, Weis RM. 2005. Site-specific and synergistic stimulation of methylation on the bacterial chemotaxis receptor Tsr by serine and CheW. BMC Microbiol 5:12.
55. Engström P, Hazelbauer GL. 1980. Multiple methylation of methyl-accepting chemotaxis proteins during adaptation of *E. coli* to chemical stimuli. Cell 20:165-171.
56. Krupski G, Götz R, Ober K, Pleier E, Schmitt R. 1985. Structure of complex flagellar filaments in *Rhizobium meliloti*. J Bacteriol 162:361-366.
57. Arapov TD, Castaneda Saldana R, Sebastian AL, Keith Ray W, Helm RF, Scharf B, E. 2020. Cellular stoichiometry of chemotaxis proteins in *Sinorhizobium meliloti*. In preparation
58. Osborn M, Munson R. 1974. Separation of the inner (cytoplasmic) and outer membranes of gram-negative bacteria, p 642-653, Methods Enzymol, vol 31. Elsevier.
59. Gegner JA, Graham DR, Roth AF, Dahlquist FW. 1992. Assembly of an MCP receptor, CheW, and kinase CheA complex in the bacterial chemotaxis signal transduction pathway. Cell 70:975-982.
60. Simon R, O'Connell M, Labes M, Puhler A. 1986. Plasmid vectors for the genetic analysis and manipulation of *rhizobia* and other gram-negative bacteria. Methods Enzymol 118:640-59.
61. Pleier E, Schmitt R. 1991. Expression of two *Rhizobium meliloti* flagellin genes and their contribution to the complex filament structure. J Bacteriol 173:2077-85.
62. Kovach ME, Elzer PH, Hill DS, Robertson GT, Farris MA, Roop II RM, Peterson KM. 1995. Four new derivatives of the broad-host-range cloning vector pBBR1MCS, carrying different antibiotic-resistance cassettes. Gene 166:175-176.
63. Schäfer A, Tauch A, Jäger W, Kalinowski J, Thierbach G, Pühler A. 1994. Small mobilizable multi-purpose cloning vectors derived from the *Escherichia coli* plasmids pK18 and pK19: selection of defined deletions in the chromosome of *Corynebacterium glutamicum*. Gene 145.

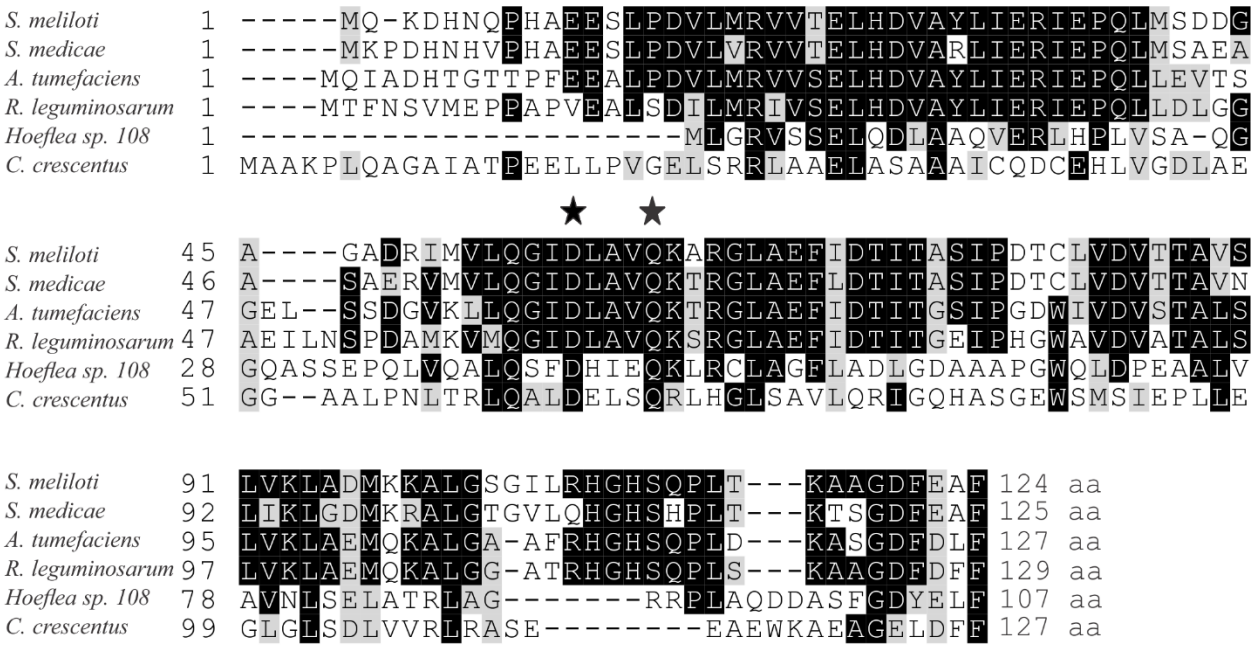

Figure 5.1 Alignment of the amino acid sequence of *S. meliloti* CheT with five paralogues from related alphaproteobacteria ; *S. meliloti* CheT (NP_384751.1), *Sinorhizobium medicae* (*YP_001325935.1*), *Agrobacterium tumefaciens* (WP_003493786.1), *Rhizobium leguminosarum* (WP_003588573.1), *Hoeflea* sp. 108 (WP_018430236.1), and *Caulobacter crescentus* CheU (NP_419258.1). GenBank accession numbers are given in parentheses. Sequences were aligned through ClustalOmega. Black shading indicates identical residues, grey indicates residues with similar side change properties. Stars indicate conserved residues indicative of a putative (DXXXQ) CheZ-like phosphatase motif.

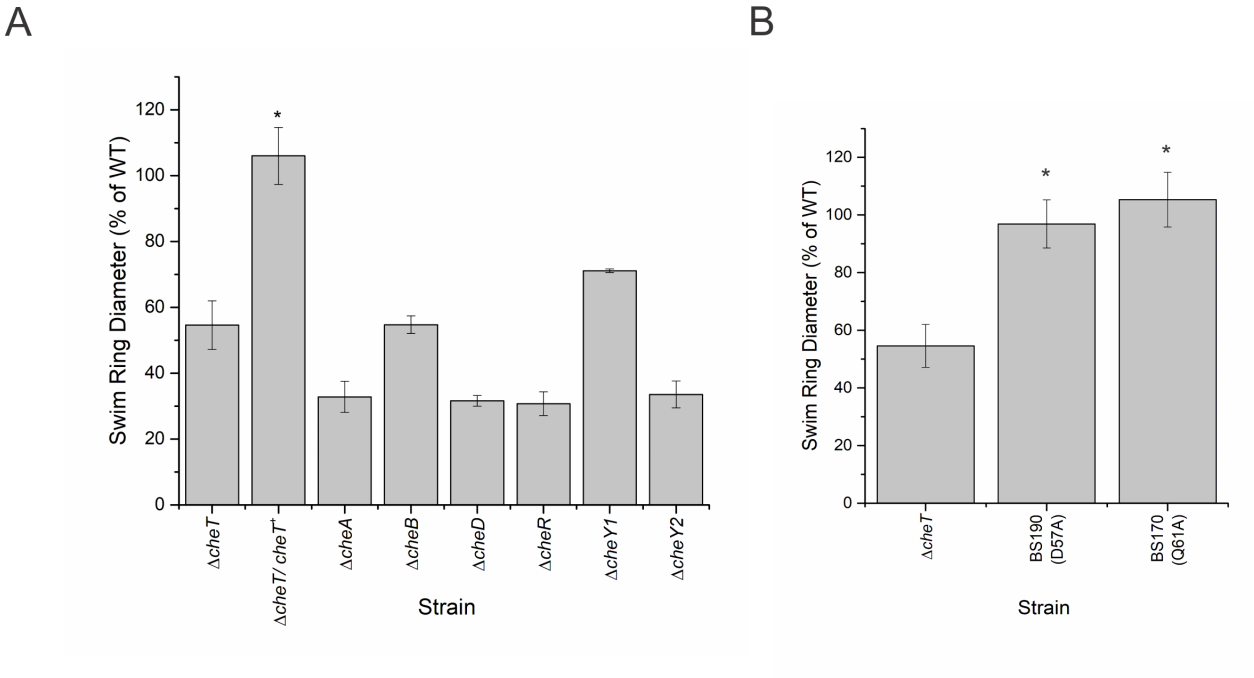

Figure 5.2 Chemotactic responses of various *S. meliloti che* mutant strains in a quantitative swim plate assay compared to the wild-type strain (RU11/001) . Strain designation: Δ*cheT*, in-frame deletion of *cheT (*RU11/319), Δ*cheT*/*cheT*$^{+}$, in-frame deletion of *cheT* (RU11/319) with pBBR1MCS-2-*cheT* (pBS445); Δ*cheA*, in-frame deletion of *cheA (*RU11/310); Δ*cheB*, in-frame deletion of *cheB (*RU11/312); Δ*cheD*, in-frame deletion of *cheD (*RU11/411); Δ*cheR*, in-frame deletion of *cheR* (RU11/306); Δ*cheY1*, in frame deletion of CheY1 (RU11/308); Δ*cheY2* in frame deletion of *cheY2* (RU11/307). Percentages of the wild-type swim diameter on 0.3% Bromfield agar are the means of seven replicates. Error bars represent the standard deviations from the mean. Statistical significance was determined by a two-tailed Student's T-test ($p < 0.05$). Asterisk symbol denotes no statistically significant difference from the wild type.

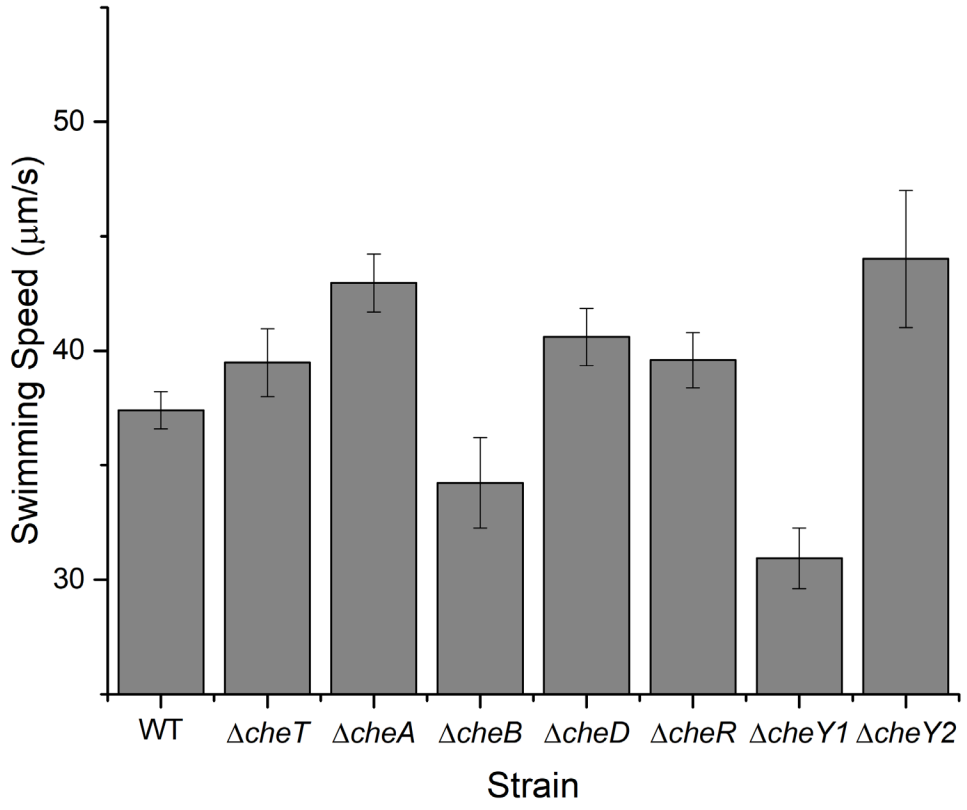

Figure 5.3 Free swimming speed of *S. meliloti* wild-type and chemotaxis gene deletion strains . Strain designation: WT (RU11/001), Δ*cheA*, in-frame deletion of *cheA (*RU11/310); Δ*cheB*, in-frame deletion of *cheB* (RU11/312); Δ*cheD*, in-frame deletion of *cheD (*RU11/411); Δ*cheR*, in-frame deletion of *cheR* (RU11/306); Δ*cheT*, in-frame deletion of *cheT* (RU11/319); Δ*cheY1*, in-frame deletion of *cheY1* (RU11/308); Δ*cheY2*, in frame deletion of *cheY2* (RU11/307).

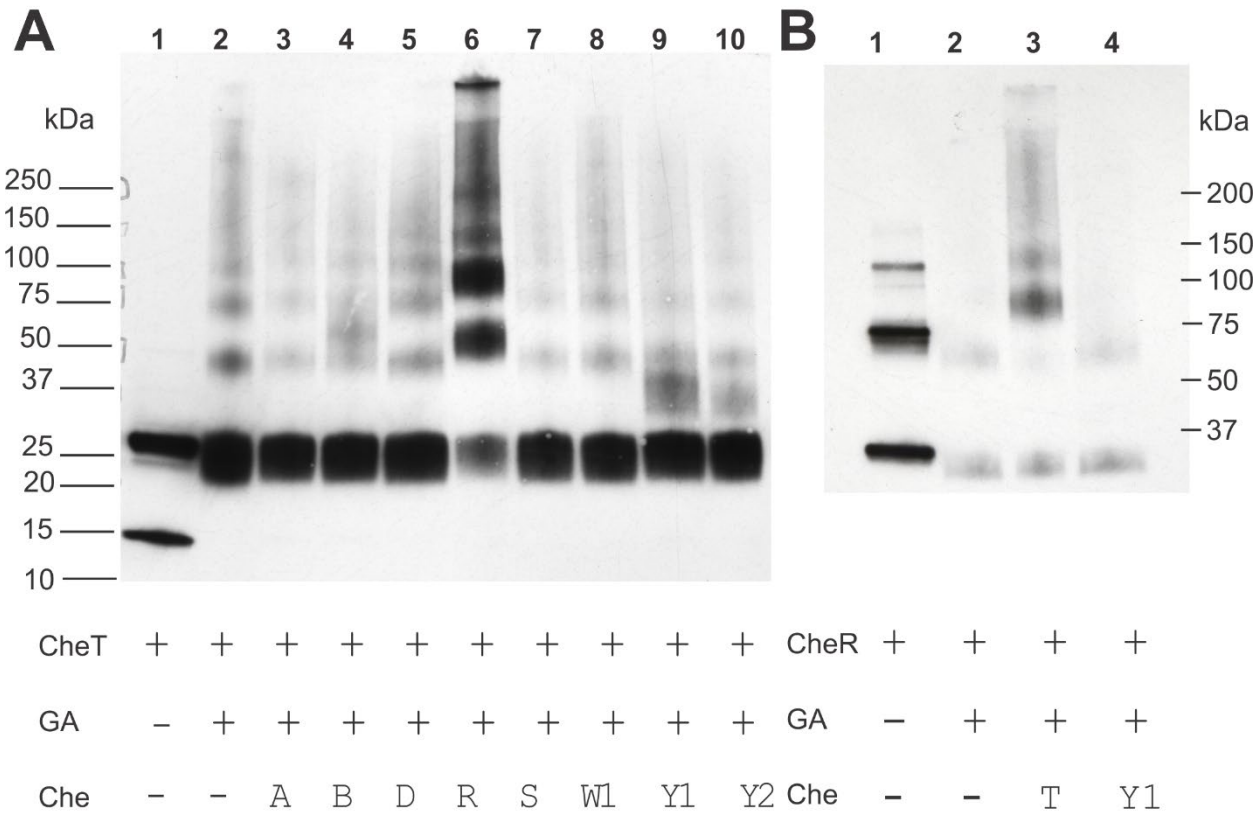

Figure 5.4 Immunoblot analysis to assess the binding of S. meliloti CheT and selected chemotaxis proteins . A. CheT (0.7 μM) was cross-linked by glutaraldehyde (GA) for 45 min to CheA, CheB, CheD, CheR, CheS, CheW1, CheY1, CheY2. Products were separated by gradient gel electrophoresis and probed with an anti-CheT antibody. B. CheR (11 μM), and cross-linked CheR (0.7 μM), and CheR cross-linked to CheT and CheY1. Products were separated by gradient gel electrophoresis and probed with an anti-CheR antibody.

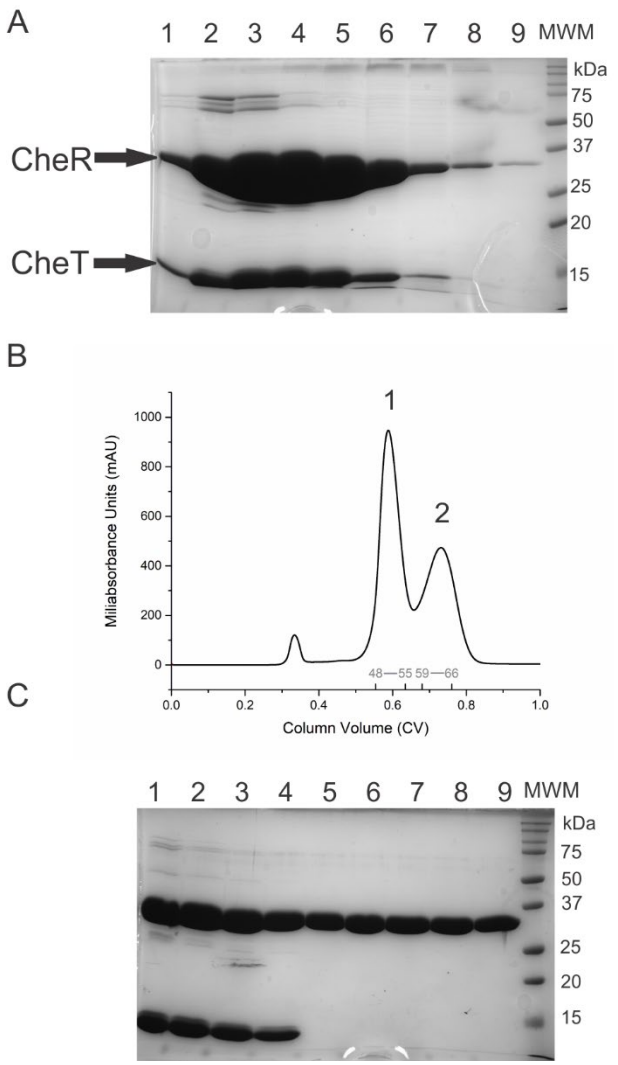

Figure 5.5 Copurification of His_6-CheR and CheT . **A.** Coomassie-stained SDS-gel of elution fractions after Ni-NTA affinity. **B.** Chromatogram of Sephacryl S-200 size exclusion chromatography. **C.** Coomassie-stained SDS-gel of fractions after Sephacryl S-200 chromatography.

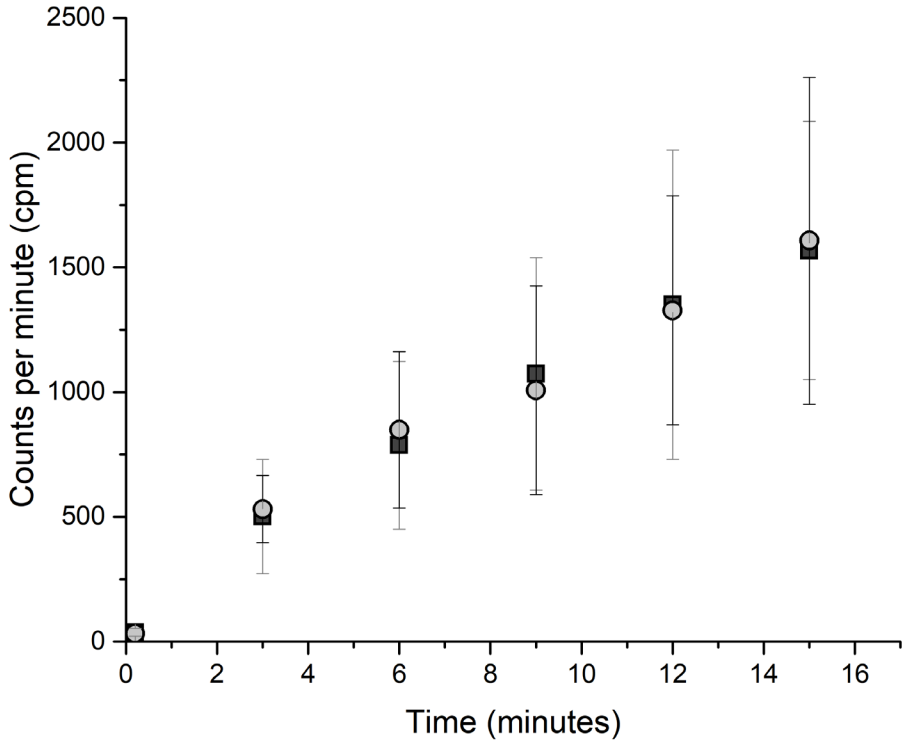

Figure 5.6 Time course of McpX methylation by CheR using [^{3}H]-S-adenosylmethionine (SAM[^{3}H]) as substrate. Reactions of 1.2 µM McpX in membrane vesicles with 0.2 µM CheR and 50 µM SAM were incubated for 0.2, 3, 6, 9, 12, 15 min at room temperature and stopped by incubation at 100 °C in the presence of Laemmli buffer. Black squares and grey circles represent the mean derived from three replicates in the absence and presence of 4.6 µM CheT,

respectively, error bars were derived from the standard deviation of three replicates.

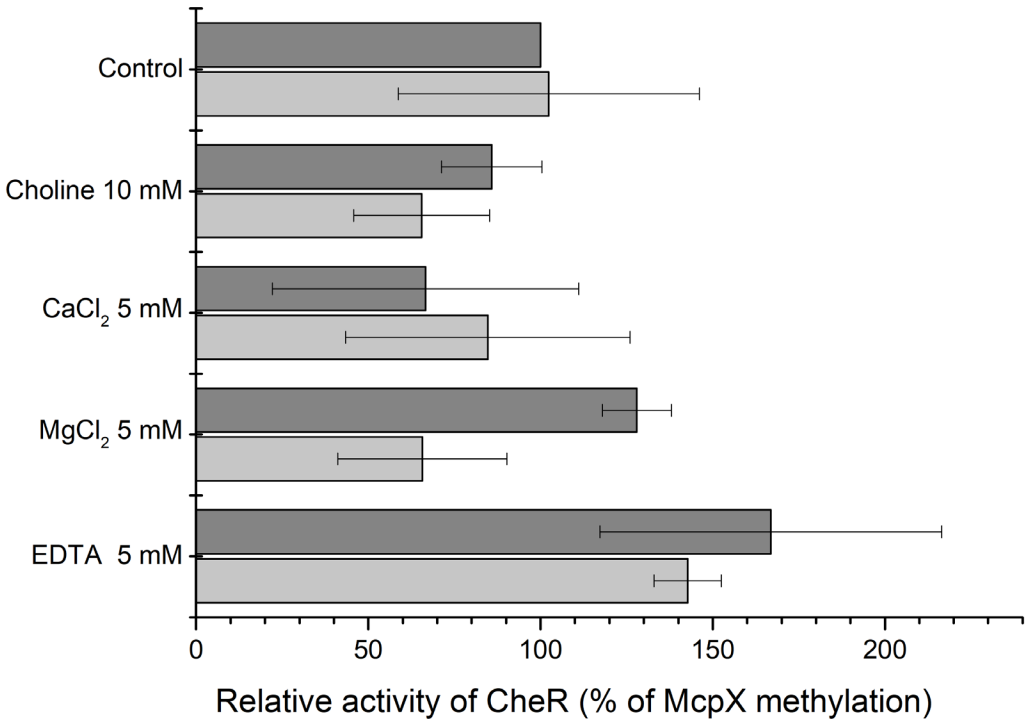

Figure 5.7 McpX methylation by CheR using [^{3}H]-S-adenosylmethionine (SAM[^{3}H]) as substrate with various supplements . Reactions of 1.2 µM McpX in membrane vesicles with 0.2 µM CheR and 50 µM SAM[^{3}H] were incubated for 15 min at room temperature and stopped by incubation at 100 °C in the presence of Laemmli buffer. All reactions were performed in TGD buffer with the specified additive for each condition. Dark and light grey bars represent the mean derived from three replicates in the absence and presence of 4.6 µM CheT.

Chapter 6 – Final Discussion

In chapters 2 and 3 we elucidated the stoichiometry of all *Sinorhizobium meliloti* chemotaxis proteins and have highlighted the major differences between *S. meliloti* and other previously characterized systems in *Bacillus subtilis* and *Escherichia coli*.

Our reported value of 423 chemoreceptors per cell is significantly lower than that observed in *E. coli* (ranging from 3,600 - 26,000 chemoreceptors) and *B. subtilis* (approximately 60,000). However, after accounting for the proportion of cells that do not express chemotaxis proteins, our value agrees closely with the estimate of 1,100–2,200 receptors per cell based on the chemoreceptor array of the related alphaproteobacterium *Caulobacter crescentus* (1-4). We discovered that the ratio of methyl-accepting chemotaxis proteins (MCPs) to CheA (22:1) is highly similar to what was discovered in *B. subtilis* (23:1) and dissimilar from *E. coli* (3.4:1) (2-4). In *E. coli*, the minimal functional unit in an array is a complex of two receptor trimer-of-dimers, one CheA dimer, and two CheW monomers. The combined high abundance of CheW1 and CheW2 in *S. meliloti* implies that many units of the array exist without CheA. It is speculated that receptors not directly interacting with CheA may indirectly influence CheA autophosphorylation activity through connected CheW proteins. One possible advantage of an increased ratio of CheW1/2 to CheA is an enhanced level of receptor cooperativity, which has been shown to occur when CheW is overexpressed in *E. coli* (5). A question remains open: why is the receptor to CheA ratio in *S. meliloti* and *B. subtilis* higher than in *E. coli*? It is known that the rate of CheA autophosphorylation in *B. subtilis* is controlled not only by receptor methylation pattern but also by the phosphorylation state of CheV and CheD binding to the receptors (6). One can speculate that in *S. meliloti* signaling through CheA is modulated by an indirect interplay of CheD, CheS and the CheR/CheB adaptation system.

The ratios of other chemotaxis proteins to CheA are also significantly variable in the three species. The CheY2:CheA (86:1) ratio is 15 and 35 times greater than the ratio of CheY:CheA in *B. subtilis* (5.5:1) and *E. coli* (2.4:1), respectively. These variations are likely are closely related to the different signal termination mechanism used by each species. Other ratios are much more challenging to explain. For instance, the ratio of *S. meliloti* CheR to MCPs is approximately 1:2 (or a 1:1 ratio of CheR to receptor dimer). CheR is an enzyme that uses MCPs as a substrate; typically, the amount of substrate is higher than its associated enzyme. This is true in *B. subtilis*, where the MCPs (excluding HemAT) to CheR ratio is 37:1, and in *E. coli*, where the lowest observed ratio of MCPs to CheR is 103:1, depending on growth conditions (3, 4). A similar observation can be made for CheB, which is only about half as abundant as CheR. Another receptor-modifying protein, CheD, is also found in high abundance with a ratio to MCPs of approximately 1:1. These stoichiometric variations imply deviations of the *S. meliloti* adaptation system from the two known paradigms. However, it is challenging to find an explanation for these differences without any information about the mechanisms involved in *S. meliloti* adaptation. This argument is only strengthened by our efforts to characterize CheT in chapter 5. Acquired data stoichiometric data will allow us to build more rigorous models of the *S. meliloti* chemotaxis system. Together with future studies focusing on rates of enzyme activities , we can form the basis for predictive mathematical modeling of *S. meliloti* chemotactic behavior.

In chapter 4 we revisited a phenomenon first discovered during the quantification of chemoreceptors described in chapter 2. It was observed that fusion of a 3xFLAG tag to the C-terminus of McpU greatly increased its cellular abundance. Using a series of epitope tag fusions, amino acid additions, and deletions at the C-terminus of McpU, we determined that the presence

of tags interferes with proteolysis. Cell-cycle dependent proteolysis had been documented extensively in the *C. crescentus* system but relatively little is known about it in *S. meliloti* (7-10). Cell-cycle dependent proteolysis has been presented to be important for the symbiosis between *S. meliloti* and its host plants, however, its importance in the free-living state is unclear (9, 11). We have shown that, similar to the flagellar component FliF in *C. crescentus*, the presence of charged residues at the C-terminus of McpU prevents its proteolysis and induces an accumulation of the tagged protein (12). This effect appears to be wide spread with five of six tested *S. meliloti* chemotaxis proteins exhibiting a significant increase in abundance when fused with a 3xFLAG epitope tag. Cell-cycle dependent proteolysis could be an important mechanism for controlling protein stoichiometry. Additionally, this work should caution researchers interested in studying protein stoichiometries in S. *meliloti* and other alphaproteobacteria about the confounding effect that even small modifications can have on cellular protein abundance.

Chapter 5 addressed the function of the *cheT* (previously known as *orf10*)gene product, which is the last gene in the major chemotaxis operon of *S. meliloti* and has no characterized homologues in any other system. Through crosslinking experiments and chromatography, we have established that CheT interacts with the methyltransferase CheR, forming a heterodimer. We have tested the methyltransferase activity of CheR with McpX as a substrate and found no influence of CheT on the rate of methylation under any conditions tested. However, there are a wide array of variables that have yet to be analyzed that could reveal when and how CheT influences methylation by CheR.

The chemotaxis system of *S. meliloti* is classified as an F7-type system (13) similar to that of *E. coli* and *Salmonella enterica*, but it appears significantly divergent from these and other members in this class. It has been well established that signal termination by a phosphate

sink mechanism is significantly different from the enzyme-based mechanism in *E. coli* (14, 15). Now it is becoming more apparent that the adaptation system is also divergent from those previously described, as evidenced by the high ratios of CheR, CheB and CheD to CheA, the interaction of CheT and CheR, and of the fact that both, CheB and CheR show a lack of homology in regions known to bind to the chemoreceptor pentapeptide motif. This idea is supported by results from past experiments investigating the *S. meliloti* adaptation system through *in-vivo* methanol release experiments. These experiments indicated that, different from *E. coli* and *B. subtilis*, methanol is not released upon removal of an attractant (16-18). The explanation for this highly unusual finding must be derived from the currently unknown unique properties of the *S. meliloti* adaptation system. Since we have shown that McpX is methylated *in vitro*, one can safely draw the conclusion that receptor modifications occur *in vivo*. Therefore, a number of investigations remain to be pursued. For example, neither the activity of CheD in receptor deamidation nor its interaction with other chemotaxis proteins has been explored. Generally, a detailed analysis of the adaptation system is required to contextualize the striking differences in the ratios of adaptation protein and the addition of CheT function in adaptation. Specifically, experiments that explore site specificity of receptor methylation and receptor activation by ligands are of high importance. In this work, we made note that the amino acid sequence of CheR differs significantly from that of other well-studied CheR proteins. Specifically, it lacks conserved residues required for binding to the pentapeptide motif at the C-terminus of MCPs (19). Although the pentapeptide motif is present in four of eight chemoreceptors, it is unclear whether effective methylation by CheR is pentapeptide-dependent or not. It is possible that CheR activity is regulated by CheT. If this is the case, it is likely that the pool of active CheR is significantly lower than what is implied by the high CheR: receptor ratio.

Alternatively, CheR is as abundant because part of its pool that is not bound to CheT serves a secondary role that is not directly related to the enzymatic activity of CheR.

The CheB:CheR ratio in *S. meliloti* is lower than that observed for *E. coli* and *B. subtilis*. CheB could be tethered to the receptor array, while CheR is not and this serves to compensate for its lower abundance relative to CheR. However, sequence alignment of *S. meliloti* CheB reveals little homology in the region responsible for pentapeptide binding in *E. coli* and *S. enterica* CheB (data not shown).

In *E. coli*, CheB and CheY have similar affinities to CheA (1.2 μM and 3.7 μM, respectively). However, this is not the case for CheB and CheY in *Thermotoga maritima*, where CheB has an affinity significantly lower than that of CheY (20-22). One possible reason for the relatively high ratio of CheB to CheA is the substantial pool of CheY1/2 with which CheB has to compete for CheA binding. It could be the case in *S. meliloti* that CheB instead binds CheA at a high affinity compared to CheY1 and CheY2. This would explain their high abundance as compensation for a relatively low affinity to CheA. Isothermal titration experiments would reveal how both adaptation proteins interact with receptors and their sub-domains, and the affinity of CheB to CheA.

While these findings need to be further examined experimentally, they contribute to the fact that the *S. meliloti* adaptation system in particular functions unlike that of the enteric paradigm.

Ultimately, this work serves as a foundation for insights into the evolution of *S. meliloti* and its symbiotic life history. A greater depth of knowledge will help us build predictive models of how bacterial cells respond to different chemical gradients exuded by the plants and what allows for effective chemotaxis in the soil. These types of models already exist for enteric

bacteria like *E. coli* and are useful tools for engineers, who wish to use bacteria for therapeutic purposes (23). Models that accurately predict *S. meliloti* behavior are critical to engineering efforts focused on creating robust and competitive strains that will outperform native soil bacteria and establish an effective symbiosis with their host plants. These more competitive strains will one day result in greater food yields, while reducing the need for exogenous nitrogen fertilizers. Finally, this work helps to establish *S. meliloti* as a model for other alphaproteobacteria, especially in processes with no direct analogs in *E. coli* or *B. subtilis* such as cell-cycle specific degradation of proteins.

REFERENCES

1. Briegel A, Ding HJ, Li Z, Werner J, Gitai Z, Dias DP, Jensen RB, Jensen GJ. 2008. Location and architecture of the *Caulobacter crescentus* chemoreceptor array. Mol Microbiol 69:30-41.
2. Zatakia HM, Arapov TD, Meier VM, Scharf BE. 2018. Cellular stoichiometry of methyl-accepting chemotaxis proteins in *Sinorhizobium meliloti*. J Bacteriol 200:e00614-17.
3. Li M, Hazelbauer GL. 2004. Cellular stoichiometry of the components of the chemotaxis signaling complex. J Bacteriol 186:3687-3694.
4. Cannistraro VJ, Glekas GD, Rao CV, Ordal GW. 2011. Cellular stoichiometry of the chemotaxis proteins in *Bacillus subtilis*. J Bacteriol 193:3220-3227.
5. Eismann S, Endres RG. 2015. Protein connectivity in chemotaxis receptor complexes. PLoS Comput Biol 11:e1004650.
6. Walukiewicz HE, Tohidifar P, Ordal GW, Rao CV. 2014. Interactions among the three adaptation systems of *Bacillus subtilis* chemotaxis as revealed by an in vitro receptor-kinase assay. Mol Microbiol 93:1104-1118.
7. Joshi KK, Chien P. 2016. Regulated proteolysis in bacteria: *Caulobacter*. Annu Rev Genet 50:423-445.
8. Smith SC, Joshi KK, Zik JJ, Trinh K, Kamajaya A, Chien P, Ryan KR. 2014. Cell cycle-dependent adaptor complex for ClpXP-mediated proteolysis directly integrates phosphorylation and second messenger signals. Proc Natl Acad Sci U S A 111:14229-34.
9. Pini F, De Nisco NJ, Ferri L, Penterman J, Fioravanti A, Brilli M, Mengoni A, Bazzicalupo M, Viollier PH, Walker GC, Biondi EG. 2015. Cell Cycle Control by the Master Regulator CtrA in *Sinorhizobium meliloti*. PLOS Genetics 11:e1005232.
10. Curtis PD, Brun YV. 2010. Getting in the loop: regulation of development in *Caulobacter crescentus*. Microbiol Mol Biol Rev 74:13-41.
11. Xue S, Biondi EG. 2019. Coordination of symbiosis and cell cycle functions in *Sinorhizobium meliloti*. Biochim Biophys Acta Gene Regul Mech 1862:691-696.
12. Grunenfelder B, Tawfilis S, Gehrig S, M OS, Eglin D, Jenal U. 2004. Identification of the protease and the turnover signal responsible for cell cycle-dependent degradation of the *Caulobacter* FliF motor protein. J Bacteriol 186:4960-71.
13. Wuichet K, Zhulin IB. 2010. Origins and diversification of a complex signal transduction system in prokaryotes. Sci Signal 3:ra50.
14. Sourjik V, Schmitt R. 1996. Different roles of CheY1 and CheY2 in the chemotaxis of *Rhizobium meliloti*. Mol Microbiol 22:427-436.
15. Dogra G, Purschke FG, Wagner V, Haslbeck M, Kriehuber T, Hughes JG, Van Tassell ML, Gilbert C, Niemeyer M, Ray WK. 2012. *Sinorhizobium meliloti* CheA complexed with CheS exhibits enhanced binding to CheY1, resulting in accelerated CheY1 dephosphorylation. J Bacteriol 194:1075-1087.
16. Greck M, Platzer J, Sourjik V, Schmitt R. 1995. Analysis of a chemotaxis operon in *Rhizobium meliloti*. Mol Microbiol 15:989-1000.
17. Robinson JB, Bauer WD. 1993. Relationships between C4 dicarboxylic acid transport and chemotaxis in *Rhizobium meliloti*. J Bacteriol 175:2284-91.
18. Greck M. 1990. Untersuchungen zur Physiologie und Genetik der Chemotaxis von *Rhizobium meliloti*. Ph.d Thesis. Universitat Regensburg, Germany

19. Perez E, Stock AM. 2007. Characterization of the *Thermotoga maritima* chemotaxis methylation system that lacks pentapeptide-dependent methyltransferase CheR:MCP tethering. Mol Microbiol 63:363-378.
20. Li J, Swanson RV, Simon MI, Weis RM. 1995. The response regulators CheB and CheY exhibit competitive binding to the kinase CheA. Biochemistry 34:14626-36.
21. Park S, Crane BR. 2011. Structural insight into the low affinity between *Thermotoga maritima* CheA and CheB compared to their *Escherichia coli*/*Salmonella typhimurium* counterparts. Int J Biol Macromol 49:794-800.
22. Park S-Y, Beel BD, Simon MI, Bilwes AM, Crane BR. 2004. In different organisms, the mode of interaction between two signaling proteins is not necessarily conserved. Proc Natl Acad Sci U S A 101:11646-11651.
23. Schauer O, Mostaghaci B, Colin R, Hürtgen D, Kraus D, Sitti M, Sourjik V. 2018. Motility and chemotaxis of bacteria-driven microswimmers fabricated using antigen 43-mediated biotin display. Sci Rep 8:9801.